Synthesis of copper oxide by thermal oxidation

熱酸化による酸化銅の合成

2012

Jianbo Liang

Nagoya Institute of Technology

Contents

Chapter – 1 Introduction

1.1 General Introduction

Nanowires are especially attractive for nano-science studies as well as for nanotechnology applications. Nanowires, compared to other low dimensional systems, have two quantum confined directions, while still leaving one unconfined direction for electrical conduction. This allows nanowires to be used in applications where electrical conduction, rather than tunneling transport is required. Because of their unique density of electronic states, nanowires in the limit of small diameters are expected to exhibit significantly different optical, electrical and magnetic properties from their bulk 3D crystalline counterparts. The increased surface area, very high density of electronic states and joint density of states near the energies of their van Hove singularities, enhanced exciton binding energy, diameter-dependent band gap, and increased surface scattering for electrons and phonons are just some of the ways in which nanowires differ from their corresponding bulk materials. Yet the sizes of nanowires are typically large enough (> 1nm in the quantum confined direction) to have local crystal structures closely related to their parent materials, thereby allowing theoretical predictions about their properties to be made on the basis of an extensive literature relevant to their bulk properties. Not only do nanowires exhibit many properties that are similar to, and others that are distinctly different from, those of their bulk counterparts, nanowires have the advantage from an applications standpoint that some of the materials parameters that are critical for certain properties can be independently controlled in nanowires, but not in their bulk counterparts, such as, for example, their thermal conductivity. Also certain properties can be enhanced non-linearly in

small diameter nanowires, by exploiting the singular aspects of the 1D electronic density of states.

Furthermore, nanowires have been shown to provide a promising framework for applying the \bottom-up" approach (Feynman, 1959) for the design of nanostructures for nanoscience investigations and for potential nanotechnology applications. Driven by: (1) these new research and development opportunities, (2) the smaller and smaller length scales now being used in the semiconductor, opto-electronics and magnetics industries, and (3) the dramatic development of the biotechnology industry where the action is also at the nanoscale, the nanowire research field has developed with exceptional speed in the last few years. Therefore a review of the current status of nanowire research is of significant broad interest at the present time. It is the aim of this review to focus on nanowire properties that differ from those of their parent crystalline bulk materials, with an eye toward possible applications that might emerge from the unique properties of nanowires and from future discoveries in this field.

For quick reference, examples of typical nanowires that have been synthesized and stud- ied are listed in Table 1. Also of use to the reader are review articles that focus on a comparison between nanowire and nanotube properties (Dresselhaus et al., 2002) and the many reviews that have been written about carbon nanotubes (Saito et al., 1998; resselhaus et al., 2001; Haddon, 2002), which can be considered as a model one-dimensional system.

Table 1.1: Selected synthesis of nanowires by material

Material	Growth Technique	Reference
Ag	DNA-template, redox template, pulsed ECD[a]	(Braun et al., 1998) (Sauer et al., 2002)
Au	Template, EDC[a]	(Hornyak et al., 1997; Zhang et al., 2001)
Bi	Stress-inducetemplate, vapor-phase template, ECD[a] template, pressure-injection	(Cheng et al., 2002) Heremans et al., 2002) (Piraux et al., 1999) (Hong et al., 1999) (Yin et al., 2001) (Zhang et al., 1998b) (Zhang et al., 1996b; Huber et al., 2000)
Bi$_2$Te$_3$	Template, dc EDC[a]	(Sander et al., 2002)
CdS	Liquid-phase (surfactant), recrystallization template, ac EDC[a]	(Chen et al., 2002b) (Xu et al., 2002a) Routkevitch et al., 1996a)
CdSe	Liquid-phase (surfactant), redox template, ac EDC[a]	(Manna et al., 2000) (Routkevitch et al., 1996b) (Xu et al., 2000b)
Cu	Vapor deposition template, ECD[a]	(Adelung et al., 2002) (Gao et al., 2001)
Fe	Template, EDC[c] shadow deposition	(Mawiawi et al., 1991) (Li and Metzger, 1997)
GaN	Template, CVD[c] VLS[b]	(Cheng et al., 1999) (Huang et al., 2002; Cui et al., 2000)
GaAs	Template, liquid/vapor OMCVD[d]	(Berry et al., 1996)
Ge	High-T, high-P liquid-phase, redox VLS[b] oxide-assisted	(Heath and LeGoues, 1993) (Wu and Yang, 2000) (Zhang et al., 2000a)
InAs	template, liquid/vapor OMCVD[d]	(Berry et al., 1996)
InP	VLS[b]	(Duan et al., 2001)
Mo	Step decoration, EDC[a]+redox	(Sun et al., 1999) (Nielsch et al., 2001; Yin et al., 2001)
Ni	template, EDC[a]	(Sun et al., 1999) (Nielsch et al., 2001; Yin et al., 2001)
PbSe	liquid phase	(Bashouti et al., 2002)
Pd	step decoration, EDC[a]	(Favier et al., 2001)
Se	liquid-phase, recrystallization template, pressure injection	(Gates et al., 2002a) (Huber et al., 1994)
Si	VLS[b] laser-ablationVLS[b] oxide-assistedlow-T VLS[b]	(Cui et al., 2001a) (Morales and Lieber, 1998) (Wang et al., 1998b) (Sunkara et al., 2001)
Zn	template, vapor-phasetemplate, EDC[a]	(Heremans et al., 2002) (Li et al., 2000b)
ZnO	VLS[b]template, ECD[a]	(Yang et al., 2002) (Zheng et al., 2002; Li et al., 2000b)

[a] Electrochemical deposition

[b] Vapor-liquid-solid

[c] Chemical vapor deposition

[d] Organometallic chemical vapor deposition (source: Ref. 1)

1.2 Synthesis

In In this section we survey the most common synthetic approaches that have successfully

afforded high quality nanowires of a large variety of materials (see Table1). In 2.1, we discuss methods

which make use of various templates with nanochannels to confine the nanowire growth in two

dimensions. In 2.2, we present the synthesis of nanowires by the vapor-liquid-solid mechanism and its

many variations. In 2.3, examples of other synthetic methods of general applicability are presented. The

last part of this section (2.4) features several approaches that have been developed to organize nanowires

into simple architectures.

1.2.1 Template-Assisted Synthesis

The template-assisted synthesis of nanowires is a conceptually simple and intuitive way to

fabricate nanostructures (Ozin, 1992; Tonucci et al., 1992; Ying, 1999). These templates contain very

small cylindrical pores or voids within the host material, and the empty spaces are filled with the chosen

material, which adopts the pore morphology, to form nanowires. In this section, we describe the templates

first, and then describe strategies for filling the templates to make nanowires.

1.2.1.1 Template Synthesis

In template-assisted synthesis of nanostructures, the chemical stability and mechanical

properties of the template, as well as the diameter, uniformity and density of the pores are important

characteristics to consider. Templates frequently used for nanowire synthesis include anodic alumina

(Al_2O_3), nano-channel glass, ion track-etched polymers and mica films.

Porous anodic alumina templates are produced by anodizing pure Al films in various acids (Diggle et al., 1969; O'Sullivan and Wood, 1970; Li et al., 1998a). Under carefully chosen anodization conditions, the resulting oxide film possesses a regular hexagonal array of parallel and nearly cylindrical channels. The self-organization of the pore structure in an anodic alumina template involves two coupled processes: pore formation with uniform diameters and pore ordering. The pores form with uniform diameters because of a delicate balance between electric-field-enhanced diffusion which determines the growth rate of the alumina, and dissolution of the alumina into the acidic electrolyte (Sullivan and Wood, 1970). The pores are believed to self-order because of mechanical stress at the aluminum-alumina interface due to expansion during the anodization. This stress produces a repulsive force between the pores, causing them to arrange in a hexagonal lattice (Jessenky et al.,1998). Depending on the anodization conditions, the pore diameter can be systematically varied from < 10 nm up to 200 nm with a pore density in the range of 10^9-10^{11} pores/cm^2 (Diggle et al., 1969; O'Sullivan and Wood, 1970; Mawiawi et al., 1991; Zhang et al., 1999b). It has been shown by many groups that the pore size distribution and the pore ordering of the anodic alumina templates can be significantly improved by a two-step anodization technique (Li et al., 1998b; Lin et al., 2000b), where the aluminum oxide layer is dissolved after the first anodization in an acidic solution followed by a second anodization under the same conditions.

Another type of porous template that is commonly used for nanowire synthesis is the template type fabricated by chemically etching particle tracks originating from ion bombardment (Ferain and Legras, 1993), such as track-etched polycarbonate membranes (Mawlawi et al., 1994; Martin, 1994;

Blondel et al., 1994; Liu et al., 1998b), and also mica films (Sun et al., 1999). There are other porous

materials that can be used as host templates for nanowire growth, as discussed by (Ozin, 1992).

Nano-channel glass (NCG), for example, contains a regular hexagonal array of capillaries similar to the

pore structure in anodic alumina with a packing density as high as 3×10^{10} pores/cm^2 (Tonucci et al.,

1992). Porous Vycor glass that contains an interconnected network of pores less than 10nm was also

employed for the early study of nanostructures (Huber and Huber, 1988). Mesoporous molecular sieves

(Beck et al., 1992), termed MCM-41, possess hexagonally-packed pores with very small channel

diameters which can be varied between 2 nm and 10 nm. Conducting organic filaments have been

fabricated in the nanochannels of MCM-41 (Wu and Bein, 1994). Recently, the DNA molecule has also

been used as a template for growing nanometer-sized wires (Braun et al.,1998). Diblock copolymers,

which consist of two different polymer chains with different properties, have also been utilized as

templates for nanowire growth. When two components are immiscible in each other, phase segregation

occurs, and depending on their volume ratio, spheres, cylinders and lamellae may self-assemble. To

form self-assembled arrays of nanopores, copolymers composed of polystyrene and

polymethylmethacrylate [P(S-b-MMA)] (Thurn-Albrecht et al., 2000) were used. By application of an

electric field while the copolymer was heated above the glass transition temperature of the two constituent

polymers, the self-assembled cylinders of PMMA could be aligned with their main axis perpendicular to

the film. Selective removal of the PMMA component afforded the preparation of 14-nm-diameter ordered

pore arrays with a packing density of 1.9×10^{11} cm^{-3}

1.2.1.2 Nanowire Template Assisted Growth by Pressure Injection

The pressure injection technique is often employed for fabricating highly crystalline nanowires from a low-melting point material or when using porous templates with robust mechanical strength. In the high-pressure injection method, the nanowires are formed by pressure injecting the desired material in liquid form into the evacuated pores of the template. Due to the heating and the pressurization processes, the templates used for the pressure injection method must be chemically stable and be able to maintain their structural integrity at high temperatures and at high pressures. Anodic aluminum oxide films and nano-channel glass are two typical materials used as templates in conjunction with the pressure injection filling technique. Metal nanowires (Bi, In, Sn, and Al) and semiconductor nanowires (Se, Te, GaSb, and Bi2Te3) have been fabricated in anodic aluminum oxide templates using this method [2].

The pressure P required overcoming the surface tension for the liquid material to fill the pores with a diameter d_W is determined by the Washburn equation (Adamson, 1982):

$$d_W = -4r\cos\theta/P \quad (1.1)$$

where r is the surface tension of the liquid, and θ is the contact angle between the liquid and the template.

To reduce the required pressure and to maximize the filling factor, some surfactants are used to decrease the surface tension and the contact angle. For example, it is found that the introduction of Cu in the Bi melt can facilitate the filling of the anodic alumina pores with liquid Bi and increase the number of nanowires that are prepared (Zhang et al., 1999b). However, some of the surfactants might cause contamination problems and therefore should be avoided. Nanowires produced by the pressure injection technique usually possess high crystallinity and a preferred crystal orientation along the wire axis.

1. 2.1.3 Electrochemical Deposition

The electrochemical deposition technique has attracted increasing attention as a promising

alternative for fabricating nanowires. Traditionally, electrochemistry has been used to grow thin films on

conducting surfaces. Since electrochemical growth is usually controllable in the direction normal to the

substrate surface, this method can be readily extended to fabricate 1D or 0D nanostructures, if the

deposition is confined within the pores of an appropriate template. In the electrochemical methods, a thin

conducting metal film is first coated on one side of the porous membrane to serve as the cathode for

electroplating. The length of the deposited nanowires can be controlled by varying the duration of the

electroplating process. This method has been used to synthesize a wide variety of nanowires e.g., metals

(Bi (Liu et al., 1998b; Piraux et al., 1999); Co (Ferre et al., 1997; Zeng et al., 2000); Fe (Mawiawi et al.,

1991; Peng et al., 2000); Cu (Piraux et al., 1994; Blondel et al., 1994); Ni (Ferre et al., 1997; Sun et al.,

1999); Ag (Bhattacharrya and Saha, 2000); Au (Hornyak et al., 1997)); conducting polymers (Martin,

1994; Piraux et al., 1999); superconductors (Pb (Yi and Schwarzacher, 1999)); semiconductors (CdS

(Routkevitch et al., 1996a)); and even superlattice nanowires with A/B constituents (such as Cu/Co

(Blondel et al., 1994; Piraux et al., 1994)) have been synthesized electrochemically (see Table 1.1).

In the electrochemical deposition process, the chosen template has to be chemically stable in the

electrolyte during the electrolysis process. Cracks and defects in the templates are detrimental to the

nanowire growth, since the deposition processes primarily occur in the more accessible cracks, leaving

most of the nanopores unfilled. Particle track-etched mica films or polymer membranes are typical

templates used in the simple dc electrolysis. To use anodic aluminum oxide films in the dc

electrochemical deposition, the insulating barrier layer which separates the pores from the bottom aluminum substrate has to be removed, and a metal film is then evaporated onto the back of the template membrane (Almawlawi et al., 1994). Compound nanowire arrays, such as Bi_2Te_3, have been fabricated in alumina templates with a high filling factor using the dc electrochemical deposition (Sander et al., 2002).

It is also possible to employ an ac electrodeposition method in anodic alumina tem-plates without the removal of the barrier layer, by utilizing the rectifying properties of the oxide barrier. In ac electrochemical deposition, although the applied voltage is sinusoidal and symmetric, the current is greater during the cathodic half-cycles, making deposition dominant over the etching, which occurs in the subsequent anodic half-cycles. Since no rec- tification occurs at defect sites, the deposition and etching rates are equal, and no material is deposited. Hence, the difficulties associated with cracks are avoided. In this fashion, metals, such as Co (Zeng et al., 2000) and Fe (Peng et al., 2000; Mawiawi et al., 1991), and semiconductors, such as CdS (Routkevitch et al., 1996a), have been deposited into the pores of anodic aluminum oxide templates without removing the barrier layer.

In contrast to nanowires synthesized by the pressure injection method, nanowires fabricated by the electrochemical process are usually polycrystalline, with no preferred crystal orientations, as observed by XRD studies. However, some exceptions exist. For example, polycrystalline CdS nanowires, fabricated by an ac electrodeposition method in anodic alumina templates (Routkevitch et al., 1996a), possibly have a preferred wire growth orientation along the c-axis. In addition, Xu et al. have prepared a number of single-crystal II-VI semiconductor nanowires, including CdS, CdSe and CdTe, by dc

electrochemical deposition in anodic alumina templates with a non-aqueous electrolyte (Xu et al., 2000b; Xu et al.,2000a). Furthermore, single-crystal Pb nanowires can be formed by pulse electrodeposition under over-potential conditions, but no specific crystal orientation along the wire axis was observed (Yi and Schwarzacher, 1999). The use of pulse currents is believed to be advantageous for the growth of crystalline wires because the metal ions in the solution can be regenerated between the electrical pulses and, therefore, uniform deposition conditions can be produced for each deposition pulse. Similarly, single crystal Ag nanowires were fabricated by pulsed electro-deposition (Sauer et al., 2002).

One advantage of the electrochemical deposition technique is the possibility of fabricating multi-layered structures within nanowires. By varying the cathodic potentials in the electrolyte which contains two different kinds of ions, different metal layers can be controllably deposited. In this fashion, Co/Cu multi-layered nanowires have been synthesized (Piraux et al., 1994; Blondel et al., 1994).

1. 2.1.4 Vapor Deposition

Vapor deposition of nanowires includes physical vapor deposition (PVD) (Heremans et al.,2000), chemical vapor deposition (CVD) (Cheng et al., 2000), and metallorganic chemical vapor deposition (MOCVD) (Berry et al., 1996). Like electrochemical deposition, vapor deposition is usually capable of preparing smaller-diameter ($\leq$20 nm) nanowires than pressure injection methods, Since it does not rely on the high pressure and the surface tension involved inserting the material into the pores.

In the physical vapor deposition technique, the material to be filled is first heated to produce a vapor, which is then introduced through the pores of the template and cooled to solidify. Using an especially designed experimental setup (Heremans et al., 2000), nearly single-crystal Bi nanowires in

anodic aluminum templates with pore diameters as small as 7 nm have been synthesized, and these Bi nanowires were found to possess a preferred crystal growth orientation along the wire axis, similar to the Bi nanowires prepared by pressure injection (Zhang et al., 1999b).

Compound materials that result from two reacting gases have also be prepared by the chemical vapor deposition (CVD) technique. For example, single-crystal GaN nanowires have been synthesized in anodic alumina templates through a gas reaction of Ga_2O vapor with a °owing ammonia atmosphere (Cheng et al., 1999; Cheng et al., 2000). A different liquid/gas phase approach has been used to prepare polycrystalline GaAs and InAs nanowires in a nanochannel glass array (Berry et al., 1996). In this method, the nanochannels are filled with one liquid precursor (e.g., Me3Ga or Et3In) via a capillary effect and the nanowires are formed within the template by reactions between the liquid precursor and the other gas reactant (e.g., AsH_3).

1.2.2 VLS Method for Nanowire Synthesis

Some of the recent successfully synthesized semiconductor nanowires are based on the socalled vapor-liquid-solid (VLS) mechanism of anisotropic crystal growth. This mechanism was first proposed for the growth of single crystal silicon whiskers 100 nm to hundreds of microns in diameter (Wagner and Ellis, 1964). The proposed growth mechanism involves the absorption of source material from the gas phase into a liquid droplet of catalyst (a molten particle of gold on a silicon substrate in the original work (Wagner and Ellis, 1964)). Upon supersaturation of the liquid alloy, a nucleation event generates a solidprecipitate of the source material. This seed serves as a preferred site for further deposition of material at the interface of the liquid droplet, promoting the elongation of the seed into a nanowire or a

whisker, and suppressing further nucleation events on the same catalyst. Since the liquid droplet catalyzes

the incorporation of material from the gas source to the growing crystal, the deposit grows anisotropically

as a whisker whose diameter is dictated by the diameter of the liquid alloy droplet. The nanowires thus

obtained are of high purity, except for the end containing the solidified catalyst as an alloy particle.

Real-time observations of the alloying, nucleation, and elongation steps in the growth of germanium

nanowires from gold nanoclusters by the VLS method were recorded by in-situ TEM (Wu and Yang,

2001).

Reduction of the average wire diameter to the nanometer scale requires the generation of

nanosized catalyst droplets. However, due to the balance between the liquid-vapor surface free energy and

the free energy of condensation, the size of a liquid droplet, in equilibrium with its vapor, is usually

limited to the micrometer range. This obstacle was overcome in recent years by several new

methodologies: 1) Advances in the synthesis of metal nanoclusters have made monodispersed

nanoparticles commercially available. These can be dispersed on a solid substrate in high dilution so that

when the temperature is raised above the melting point, the liquid clusters do not aggregate (Cui et al.,

2001a). 2) Alternatively, metal islands of nanoscale sizes can self-form when a strained thin layer is

grown or heat treated on a non-epitaxial substrate (Wu and Yang, 2000). 3) Laser-assisted catalytic VLS

growth is a method used to generate nanowires under non-equilibrium conditions. By laser ablation of

a target containing both the catalyst and the source materials, a plasma is generated from which catalyst

nanoclusters nucleate as the plasma cools down. Single crystal nanowires grow as long as the particle

remains liquid (Morales and Lieber, 1998). 4) Interestingly, by optimization of the material properties of the catalyst-nanowire system, conditions can be achieved for which nanocrystals nucleate in a liquid catalyst pool supersaturated with the nanowire material, migrate to the surface due to a large surface tension, and continue growing as nanowires perpendicular to the liquid surface (Sunkara et al., 2001). In this case, supersaturated nanodroplets are sustained on the outer end of the nanowire due to the low solubility of the nanowire material in the liquid (Sharma et al., 2001).

A wide variety of elemental, binary and compound semiconductor nanowires has been synthesized via the VLS method, and relatively good control over the nanowire diameter and diameter distribution has been achieved. Researchers are currently focusing attention on the controlled variation of the materials properties along the nanowire axis. To this context, researchers have modified the VLS synthesis apparatus to generate compositionally-modulated nanowires. GaAs/GaP modulated nanowires have been synthesized by alternately ablating targets of the corresponding materials in the presence of gold nanoparticles (Gudiksen et al., 2002). p-Si/n-Si nanowires were grown by chemical vapor deposition from alternating gaseous mixtures containing the appropriate dopant (Gudiksen et al., 2002). Si/Si$_{1-x}$Ge$_x$ nanowires were grown by combining silicon from a gaseous source with germanium from a periodically ablated target (Wu et al., 2002). Finally, using an ultra-high vacuum chamber and molecular beams, InAs/InP nanowires with atomically sharp interfaces were obtained (Bjork et al., 2002a). These compositionally-modulated nanowires are expected to exhibit exciting electronic, photonic, and thermoelectric properties. Interestingly silicon and germanium nanowires grown by the VLS method

consist of a crystalline core coated by a relatively thick amorphous oxide layer. These layers are too thick

to be the result of ambient oxidation, and it has been shown that these oxides play an important role in the

nanowire growth process (Wang et al., 1998a; Wang et al., 1998b). Silicon oxides were found to serve as

a special and highly selective catalyst that significantly enhances the yield of Si nanowires, without the

need for metal catalyst particles (Wang et al., 1998b; Wang et al., 1998a; Zhang et al., 1999a). A similar

yield enhancement was also found in the synthesis of Ge nanowires from the laser ablation of Ge powder

mixed with GeO_2 (Zhang et al., 2000a).

1.2.3 Other Synthesis Methods

In this section we review several other general procedures available for the synthesis of a

variety of nanowires. We focus on "bottom-up" approaches, which afford many kinds of nanowires in

large numbers, and do not require highly sophisticated equipment (such as scanning microscopy or

lithography based methods), and exclude cases for which the nanowires are not self-sustained (such as in

the case of atomic rows on the surface of crystals). A solution-phase synthesis of nanowires with

controllable diameters has been demonstrated (Gates et al., 2000; Gates et al., 2002a), without the use of

templates, catalysts, or surfactants. Instead, Gates et al. make use of the anisotropy of the crystal structure

of trig-onal selenium and tellurium, which can be viewed as rows of 1D helical atomic chains. Their

approach is based on the mass transfer of atoms during an aging step from a high free-energy solid phase

(e.g., amorphous selenium) to form a seed (e.g., trigonal selenium nanocrystal) which grows

preferentially along one crystallographic axis. The lateral dimension of the seed, that dictates the diameter

of the nanowire, can be controlled by the temperature of the nucleation step. Furthermore, Se/Te alloy

nanowires were synthesized by this method, and Ag_2Se compound nanowires were obtained by treating selenium nanowires with $AgNO_3$ (Mayers et al., 2001; Gates et al., 2001; Gates et al., 2002b). More often, however, the use of surfactants is necessary to promote the anisotropic 1D growth of nanocrystals. Solution phase synthetic routes have been optimized to produce monodispersed quantum dots, i.e., zero-dimensional isotropic nanocrystals (Peng et al., 1998). Surfactants are necessary in this case to stabilize the interfaces of the nanoparticles and retard oxidation and aggregation processes. Detailed studies on the e®ect of growth conditions revealed that they can be manipulated to induce a directional growth of the nanocrystals, usually generating nanorods (aspect ratio of ¼ 10), and in favorable cases, nanowires of high aspect ratios. Heath and LeGoues synthesized germanium nanowires by reducing a mixture of $GeCl_4$ and phenyl-$GeCl_3$ at high temperature and high pressure. The phenyl ligand was essential for the formation of high aspect ratio nanowires (Heath and LeGoues, 1993). In growing CdSe nanorods (Manna et al., 2000), a mixture of two surfactants was used, whose concentration ratio influenced the structure of the nanocrystal. It is believed that different surfactants have different affinities, and different absorption rates, for the different crystal faces of CdSe, thereby regulating the growth rate of these faces. A coordinating alkyl-diamine solvent was used to grow polycrystalline PbSe nanowires at low temperatures (Bashouti et al., 2002). Here, the surfactant-induced directional growth is believed to occur, due to the formation of organometallic complexes in which the bidentate ligand assumes the equatorial positions, thus hindering the ions from approaching each other in this plane. Additionally, the alkyl-amine molecules coat the external surface of the wire, preventing lateral growth. The aspect ratio of

the wires increased as the temperature was lowered in the range $10 < T < 117°C$. Ethylenediamine was

used to grow CdS nanowires and tetrapods by a solvo-thermal recrystallization process starting with CdS

nanocrystals or amorphous particles (Chen et al., 2002b). While the coordinating solvent was crucial for

the nanowire growth, its role in the shape and phase control was not clarified.

1.2.4 Hierarchical Arrangement and Superstructures of Nanowires

Ordering nanowires into useful structures is another challenge that needs to be addressed in

order to harvest the full potential of nanowires for applications. We will first review examples of

nanowires having a non-trivial structure, and then proceed to describe methods to create assemblies of

nanowires of a predetermined structure. We have already mentioned in 2.2 that the preparation of

nanowires with a graded composition or with a super-lattice structure along their main axis was

demonstrated by controlling the gas-phase chemistry as a function of time during the growth of the

nanowires by the VLS method. Control of the composition along the axial dimension was also

demonstrated by a template-assisted method, for example by the consecutive electrochemical deposition

of different metals in the pores of an alumina template (Nicewarner-Pena et al., 2001). Alternatively, the

composition can be varied along the radial dimension of the nanowire, for example, by first growing a

nanowire by the VLS method and then switching the synthesis conditions to grow a different material on

the surface of the nanowire by CVD. This technique was demonstrated for the synthesis of Si/Ge and

Ge/Si coaxial (or core-shell) nanowires (Lauhon et al., 2002), and it was shown that by a thermal

annealing process, the outer shell can be formed epitaxially on the inner core. A different approach was

adopted by Wang et al. who generated a mixture of coaxial and biaxial $SiC-SiO_x$ nanowires by the

catalyst-free high-temperature reaction of amorphous silica and a carbon/graphite mixture (Wang et al., 2000).

A different category of non-trivial nanowires is that of nanowires having a non-linear structure, resulting from multiple one-dimensional growth steps. Members of this category are tetrapods that were mentioned in the context of liquid-phase synthesis 2.3. In this process, a tetrahedral quantum-dot core is first grown, and then the conditions are modified to induce a one-dimensional growth of a nanowire from each one of the facets of the tetrahedron. A similar process produced high-symmetry In_2O_3/ZnO hierarchical nanostructures. From a mixture of heat-treated In_2O_3, ZnO, and graphite powders, faceted In_2O_3 nanowires were first obtained, on which oriented shorter ZnO nanowires were crystallized (Lao et al., 2002b). Brush-like structures were obtained as a mixture of 11 structures of different symmetries. Comb-like structures entirely made of ZnO were also reported (Yang et al., 2002). Control of the position of a nanowire in the growth process is important for preparing devices or test structures containing nanowires, especially when involving a large array of nanowires. Post-synthesis methods to align and position nanowires include microfluidic channels (Messer et al., 2000), Langmuir-Blodgett assemblies (Yang and Kim, 2002), and electric-field assisted assembly (Smith et al., 2000). The first method involves the orientation of the nanowires by the liquid flow direction and by the interaction of the nanowires with the side walls of the channel. The second method involves the alignment of nanowires at a liquid- gas or liquid-liquid interface by the application of compressive forces on the interface. The third technique is based on dielectrophoretic forces that pull polarizable nanowires toward regions of high field strength.

The nanowires align between two isolated electrodes which are capacitatively coupled to a pair of buried electrodes biased with an AC voltage. Once a nanowire shorts the electrodes, the electric field is eliminated, preventing more nanowires from depositing. The above techniques have been successfully used to prepare electronic circuitry and optical devices out of nanowires (see 4.1 and x4.3). Alternatively, alignment and positioning of the nanowires can be specified and controlled during their growth by proper design of the synthesis method. For example, ZnO nanowires prepared by the VLS method was grown into an array in which both their position on the substrate and their growth direction and orientation were controlled (Yang et al., 2002). The nanowire growth region was defined by patterning the gold film, which serves as a catalyst for the ZnO nanowire growth, employing soft-lithography, e-beam lithography, or photolithography. The orientation of the nanowires was achieved by selecting a substrate with a lattice structure matching that of the nanowire material to facilitate the epitaxial growth. These conditions result in an array of nanowire posts at predetermined positions, all vertically aligned with the same crystal growth orientation. A similar structure could be obtained by the template-mediated electrochemical synthesis of nanowires (see 2.1.3), particularly if anodic alumina with its parallel and ordered channels is used. The control over the location of the nucleation of nanowires in the electrochemical deposition is determined by the pore positions, which can be precisely controlled by imprint lithography (Masuda et al., 1997), and by growing the template on a patterned conductive substrate that serves as a back electrode (Rabin et al., 2001a), different materials can be deposited in the pores at different regions of the template.

1.3 Basic properties of copper oxide

Two copper oxides, cuprous oxide (Cu_2O) and cupric oxide (CuO) are stable in the copper oxygen system. Cu_2O is insoluble in water and organic solvents. It dissolves in concentrated ammonia solution to form the colorless complex $[Cu(NH_3)_2]^+$, which easily oxidizes in air to the blue $[Cu(NH_3)_4(H_2O)_2]^{2+}$ and in hydrochloric acid to form $HCuCl_2$ (a complex of $CuCl$), while dilute sulfuric acid and nitric acid produce copper(II) sulfate and copper(II) nitrate, respectively. Cu_2O is found as the mineral cuprite in some red-colored rocks. When it is exposed to oxygen, copper will naturally oxidize to Cu_2O, but this takes extensive time. Artificial formation is usually accomplished at high temperature or at high oxygen pressure. With further heating, Cu_2O will form CuO. CuO is a black solid with an ionic structure which melts above 1200 °C with some loss of oxygen. It can be formed by heating copper in air, but in this case it is formed along with Cu_2O; thus, it is better prepared by heating copper(II) nitrate, copper(II) hydroxide or copper(II) carbonate ($2Cu(NO_3)_2 \rightarrow 2CuO + 4NO_2 + O_2$, $Cu(OH)_2 \rightarrow CuO + H_2O$ or $CuCO_3 \rightarrow CuO + CO_2$). CuO is a basic oxide, so it dissolves in mineral acids such as hydrochloric acid, sulfuric acid or nitric acid to give the corresponding copper (II) salts ($CuO + 2HNO_3 \rightarrow Cu(NO_3)_2 + H_2O$, $CuO + 2HCl \rightarrow CuCl_2 + H_2O$ or $CuO + H_2SO_4 \rightarrow CuSO_4 + H_2O$). It is also made by reacting solid copper with oxygen gas ($2Cu + O_2 \rightarrow 2CuO$)

Cu_2O is known to be a metal deficient, p-type semiconductor with cation vacancies and electron holes as the primary defects [3]. The deviation from stoichiometry has been studied as a function of temperature and oxygen partial pressure by chemical analysis of quenched samples [4], by

thermogravimetry [5-7] and by high-temperature solid-state coulometric titration [8]. These studies generally conclude that Cu_2O is metal-deficient and that the prevailing atomic defects are neutral copper vacancies. However, on the basis of previous studies, several different models were proposed for the defect structure of nonstoichiometric Cu_2O. These include neutral (depicted in Eqs. (1) and (4) of Table 1.2), singly-ionized copper vacancies (Eq. 5), singly-ionized oxygen interstitials (Eq. 2) and doubly-ionized oxygen interstitials (Eq. 3) [4-7, 9, 10]. Also shown in Table 1.2 is the oxygen-partial-pressure (pO_2) dependence of the electrical conductivity of Cu_2O with various defects.

The electrical conductivity (σ) of Cu_2O has been measured over a wide range of temperatures and pO_2 levels [9, 11-15] Maluenda et al. [16] measured electrical conductivity of Cu_2O over the temperature range from 700 to 1100°C at a pO_2 corresponding to the Cu_2O phase, down to 10^{-6} atm. According to their results, the slope (dlog σ/dlog pO_2) is greater than 1/8, which is not expected if $V{'}_{Cu}$ is the only charged atomic defect. To account for the observed pO_2 dependence of σ, Maluenda et al. [16] Suggest that a defect pair ($V{'}_{Cu}$) may become important with increasing pO_2. However, Peterson and Wiley [15] developed the exact expression for electrical conductivity, which includes the coupling of singly-ionized copper vacancies $V{'}_{Cu}$ and oxygen interstitials $O{'}_i$. They made two assumptions in analyzing their data: the mobility of the hole μ_{h}· was assumed to be independent of temperature; and the mobilities of $V{'}_{Cu}$ and V_{Cu}^x were assumed to be equal. The enthalpy of formation values for the defects obtained from electrical-conductivity measurements appear to be a function of both temperature and partial pressure [9] and the values are not consistent with those deduced from thermo-gravimetric

measurements [5, 7].

Table 1.2 Possible Defects in Nonstoichiometric Cu_2O

Point defect	Charge	Expected defect reaction	Eq.no.	Exponent n^a
O_i^o	0	$1/2O_2 (g) = O_i^o$	1	0
$O_i^{\cdot}$	-1	$1/2O_2 (g) = O_i^{\cdot} + h^{\cdot}$	2	1/4
$O_i^{\cdot\cdot}$	-2	$1/2O_2 (g) = O_i^{\cdot\cdot} + 2h^{\cdot}$	3	1/6
V_{Cu}^x	0	$1/2O_2 (g) = 2 V_{Cu}^x + O_o^x$	4	0
$V_{Cu}^{\cdot}$	-1	$1/2O_2 (g) = 2 V_{Cu}^{\cdot} + O_o^x + 2h^{\cdot}$	5	1/8
$V_{Cu}^{\cdot\cdot}$	-2	$1/2O_2 (g) = V_{Cu}^{\cdot\cdot} + O_o^x + 2h^{\cdot}$	6	1/6
Intrinsic	$e^{\backprime}$ and $h^{\cdot}$	$O = e^{\backprime} + h^{\cdot}$	7	0

^{a}Exponents, n, in $\sigma \propto (pO_2)^{1/n}$ (pO_2 dependence of electrical conductivity).

Because the deviation from stoichiometry in Cu_2O is rather small, quantitative agreement among different studies is only fair. Peterson and Wiley [15] measured the temperature and pO_2 dependence of cation-tracer diffusion in Cu_2O. The results suggested that both neutral and singly-charged copper vacancies contribute mainly to cation self-diffusion. However, a defect model [15] involving both neutral and singly-charged copper vacancies, holes and singly-charged oxygen-interstitial ions was developed and compared with the tracer-diffusion data, the electrical-conductivity data obtained by Maluenda et al.[16] and the stoichiometry data of O'Keefe et al.[17]. The model (see for example, Eq. 5 in Table 1.2) suggests that majority of the neutral species in Cu_2O are neutral copper vacancies and therefore may not provide a good explanation for electronic transport.

1.4 Oxidation of copper

Multiphase scales of Cu_2O and CuO form on Cu oxidized in oxygen or air at high temperatures, depending on the thermodynamic stability of the oxides [5, 19, 20]. The parabolic rate constant k_p for the oxidation of copper depends on $pO_2^{1/4}$ when only Cu_2O forms. Mass transport mainly involves neutral copper vacancies [21-24]. This implies that the majority of the copper vacancies in the outer layer of the scale have zero effective charges. The formation of neutral copper vacancies, V_{Cu}^x was considered in Eq. (3). According to Mrowec and Stoklosa studies on the oxidation of copper as a function of oxygen partial pressures, at high pO_2 the scale consists of Cu_2O and CuO at the scale/gas interface and the parabolic rate constant is independent of pO_2 [24]. However, to verify this pO_2 independence of oxidation high-purity specimens are needed because impurities can have a significant effect on defect concentration in nonstoichiometric Cu_2O. The existence of even a very thin layer of a compound of a higher metal - oxidation state on the scale surface can alter the dependence of the reaction rate on oxidant pressure. Onay and Rapp performed in situ oxidation of copper at 10^{-4} atm and 300°C [25]. Their results indicate that the multiphase, multilayer scales form by dissociation of the Cu_2O scale, which loses contact with the copper substrate upon thickening and also leads to microchannels and formation of oxygen-rich CuO in Cu_2O scales. Kaufman and Hawkins performed optical-luminescence measurements on thin films of Cu_2O on copper [26]. They suggest that the rate of copper oxidation is limited by the diffusion of copper vacancies.

Table 1.3 Physical Parameters of Cu_2O and CuO

Parameter	Cu_2O	CuO
Formula weight	143.08	79.54
Melting point	1235	1326
Crystal system	Cubic	Monoclinic
Space group	Pn3m(224)	C2/$_c$
Z^a	2	4
Lattice parameters(A)	A = 4.2696	A = 4.684, B = 3.425, C = 5.129, β = 99.54°
Cell volume(10^{-24} cm^3)	77,8334	81.164
Molar volume (cm^3)	23.437	12.02
X-ray density (g/cm^3)	6.1047	6.509

"Z=number of gram formula weight per unit cell (source: Ref. 18).

Formation of one-dimensional metal oxide nanowires or whiskers has been intensively investigated, because of wide technological applications and the intrinsic interest in structures with reduced dimensions. More recently, considerable attention has been directed to oxide nanowires formation by thermal oxidation of metals in oxygen atmosphere [27-35], largely due to its technical simplicity and large-scale growth capability. Oxide whisker growth from the oxidation of metals was first observed back in the 1950s [36, 37] and since then numerous observations have been performed but have led to different theories regarding the mechanisms for the spontaneous oxide nanowires formation. Some are based on evaporation and condensation mechanism, i.e., vapor-solid (VS) model [34, 38, 39], or short-circuit diffusion up the center of the nanowires [40-44]. Other work suggested that growth of oxide nanowires occurs as a result of the accumulation and relaxation of compressive stresses in the oxidation processes [45-47]. Unclear to date, however, is the origin of the compressive stresses in the oxide layer and how they result in oxide nanowire growth.

Recent studies by several groups indicate that CuO could exist in as many as three different magnetic phases [36]. It was a 3D collinear antiferromagnet at temperatures below 213 k. when the temperature was raised; it first became an intermediate non-collinear incommensurate magnetic phase up to 230 k and the acted like a 1D quantum antiferromagnetic material. Ever since the discovery of carbon nanotubes, there has been a steadily growing interest in the studies of one-dimensional (1D) nanostructures, such as nanowires and Nano rods. By definition, 1D nanostructure is anisotropic Nano crystals with large aspect ratio and diameter in the range of 1 – 200 nm. These 1D nanostructures not only open new opportunities in the field of microelectronics but also provide models for studying the effect of dimensionality and size confinement on electrical, transport and mechanical properties. For example, transport properties of a single SnO_2 nanowires exhibit strong correlation effects in comparison to the bulk or thin films of SnO_2 whose temperature dependent conductivity is well described by the thermal activation model [37]. During the last 3–4 years, nanowires of various inorganic materials have been synthesized due to the realization of their applications in different filed. High capacity, longer cycle life and higher C - rate performance compared to the bulk have been reported for SnO_2 nanofibres used as the anode material for Li ion batteries [38].

The phenomenon of oxide nanowire formation from the oxidation of metals is not tied up with a single metal system but the oxidation of copper remains the most representative one [43,45-51]. It was proposed that the driving force for CuO whisker formation during the oxidation of copper is related to the high compressive stress in the oxide layer resulting from the large difference in the molar volumes of the

metal and oxides [43, 52, 53]. Since both Cu_2O and CuO are cation-deficient p-type oxides, it has been shown univocally that the oxide growth is controlled via outward diffusion of cations during the oxidation of Cu [41, 43, 54-58]. The new oxide formation occurs at the gas/oxide interface so that the oxide layer grows preferentially into free space. Such unconstrained growth would not be expected to develop stress (the effect of epitaxial stress is limited to the first ~ 50 nm of oxide and is not applicable to oxide nanowires formation, which requires the first growth of macro-thick surface oxide layers) [54].

Some unique experiments have been performed and suggested that CuO nanowires grow from the tip and are not extruded from the base oxide layers during the oxidation of Cu substrates [43, 59]. For such a process, the nanowire growth must call for transport of Cu ions from the base to growth tip. It was suggested that oxide nanowires or whiskers grow predominately by surface diffusion of metal species from the nanowires base to top along a tunnel centered on the core of a screw dislocation [40-44]. However, such a scenario contradicts with many recent experimental observations, which reveal that oxide nanowires have a bi-crystal or single crystal structure (i.e., no hollow pipe present along the axial core of nanowires) [32, 34, 46, 49, 59]. Therefore, it is paramount to identify the driving force leading to the initiation of oxide NW formation and the mass transport mechanisms governing the one-dimensional nanowire growth. In this work we choose to study CuO nanowire formation during the oxidation of copper as a model system to understand the mechanism of oxidation-induced oxide nanowire growth. Meanwhile, our interest in this system also stems from the prospective broad applications of nanostructured CuO. A number of interesting properties have been found in this p-type semiconductor

material that have led to its myriad technological applications in important fields including solar energy

conversion [60, 61], photocatalysts [62], fuel cells [63, 65], emission control [65-66], cathode materials

in lithium ion batteries [68], gas sensing [33, 35, 69], and heterogeneous catalysis for hydrocarbons

conversion reactions [70, 71].

1.5 CuO nanowires synthesis methods

During the last couple of years 1D nanowires of CuO has been synthesized by various methods

such as sonochemical method [72]. It is very useful for conducting research on novel materials with

salient properties. It depends on the acoustic cavitation phenomenon of the formation, growth, and

implosive collapse of bubbles in a liquid medium. High temperatures (>5000K), pressures (>20Mpa), and

high cooling rates (>10^7Ks^{-1}) comes out when cavity collapses. These extreme properties are useful in

irradiated solution. R.Vijiaya and co-workers have prepared nanoparticles of copper oxide which had

solidified either in an amorphous state or as crystalline phases. The process of producing CuO

crystallization in poly (vinyl alcohol) has been carried as below: a 0.015 M solution of copper nitrate

(Aldrich) is heated to a certain temperature in a water-jacketed cell of capacity to prevent the formation of

copper hydroxide later on. The admixtures (pristine polymer, CuO nanoparticles, or CuO PVA composite)

and a 0.015 M solution of hexamethylenetetramine (Aldrich; HMT) are added to the hot solution. HMT

decomposes in the hot solution to ammonia and formaldehyde. The pH of the solution changes from 5 to

a pH of about 6 which is enough to exceed the solubility product of CuO. Then the vessel is putted in ice

to stop the crystallization. After 3 h, the reaction mixture is centrifuged, washed first with water and

finally with ethanol for several times then dried in a vacuum at room temperature for a while. The copper oxide is embedded in the poly (vinyl alcohol). Similarly, Xu et al [73] obtained nanorods of CuO having diameter in the range of 30-100 nm and lengths of 1-3 μm by thermal decomposition of precursor CuC_2O_4. Based on the reaction as follows: $C_2O_4^{2+} + Cu^{2+} \rightarrow CuC_2O_4$, $CuC_2O_4 \rightarrow CuO + CO_2$. Copper acetate Cu $(CH_3COO)_2 \cdot H_2O$, oxalic acid $H_2C_2O_4 2H_2O$, nonyl phenyl ether(9)/(5)(NP-(9)/(5)),and NaCl are prepared. $Cu(CH_3COO)_2 \cdot H_2O$ and $H_2C_2O_4 2H_2O$ are mixed in (NP-(9)/(5)) and ground for several minutes, and kept in an oven for hours to supported as precursor. Then the product is washed several times with distilled water and acetone to take away the remained reactants and dried in an oven for hours. Mixed with CuC_2O_4 and NaCl powder the product is ground for several minutes. The mixture is annealed in the porcelain crucible placed in the alumina tube at hundreds degree. Then it is gradually cooled to normal temperature and washed with water, ethanol and ethyl in the ultrasonic bath. This is a chemical method that produces CuO nanorods in powder form. Wang et al. [74] obtained CuO nanowires by a novel one-step, solid-state reaction in the presence of a nonionic surfactant. This is based on the reaction as follow: $CuCl_2 \bullet 2H_2O(s) + 2NaOH(s) \rightarrow CuO(s) + 2NaCl + 3H_2O$ The typical process for producing CuO nanowhiskers is as follows. CuCl$_2$ and solid NaOH are ground for several minutes. Then PEG400 is mixed. After adequate grinding, the mixtures are washed several times with distilled water in the ultrasonic bath and then with ethanol. Finally, the product is dried in the oven. And the CuO nanowhiskers are embedded in the presence of a nonionic surfactant-PEG 400. This method also can be used to produce other nanowhiskers such as ZnS, CuS, PbS, NiS, FeS and so on. Thus, the techniques

based on precursor templates require a deep knowledge of the chemical reaction for adopting a variety of procedures for producing various precursors for synthesizing Nano-rods having a choice of diameters.

Moreover, normally the lengths of the Nano-rods produced by these methods are also less than a micron and these does not seem to be way to control the length and hence the aspect ratio of these nanorods.

From the point of view of studies of nanostructures should be simple, suitable for producing bulk quantities and amenable to control of diameter and length. In comparison to complex chemical methods, thermal annealing of copper foil provides simple, convenient and fast method for synthesizing CuO nanowires. Thermal oxidation is becoming an increasingly attractive method for the synthesis of nanostructures.

1.6 purpose and organization of thesis

This thesis describes the copper oxide thin films and cupric oxide nanowires grown by thermal oxidation of copper foils at different temperatures. The morphology and structure of the copper oxide thin films and cupric oxide nanowires have been studied. The optical parameters such as absorption coefficient and band gap are determined from optical absorption measurements. In the first chapter, gives an introduction of nanowires and their common methods of synthesis are described. Copper oxide film, cupric oxide nanowires and its synthesis method are also discussed.

The second chapter describes CuO nanowires preparation and characterization of CuO nanowire nanostructures on copper foils with different oxidation temperature from 300 to 900 °C in an ambient condition. The diameters of nanowires can be controlled by changing the annealing temperature. The morphology, composition, and structure were analyzed by using X-Ray Diffraction (XRD) and Scanning

Electron Microscope (SEM). The cross-sectional analysis was also performed by using field emission-SEM and energy dispersive X-ray spectroscopy (EDX). It indicates that the CuO nanowires were grown on the CuO/Cu_2O layer, which was formed on the surface of Cu foil.

In the third chapter investigated the effects of the grain size, orientation and surface roughness of copper substrates on the growth of cupric oxide nanowires by thermal oxidation method. Long, high density and aligned cupric oxide nanowires have been synthesized by heating (200) oriented copper foils with small grain size in an air gas flow. Long and aligned nanowires can only be formed within a narrow temperature range at around 500 °C, with diameters of 80 nm. On the other hand, uniform and aligned nanowires don't grow with case of the bigger crystallite size of copper foils with random orientation. We have studied how the surface roughness of substrates affects the growth of cupric oxide nanowires. It is observed that the growth of nanowires does not depend on the surface roughness of substrates. The smaller grain size of thin copper foil with (200) orientation is favorable for the growth of highly-aligned nanowires by thermal oxidation method.

In the fourth chapter CuO thin films on quartz substrates have been synthesized by thermal oxidation in air with water vapor. It was found that single CuO phase are synthesized by oxidation in cylinder air with water vapor, whereas mixture of random oriented CuO and Cu_2O are formed when oxidized in atmospheric air. The effects of the oxidation ambient, heating temperature and film thickness are systematically investigated. In addition, the optical band gaps of CuO thin films have been characterized by measuring the transmittance and reflectance spectra.

In the fifth chapter the growth of high quality crystals of cuprous oxide films grown on copper foils

by thermal oxidation of cupper foils with water vapor. This method proved to be good for preparing cuprous oxide films with high purity and large grain size. X-ray diffraction studies revealed the formation of Cu_2O films with preferred (111) orientation.   The cuprous oxide diodes fabricated by the above technique have been studied using current-voltage method.

In the sixth chapter high quality cuprous oxide thin films with large grain size were grown by thermal oxidation of copper foil in water vapor with N_2 gas. It was found that in water vapor (111) oriented Cu_2O are preferentially formed, whereas mixture of random oriented CuO and Cu_2O are formed when oxidized in air. The effects of the film oxidation method, heating temperature are investigated. In addition, the optical band gaps of cuprous oxide thin films have been determined by measuring the transmittance and reflectance spectra.

In the seventh chapter present the overall conclusion and recommendation for future work in this research area.

Reference

[1] M. J. Factoran, "Silicon's Usefulness in Photovoltaics," IEEE Potentials (1995) 8.

[2] J. Nozik , John Miller" Introduction to Solar Photon Conversion" Chem. Rev. 110 (2010) 6443.

[3] P. Kofstad, *Non-Stoiehiometry, Diffusion, and Electrical Conductivity in Binary Metal Oxides* (Wiley

Interseience, New York, 1972).

[4] C. Wagner and H. Hammen, *Z. Physik. Chem.* B 40 (1938) 197.

[5] M. O'Keefe and W. J. Moore, *J. Chem. Phys.* 36, 3009 (1962); H. L. McKinzie and M. O'Keefe, *Phys.*

Lett. A 24 (1967) 137.

[6] S. Mrowee, A. Stoklosa, and K. Godlewski, *Cryt. Lat. Def.* 5 (1974) 239.

[7] M. Yoshimura, A. Revcolevschi, and J. Castaing, *J. Mater. Sci.* 11 (1976) 384.

[8] Y. D. Tretyakov, V. F. Komarov, N. A. Prosvirhina, and I. B. Kusenok, *J. Solid St. Chem.*5 (1972) 157.

[9] J. Maluenda, R. Farhi, and G. Petot-Ervas, *J. Phys. Chem. Solids* 42 (1981) 911.

[10] F. Perinet, S. Barbezat, and C. Nonty, *J. Phys. Colloq.* C 6 (1980) 315.

[11] J. Gunderman, K. Hauffe, and C. Wagner, *Z. Physik. Chem.* B 37 (1937) 148.

[12] M. O'Keefe and W. J. Moore, *J. Chem. Phys.* 35 (1961) 1324.

[13] R. S. Toth, R. Kilkson, and D. Trivich, *Phys. Rev.* 122 (1961) 482.

[14] K. Stecker, *Ann. Phys.* 7 (1959) 55.

[15] N. L. Peterson and C. L. Wiley, *J. Phys. Chem. Solids* 45 (1984) 281.

[16] J. Maluenda, R. Farhi, and G. Petot-Ervas, *J. Phys. Chem. Solids* 42 (1981) 697.

[17] M. O'Keefe, Y. Ebisuzaki, and W. J. Moore, *J. Phys. Soc. Jpn.* 18 (1963) 131.

[18] *Handbook of Chemistry and Physics,* 61st Ed. (CRC press, 1981).

[19] W. J. Tomlinson and J. Yates, J. Phys. Chem. Solids 38 (1977) 1205.

[20] E. lguchi, K. Yajima, and Y. Saito, *Trans. Jpn. Inst. Met.* 14 (1973) 423.

[21] C. Wagner and K. Grunewald, *Z. Phys. Chem.* B 40 (1938) 197.

[22] J. P. Baur, D. W. Bridges, and W. M. Fassell, Jr., J. *Eleetrochem. Soc.* 103 (1956) 273.

[23] W. Feitknecht, *Z. Elektrochem.* 35 (1929) 142.

[24] S. Mrowec and A. Stoklosa, *Oxid. Met.* 3 (1971) 142.

[25] B. Onay, *J. Eleetroehem. Soe.* 136 (1989) 1578.

[26] R. G. Kaufrnan and R. T. Hawkins, *J. Electrochem. Soc.* 131(2), 385; 133(12), 2652 (1986); 135(8), 2096 (1988); *J. Luminesc.* 31 & 32 (1984) 509.

[27] E. Comini, C. Baratto, G. Faglia, M. Ferroni, A. Vomiero, S. Sberveglieri, Prog Mater Sci 54 (2009)1.

[28] Y. H. Sun, J. Y. Gao, R. Zhu, J. Xu, L. Chen, J. M. Zhang, J Chem Phys 132 (2010) 124705.

[29] A. G. Nasibulin, S. Rackauskas, H. Jiang, Y. Tian, P. R. Mudimela, S. D. Shandakov, Nano Res 2 (2009) 373.

[30] R. M. Wang, Y. F. Chen, Y. Y. Fu, H. Zhang, C. Kisielowski, J Phys Chem B 109 (2005) 12245.

[31] X. G. Wen, S. H. Wang, Y. Ding, Z. L. Wang, S. H. Yang, J Phys Chem B 109 (2005) 215.

[32] L. Liao, Z. Zhang, B. Yan, Z. Zheng, Q. L. Bao, T. Wu, Nanotechnology 20 (2009)085203.

[33] Y. Y. Fu, J. Chen, J. Zhang, Chem Phys Lett 350 (2001) 491.

[34] X. C. Jiang, T. Herricks, Y. N. Xia, Nano Lett 2 (2002)1333.

[35] M. L. Zhong, D. C. Zeng, Z. W. Liu, H. Y. Yu, X. C. Zhong, W. Q. Qiu, Acta Mater 58 (2010) 5926.

[36] S. M. Arnold, S. E. Koonce, J Appl Phys 27 (1956) 964.

[37] J. A. Sartell, R. J. Stokes, S. H. Bendel, T. L. Johnson, C. H. Li, Trans Metall Soc AIME 215 (1959)

420.

[38] C. T. Hsieh, J. M. Chen, H. H. Lin, H. C. Shih, Appl Phys Lett 82 (2003) 3316.

[39] L. S. Huang, S. G. Yang, T. Li, B. X. Gu, Y. W. Du, Y. N. Lu, J Cryst Growth 260 (2004)130.

[40] Kofstad P. High temperature corrosion. New York: Elsevier Applied Science; 1988.

[41] R. A. Rapp, Metall Trans B 15B (1983)195.

[42] R. A. Rapp, Metall Mater Trans A 15A (1984)765.

[43] G. M. Raynaud and R. A. Rapp, Oxid Metals 21 (1984)89.

[44] D. A. Voss, E. P. Bulter, T. E. Michell, Metall Trans A 13A (1982) 929.

[45] A. M. Goncalves, L. C. Campos, A. S. Ferlauto, R. G. Lacerda, J Appl Phys 106 (2009) 34303.

[46] A. Kumar, A. K. Srivastava, P. Tiwari, R. V. Nandedkar, J Phys: Condens Matter 16 (2004) 8531.

[47] J. T. Chen, F. Zhang, J. Wang, G. A. Zhang, B. B. Miao, X. Y. Fan, J Alloys Compd 454 (2008) 268.

[48] C. H. Xu, C. H. Woo, S. Q. Shi, Chem Phys Lett 399 (2004) 62.

[49] M. Kaur, K. P. Muthe, S. K. Despande, S. Choudhury, J. B. Singh, N. Verma, J Cryst Growth 289 (2006) 570.

[50] K. Zhang, C. Rossl, C. Tenalleau, P. Alphonse, J. Y. Chane-Ching, Nanotechnology 19 (2007)

275607.

[51] N. Chopra, B. Hu, B. Hinds, J Mater Res 22 (2007) 2691.

[52] W. K. Appleby, R. F. Tylecote, Corros Sci 10 (1970) 325.

[53] F. Morin, J Mater Sci Lett 2 (1983) 383.

[54] H. E. Evans, Int J Mater Res 40 (1995)1.

[55] Y. Zhu, K. Mimura, M. Isshiki, Oxid Metals 62 (2004) 207.

[56] Y. F. Zhu, K. Mimura, M. Isshiki, Mater Trans 43 (2002) 2173.

[57] Z. Grzesik, M. Migdalska, Def Diffus Forum 429 (2009) 289.

[58] Y. F. Zhu, K. Mimura, J. W. Lim, M. Isshiki, Q. Jiang, Metall Mater Trans A 37A (2006) 1231.

[59] M. Komatsu, H. Mori, J Electron Microsc 54 (2005) 99.

[60] A. O. Musa, T. Akomolafe, M. J. Carter, Solar Energy Mater Solar Cells 51 (1998) 305.

[61] C. A. N. Fernando, P. H. C. de Silva, S. K. Wethasinha, I. M. Dharmadasa, T. Delsol, M. C. Simmonds, Renew Energy 26 (2002) 521.

[62] W. Siripala, A. Ivanovskaya, T. F. Jaramillo, S. H. Baeck, E. W. McFarland, Solar Energy Mater Solar Cells 77 (2003) 229.

[63] L. Zhou, S. Gunther, D. Moszynski, R. Imbihl, J Catal 235 (2005) 359.

[64] X. Q. Wang, J. A. Rodriguez, J. C. Hanson, D. Gamarra, A. Martinez-Arias, M. Fernandez-Garcia, J Phys Chem B 109 (2005)19595.

[65] J. B. Wang, D. H. Tsai, T. J. Huang, J Catal 208 (2002) 370.

[66] W. Liu, M. Flytzani-stephanopoulos, J Catal 153 (1995) 317.

[67] X. Q. Wang, J. C. Hanson, A. I. Frenkel, J. Y. Kim, J. A. Rodriguez, J Phys Chem B 108 (2004)13667.

[68] P. Poizot, S. Laruelle, S. Grugeon, L. Dupont, J. M. Tarascon, Nature 407 (2000) 496.

[69] S. T. Shishiyanu, T. S. Shishiyanu, O. L. Lupan, Sens Actuat B: Chem 113 (2006) 468.

[70] S. Pradhan, A. S. Reddy, R. N. Devi, S. Chilukuri, Catal Today 141 (2009)72.

[71] A. Horne, A. B. Hungria, P. Bera, A. L. Camara, M. Fernandez-Garcia, A. Martinez-Arias, J Am Chem Soc 132 (2010) 34.

Chapter – 2 Cross-sectional characterization of Cupric Oxide Nanowires

2.1 Introduction

Nanostructurd materials have attracted much scientific attention due to their interesting size-dependent chemical and physical properties and potential technological applications. One-dimensional (1D) nanostructures such as nanowires, nanobelts, nanorods, and nanotubes have become one focus of intensive research as a result of their unique properties and potential usages [1]. Nanowires and nanorods of various semiconductor materials including Si, Ge, GaN, ZnO etc, have been synthesized for different potential applications. Various growth techniques have been employed, including the vapor-liquid-solid growth [2], epitaxial growth [3], vapor-solid growth [4], wet chemical methods [5], and electrospinning [6]. For vapor-solid growth, it has been known since the 1950s that the oxidation of various metals, including Cu, Zn, Fe and Ta at intermediate temperatures results in a parallel oxide layering with high density oxide wires at the surface [7].

Nanowires, nanorods, nanowhiskers and nanosheets of CuO can be synthesized by thermal decomposition of CuC_2O_4 precursors [8], hydrothermal decomposition route [9], self-catalytic growth processes [10]. In addition, bulk CuO with a known band gap of 1.2 eV has an interesting monoclinic crystal structure belonging to the Mott insulator material class whose electronic structure cannot be described by conventional band theory [11]. There has been increasing interest in developing 1D

nanostructures of CuO for device applications such as high-critical-temperature superconductors [12], gas sensor [13, 14], magnetic storage media [15], nanodevices for catalysis [16-18] and field emitters [19]. Few studies of the growth of CuO nanowiers by thermal annealing of the copper foils in oxygen atmosphere have been reported [4]. In comparison to complex chemical methods, thermal annealing of copper foils provides simple, convenient and fast methods for synthesizing CuO nanowires. Thermal oxidation is becoming an increasingly attractive method for synthesizing the nanostructures. There were many literatures which have discussed the hypothesis of the layering structure of copper oxidation. It is reported that the nanowires present in CuO phase which possibly grow on the surface of a $CuO/Cu_2O/Cu$ multilayer structure according to X-ray diffraction (XRD) analysis investigation [20]. The nanowires formed on the surface of the scale should be CuO phase according to thermodynamics analysis [21]. A copper foil is heated in air at 500 °C for 4 h, and XRD pattern shows that the majority of this copper foil converted into Cu_2O, with only a small amount of CuO on the surface in the form of nanowiers [4]. But there are no literatures that are reported for determining the cross-section of the nanowires on substrate.

The present work reports the preparation of CuO nanowires through heating copper foils in air at various temperatures. The morphology of the nanowires depends on the preparation conditions. To investigate the layering structures of the oxidized substrate, cross-sectional characterizations of energy dispersive X-ray spectroscopy (EDX) were performed. The EDX measurements indicate that the CuO nanowires are grown on the CuO/Cu_2O layer, which is formed on the surface of Cu foil. The thermal annealing of the copper is demonstrated to be a convenient route to produce CuO nanowires.

2.2 Experimental procedure

CuO nanowires were synthesized by using the thermal oxidation method [4]. Figure 2.1 shows

the schematic diagram of the experimental setup for oxidation in atmospheric air. Copper foils (0.1 mm

thick, 4N) were used as substrates. The copper foils were cut into standard sizes of 1cm×1cm. The

substrates were first cleaned in dilute nitric acid to remove the native oxide layer and adsorbed impurities,

and then they were cleaned with acetone, methanol, and deionized water under an ultrasonic bath for

5min. Finally, they were dried by N_2 flow. The cleaned Cu substrate was placed inside an electric box

furnace (KOYO, KBF – 828N). The oxidation was carried out at 300 – 800 °C in static air.
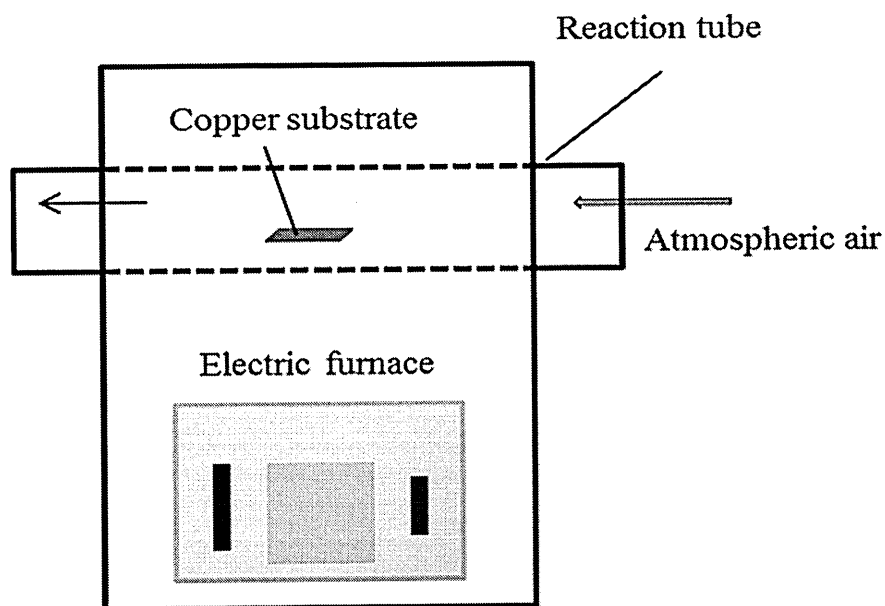
Figure 2.1 Schematic representation of the experimental setup.

The crystal structure and phase composition were identified by XRD, (Rigaku RINT-2100) using a 40 kV,

30 mA, Cu-Kα X-ray. A scanning step of degree of 0.02^0 was applied to record the XRD patterns in the

2θ range of degree of 25 - 65^0. The morphology of the CuO nanowires were characterized by scanning

electron microscope (SEM, Hitachi S-3000H) operated at 15 kV. The cross-sectional characterizations

were performed by field emission scanning electron microscopy (FE-SEM, JEOL JSM7001FF) equipped

with an EDX (THERMO SCIENTIFIC NSS). Transmission electron microscopy (TEM) observation and

electron diffraction investigation were carried out using a JEOL JEM-4000 EXII.

2.3 Results and discussions

2.3.1 Growth of CuO nanowires by thermal oxidation method

2.3.1.1 Annealing temperature dependence of CuO nanowires

In order to study the influence of the heating temperature on the growth of CuO nanowires, six

samples have been prepared at the temperatures of 300, 400, 500, 600, 700 and 800 °C for 2 h, as shown

in Figure 2.2. The round oxide grains with diameters of about 450 nm are observed after oxidation at

300 °C, without nanowires on the surface of the specimen (Figure 2.2A). From the morphology of the

samples, it is observed that nanowires formed at 400 °C are very small and the orientation of the

nanowires is not conformed. Figure 2.2(B) shows the morphologies of oxide scales formed at 400 °C,

showing a high density of uniformly curved nanowires. After 2 h of heating at 500 °C, nanowire with a

high density (but non - uniform size) is formed. In this process, the longer nanowires can be formed,

which are larger than that of 400 °C, with length ranging from 2 to 15μm and diameter from 100 to 250

nm as shown in Figure 2.2(C). In Figure 2.2(D) a large amount of nanowires, which have a high density,

was observed in the samples prepared at 600 °C with length of 3 to 10μm and diameter of the nanowires

about 350 nm. In comparison with the nanowires formed at 500 °C, the nanowires formed at 600 °C are

more straightly. The diameter of the nanowires synthesized at 700 °C is about 500 nm. A consistent

decreasing in the number of density of nanowires is observed in Figure 2.2(E), while only few of nanowires are observed. Nanowires are always nearly unidirectional and are almost perpendicular to the surface of the substrate. Figure 2.2(F) shows large oxide grains, which were formed during oxidation at 800 °C. The morphologies of CuO nanowires change, from curved to straight, as the oxidation temperature increases from 400 to 700 °C. This is due to the difference of diameter of the nanowires.
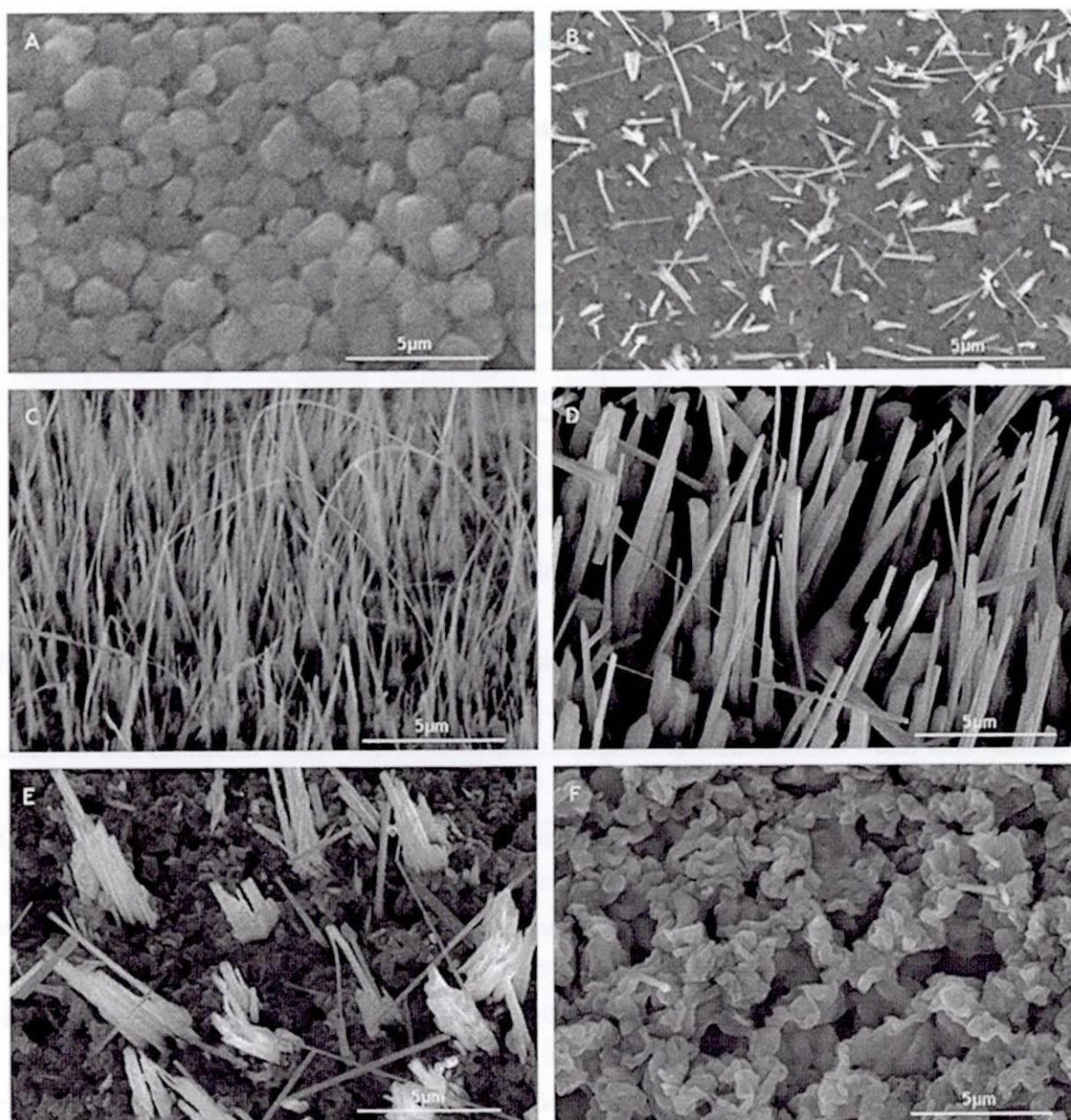
Figure 2.2 SEM images of CuO nanowires by directly heating of copper foils in air at (A) 300, (B) 400, (C) 500, (D) 600, (E) 700 and (F) 800 °C for 2 h.
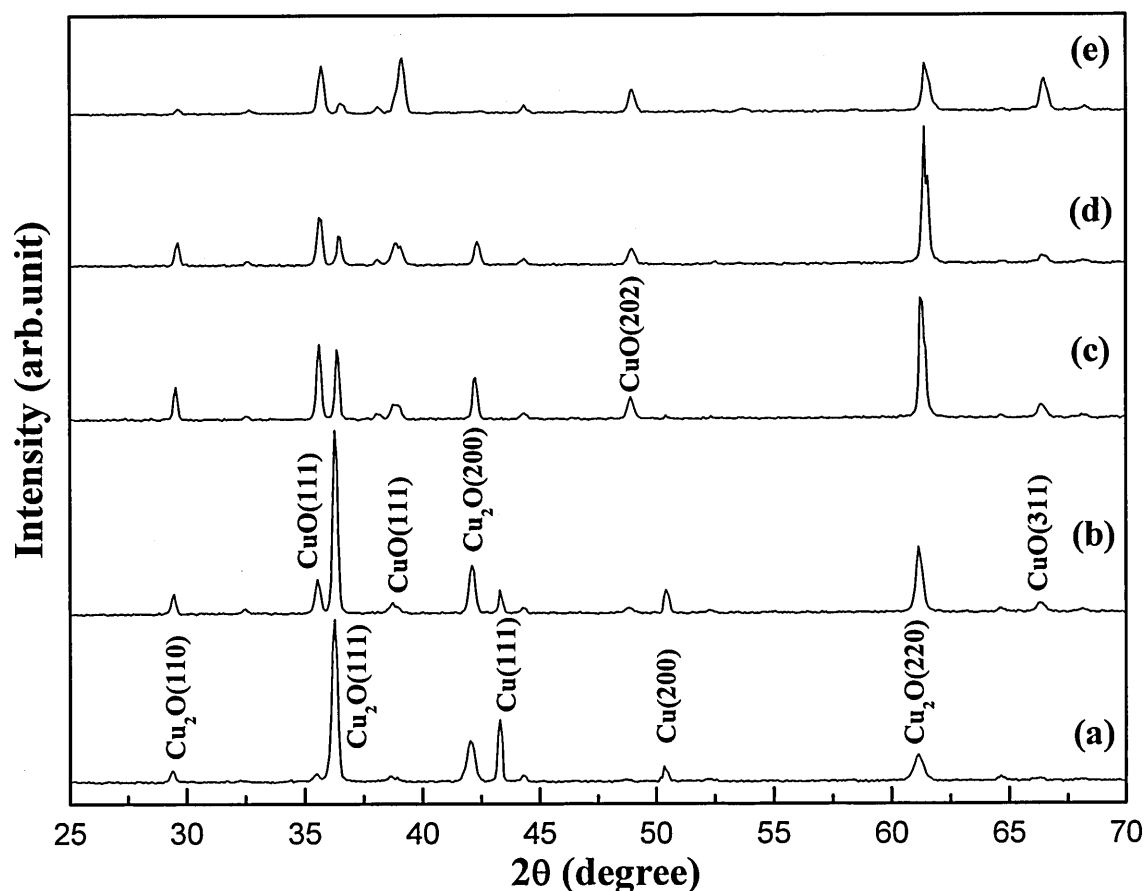
Figure 2.3 XRD patterns of CuO nanowires with heating in air at (a) 400, (b) 500, (C) 600, (d) 700, and (e) 800 °C for 2 h.

Figure 2.3 shows the XRD patterns of the samples after oxidation at 400, 500, 600, 700, and 800 °C for 2 h. The XRD results show that Cu_2O is the main oxidation products with a small amount of CuO after the oxidation at 400 and 500 °C. XRD peak at $2\theta = 36.3°$corresponding to (111) plane of cubic Cu_2O structure is the most prominent peak. The weak two peaks at $2\theta = 35.5°$and $2\theta = 38.7°$ can be readily indexed as ($\bar{1}$ 11) and (111) crystal plane of monoclinic CuO. Copper is sufficient for oxidizing to Cu_2O at the temperature up to 600 °C. However, in the case of annealing at 700 °C most of copper phases were oxidized, and the cupric oxide became the main oxidation product. This indicates a conversion from

Cu_2O to CuO, and this is also confirmed by the fact that the colors of the samples changed from brick red

(Cu_2O) to black (CuO). These two peaks become strong with increasing the annealing temperature. But

(111) plane of Cu_2O becomes weak while CuO is formed through a second step of oxidation of Cu_2O.

Other weak peaks corresponding to Cu_2O and CuO phases have also been observed. When the

temperature rose to 800 °C, CuO became the main oxidation product with a small Cu_2O peak. We have

checked the sample with annealing temperature at 300 for 2 h. CuO peak is not found, and only Cu_2O and

Cu were observed. This result reveals that the growth planes of the nanowires are along the ($\bar{1}$ 11) and

(111) planes which increase with the temperature, and the copper forms two thermodynamically stable

oxides, CuO and Cu_2O, in the reaction with molecular oxygen. The oxide consists of either Cu_2O or CuO,

depending on the oxidation temperature.

Figure 2.4 presents Raman spectra of the as-prepared products. CuO belongs to the C_{2h}^6 space

group with two molecules per primitive cell. One can find for the zone center normal modes:

$$\Gamma = 4\,Au + 5\,Bu + Ag + 2\,Bg$$

These are three acoustic modes (Au + 2Bu), six infrared active modes (3Au + 3Bu), and three Raman

active modes (Ag + 2Bg). As Figure 2.4 shown, three Raman peaks at 621.4, 339.8 and 295.4 Cm^{-1}

were observed, with first one being broad and the second one being weakest. In comparison with the

vibration spectra of a CuO single crystal [22], the peak at 295.4 cm^{-1} is assigned to the Ag mode and the

peak at 339.8 and 621.4 cm^{-1} to the Bg modes. The results are in agreement with the literature reference

value for nanocrystal CuO [23].
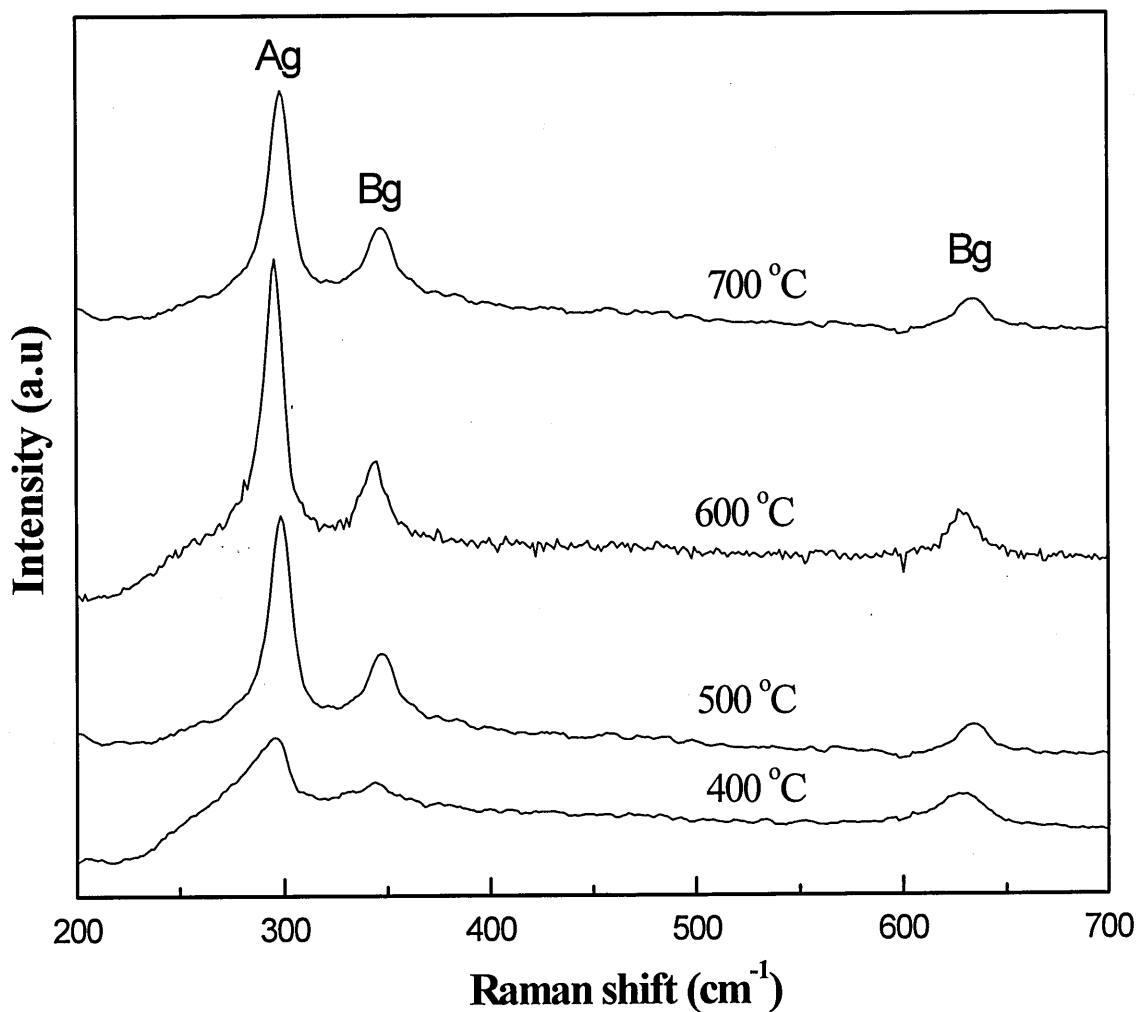
Figure 2.4 Raman spectra of the as-prepared CuO nanowires

2.3.1.2 Annealing time dependence of CuO nanowires

In order to study the influence of the evaporation times on the growth of CuO nanowires, four

samples have been prepared with different annealing time at 600 °C. Figure 2.5 shows the annealing time

affects the length of the nanowires. The longtime of annealing, the longer length of the nanowires will be.

From the SEM measurements, 3-10 μm long nanowires can be formed after 2 h of annealing. The lengths

of the nanowires are about 10, 15 and 25 μm for the annealing and time of 4, 6 and 12 h, respectively.

However, the average diameter of the nanowires is found to be the same, irrespective of the time of annealing. Thus, annealing time does not seem to have an effect on the average diameter of the nanowires and affects only their length, the longer the time of thermal annealing, the longer the nanowires. Moreover, it is also evident from Figure 2.5(a) – (d) that the number density of nanowires is also almost independent of the annealing time.
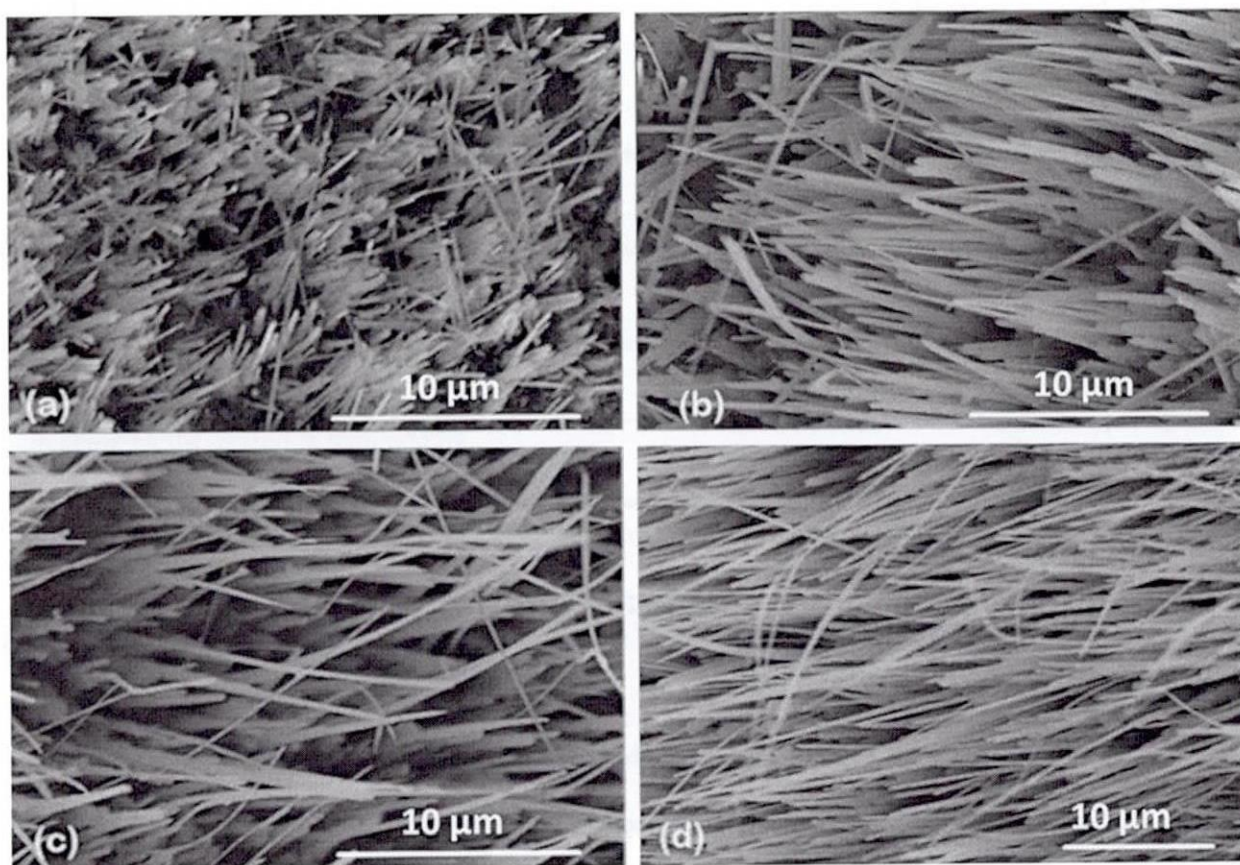
Figure 2.5 SEM morphologies of CuO nanowires prepared at 600 °C for different times (a) 2 h, (b) 4 h, (c) 6 h and (d) 12 h.

Figure 2.6 shows the XRD pattern of films were annealed at 600 °C in air for 2, 4, 6 and 12 h respectively. With an increase in oxidation times, the peak at $2\theta = 32.5°$ d = 0.274 nm corresponded to (110) plane of monoclinic CuO, the cupric oxide diffraction peaks become more intense and sharper, which suggests that the nanowires size becomes larger and the crystal quality has improved. This result

reveals that the growth planes of the nanowires are along the ($\bar{1}$ 11) and (111) planes with increase the

temperature, and along the (110) plane with increase the time.
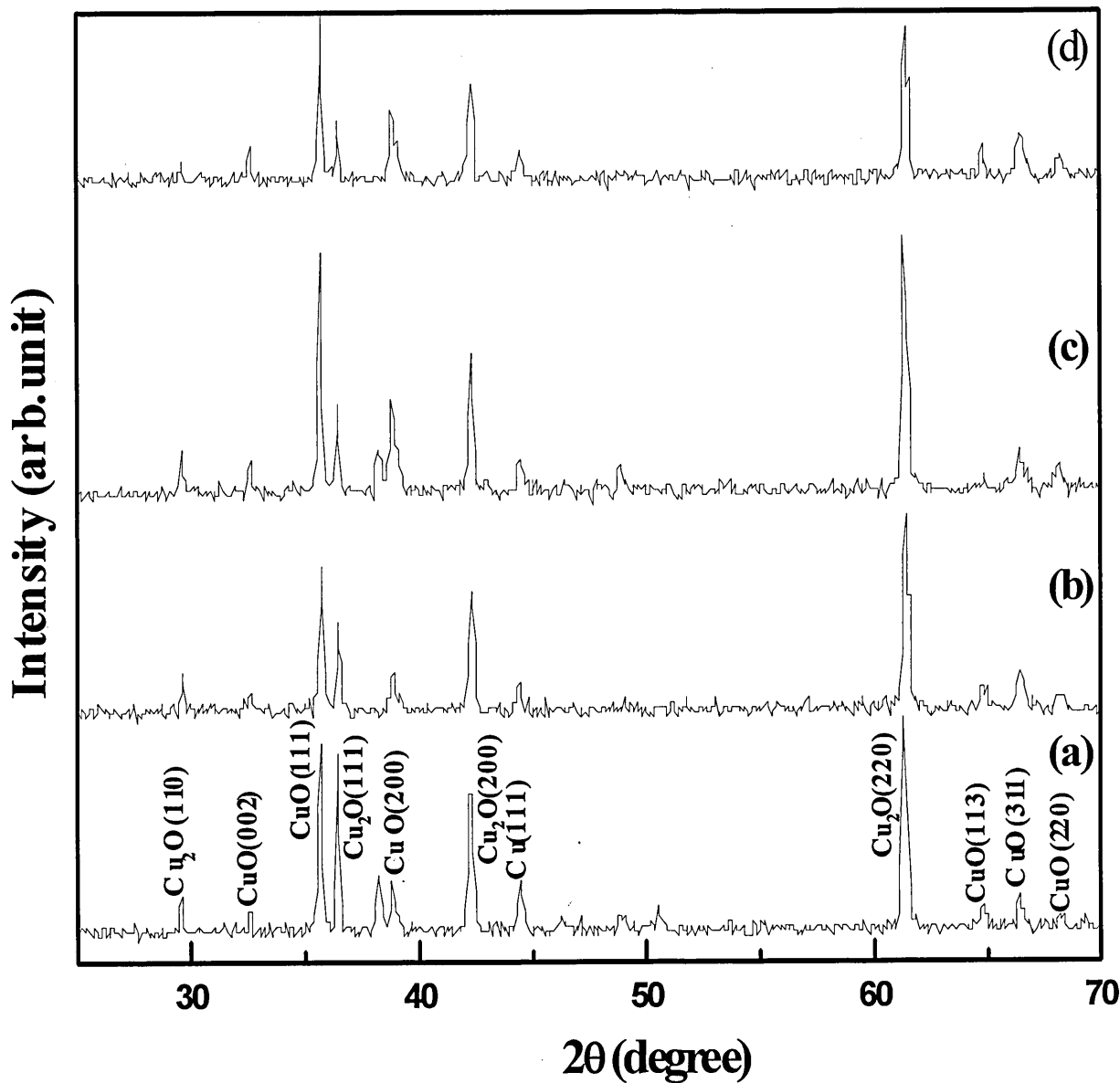
Figure 2.6 XRD morphologies of CuO nanowires prepared at 600 °C for different times (a) 2 h, (b) 4 h, (c) 6 h and (d) 12 h.

2.3.1.3 Diameter distribution and aspect of CuO nanowires

In Figure 2.7 (a)-(b), the average diameter and aspect ratio of CuO nanowires are plotted as

annealing temperature and annealing time. From these two figures, it is clear that the diameter of the nanowires increases monotonically with annealing temperature. Moreover, under similar conditions of annealing time, there is an optimum value of temperature at which the aspect ratio of the nanowires is the maximum. For example, we find that the optimum temperature is 400 °C for 2 h. Thus, it is apparent that while nanowires of different diameter can be synthesized with high number density by varying the annealing temperature which is conducive for the creation of nanowires can be achieved by increasing the annealing time (Figure 2. 7 (b)).

In order to obtain an estimate of the dispersion in the diameter of nanowires, we plot the percentage of nanowires with different diameter synthesized by thermal annealing at 600 °C for 2, 4, 6 and 12 h in Figure 2.8 (a)-(d), respectively. Although the mean diameter of the nanowires are almost same for the four annealing times, the dispersion in the diameter of the nanowires is considerably less for the annealing time of 12 h compared to that for the annealing time of 2 h, 4 h and 6 h. At 12 h of annealing time, almost 65 % of the nanowires have their diameter in the narrow range of 400 nm. The standard deviation in the diameter of thenanowires at these four annealing times is found to be 4.6, 6.5, 8.5 and 11.2 nm for 2 h, 4 h, 6 h and 12 h, respectively. The observed standard deviation of 4.6 nm for nanowires with a mean diameter of 350 nm is thus comparable with these results, indicating that it may be possible to further narrow down the distribution in diameter by annealing for longer time periods.
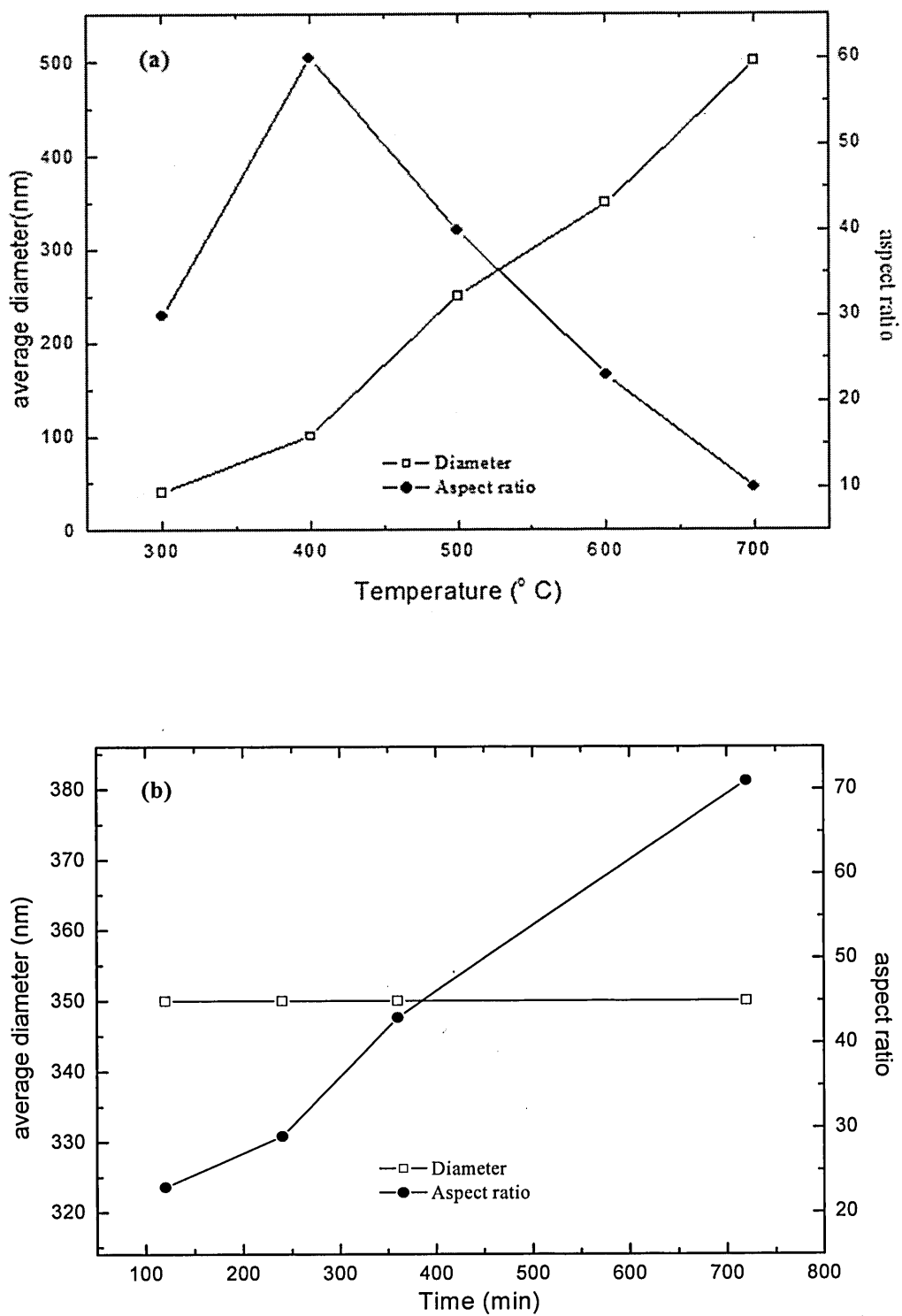
Figure 2.7 The effect of the different growth conditions, namely, (a) Annealing temperature (b) Annealing time on the diameter and aspect ratio of CuO nanowires.
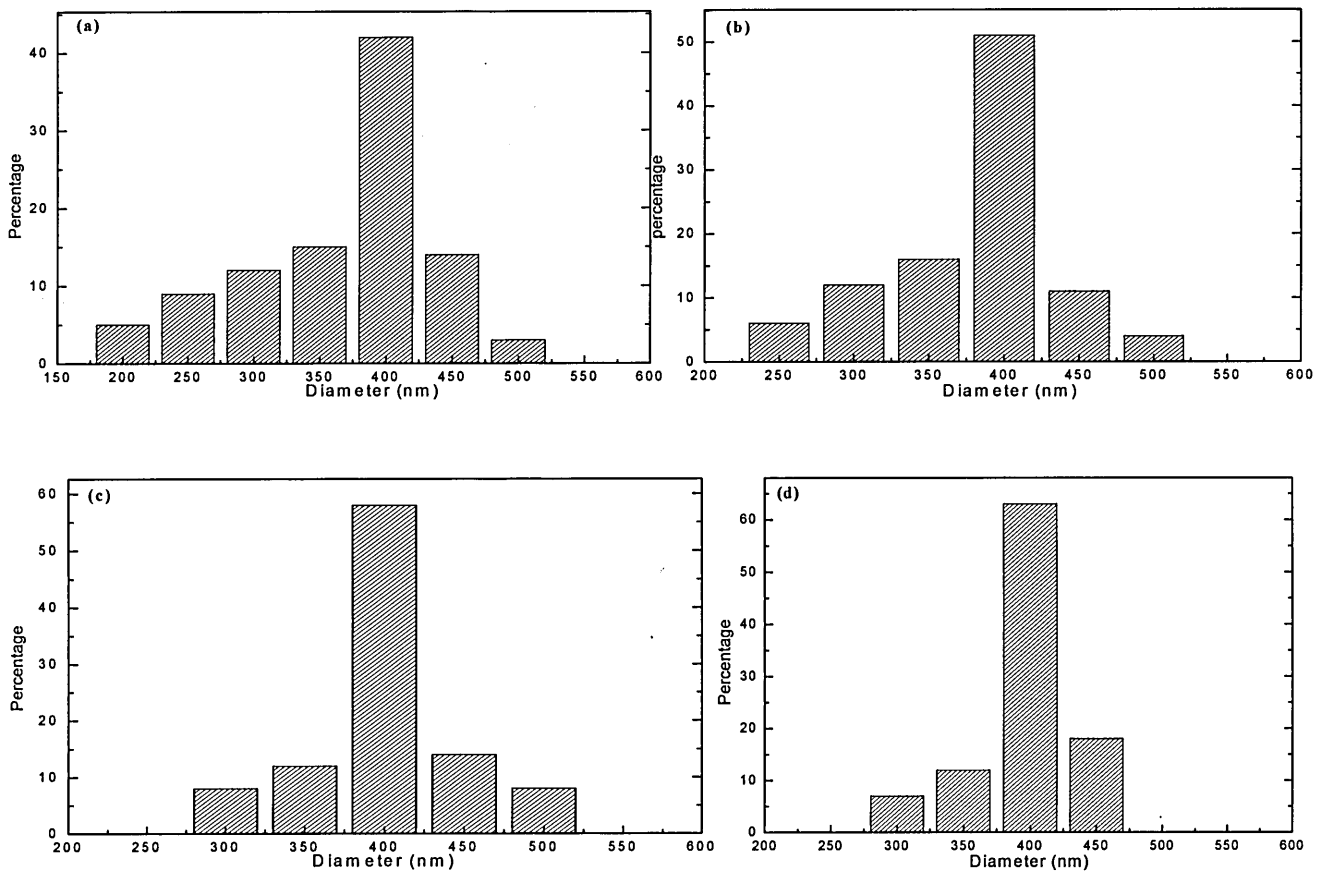
Figure 2.8 The dispersion in the diameter of the nanowires prepared under annealing temperature 600 °C for annealing time of (a) 2 h (b) 4 h (c) 6 h and (d) 12 h.

2.3.2 Cross sectional characterization of CuO nanowire samples by FE-SEM and EDX

Our results indicate that the growth of CuO nanowire is performed only at 400 – 700 °C. If the oxidation temperature is too high or too low, nanowires cannot be obtained, even though the CuO phase exists. Figure 2.3 indicates the presence of both Cu_2O and CuO in this temperature range. However, no information on the individual layer composition can be extracted. The theoretical layering composition has been discussed in the reference [21] with CuO, as nanowires and intermediate layer, and Cu_2O, as the

bottom layer. The theoretical hypothesis on the nanowires will be proved by our experiments.
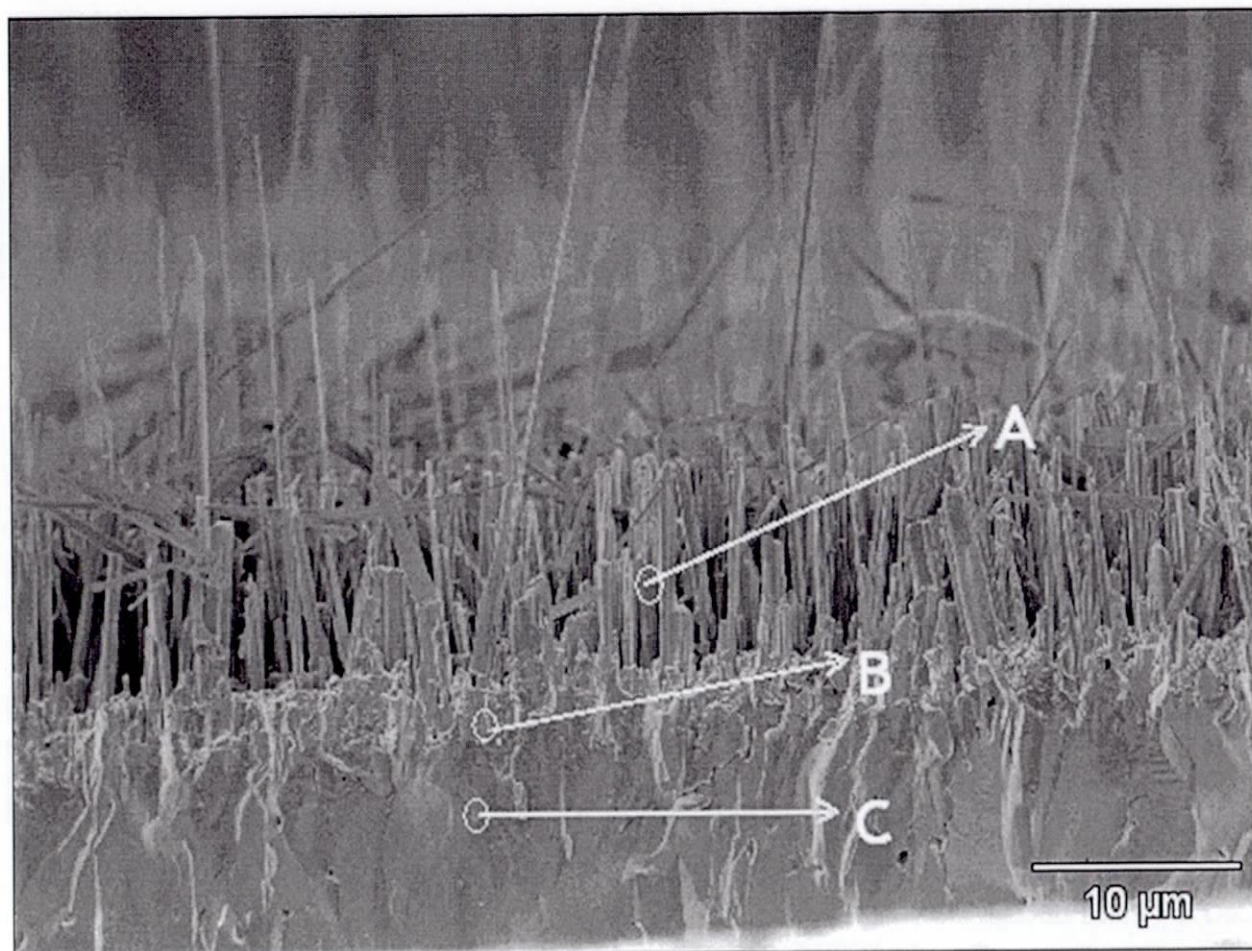
Figure 2.9FE-SEM cross-section images of CuO nanowires heated at 500 °C for 2 h.

The FE-SEM cross-section image of nanowires heated at 500 °C is shown in Figure 2.9. Three layers are

observed in copper substrate. The bottom layer is a thick layer that lies directly above the copper substrate,

an intermediate layer that the nanowires grow from, and a top nanowire; (C), (B), and (A) in Figure 2.9,

respectively. To confirm the rest of the layering composition, we measured EDX at each layers. EDX

spectra were obtained from the top layer, intermediate layer and the bottom layer of an oxide on copper

substrate shown in Figure 2.10 (A), (B) and (C), respectively. In addition, EDX spectra were produced

from compacted CuO (3Ns) and Cu_2O (2Ns) powder of standard samples. The resulting spectra are

presented in Figure 2.10 (D), (E), respectively. The spectra were taken at identical parameters of 3 KeV and with a 34.5 degree sample tilt. Regions of 0.40 – 0.60 keV and 0.62 – 1.08 keV were created about the O K and Cu L peaks, respectively. The results indicate that the atomic ratio of copper and oxygen taken from the top of nanowires and intermediate layer (B) in Figure 2.9 matches with that of the standard CuO. Likewise, the atomic ratio of copper and oxygen taken from the bottom of the layer (C) in Figure 2.9 matches that of the standard Cu_2O. Our experimental results, which indicate distinct oxide layers directly, agree with the theoretical speculation [21] of the bottom layer of Cu_2O and the intermediate layer of CuO. The topmost layer is always of CuO if the oxide consists of both Cu_2O and CuO. The fractional thickness of the CuO topmost layer in this bi-layer oxide scale mainly depends on the annealing temperature. When copper foil is oxidized in air, at first, the major product is Cu_2O, and it is expected that CuO is formed through a second step of oxidation of Cu_2O. In this case, Cu_2O serves as a precursor to CuO. Eshelby earlier suggested that the stress-induced mechanism is the growth mechanism for whiskers [24]. The energy required to form fresh surface was provided by interaction of metal with atmosphere. Kumar et al reported that the mechanism of nanowires growing in this case is due to relaxation of stress [25]. Oxidation leads to stress in the foil, and it is maybe expected that substantial stress exists on the CuO and Cu_2O interface or phase boundaries, which are different in their crystallographic structures, molar volumes and densities. The stress also exists on the Cu_2O and Cu interface. But due to the difference in thermal expansion coefficient between Cu (1.7×10^{-5} °C^{-1}) and Cu_2O (1.9×10^{-6} °C^{-1}), the metal substrate at higher temperatures becomes more ductile which provides a mechanical mechanism for

stress relaxation with increasing temperature.
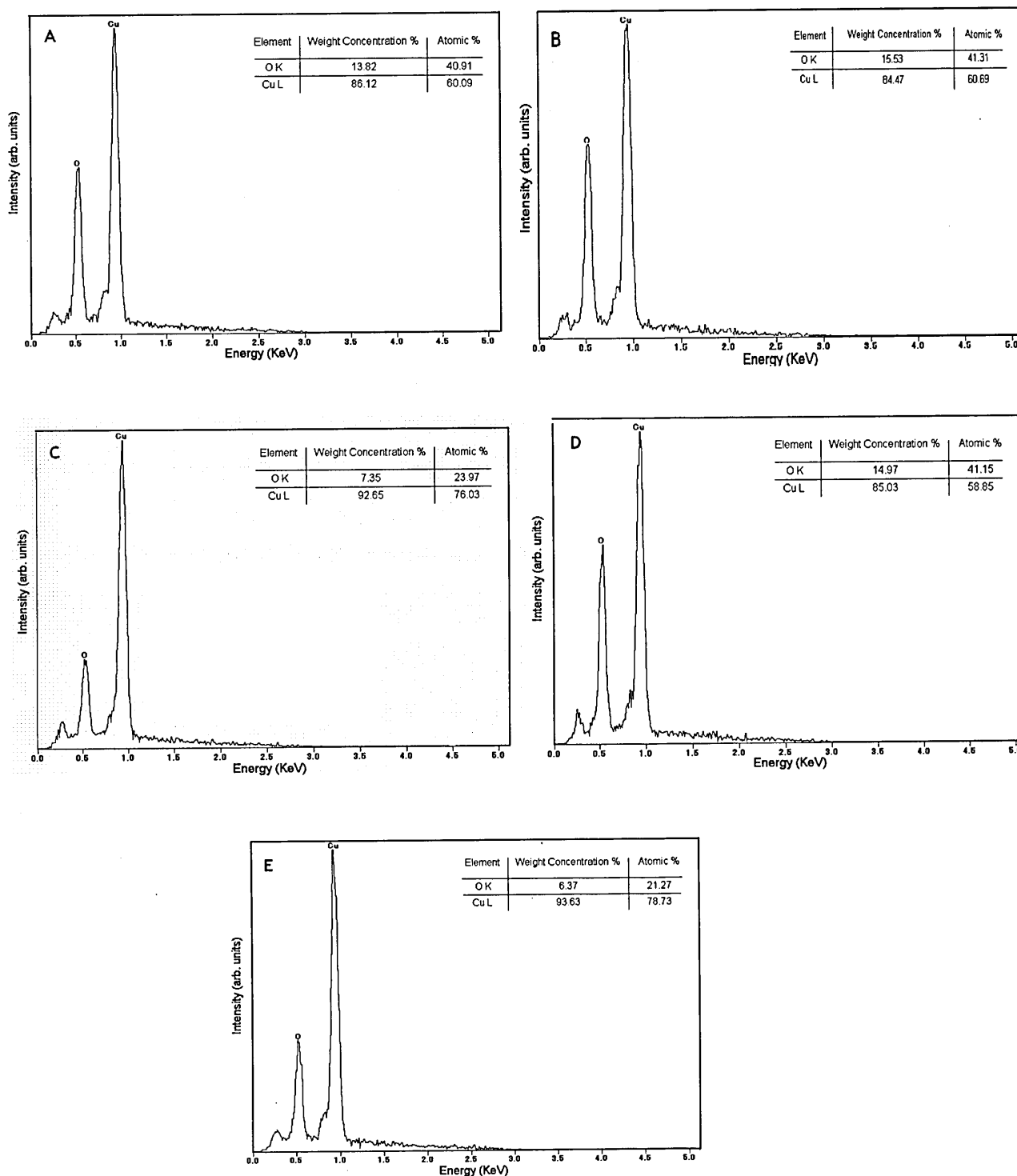
Figure 2.10 EDX spectra of (A) top of the oxide nanowires, (B) intermediate oxide layer, (C) bottom oxide layer, (D) CuO standard sample, and (E) Cu_2O standard sample.

The lattice mismatch becomes smaller, and this lattice mismatch induced stress becomes smaller too. So

this could explain that the nanowires do not grow during oxidation of Cu_2O. CuO is different of metal

copper with no more ductile and no bigger thermal expansion coefficient. Cu_2O oxidizing to CuO leads to

stress on the interface due to volume and structural change. The oxidation process continues through the

surface diffusion of oxygen. The growth of nanowires occurs to reduce the stress generated during

oxidation of copper. So we believe that growth of CuO nanowires may be described by strees relaxation

model.
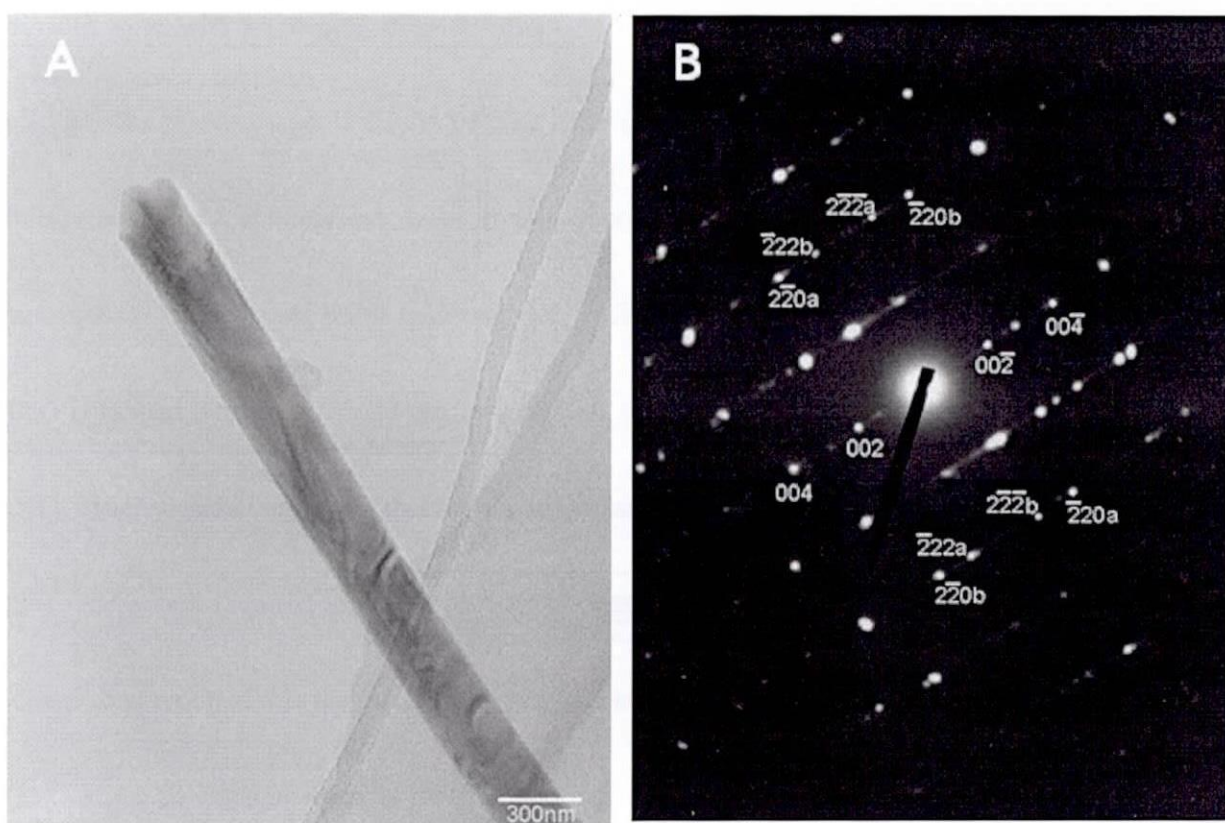
Figure 2.11 (A) TEM image of a single CuO nanowire prepared at 500 °C for 2 h. (B) SAD pattern from a single CuO nanowire. Indices with subscript a refer to a single crystal of a nanowire, and indices with subscript b refer to the other single crystal of a nanowire.

2.3.3 TEM characterization of CuO nanowires

We further characterized the size, structure, and crystal of these nanowires using TEM and

selected area diffraction (SAD) pattern. The used sample was prepared at 500 °C for 2 h. The TEM image

of the CuO nanowiers is shown in Figure 2.11 (A). It can be seen that the products have wire-like shapes

and smooth surfaces with the diameter of about 250 nm. Figure 2.11 (B) shows a diffraction pattern that

would be typically observed when the electron beam was focused on an individual nanowire along the

[110] direction. The mirror-image relationship between the two sets of diffraction spots confirmed the

formation of a bi-crystalline structure within each nanowire. The relevant SAD pattern includes two sets

of diffraction spots as shown in Figure 2.11 (B), where each set diffraction spot is a single crystal which

corresponds to the monoclinic structure of CuO with the lattice constants, $a = 0.469$ nm, $b = 0.343$ nm, c

$= 0.513$ nm, and $\beta = 99.55°$.

2.4 Conclusion

Large scale cupric oxide nanowires have been prepared by thermal oxidation methode, the thermal oxidation conditions can affect the formation of the nanowires. At low temperature, nanowires with small diameter can be formed. CuO anowires with diameter between 50 and 500 nm and lengths between 1 and 25 μm can be obtained by oxidizing copper foil in air at temperature between 400 and 800 °C. Increasing the oxidation temperature may produce a reduction in the density, but increase in the diameter and strength of the nanowires, causing them to adopt a straight morphology. It is observed that the aspect ratio and number density of these nanowires are critical functions of various growth parameters, namely, the annealing time and the annealing temperature. While the annealing temperature affect both the aspect ratio and number density, the main effect of the annealing time is on the aspect ratio of these nanowires. After heating, the color of the copper foil turned black. It was found that the black products were CuO. Analyses on the oxidized substrates indicated that the growth process began with the formation of thin layer of Cu_2O, then thick layer of CuO, and finally CuO nanowiers. Moreover, from TEM analysis, the CuO nanowires exhibited bi-crystalline property with monoclinic structure.

References

[1] Y. Xia, P. Yang, Y. Sun, Y. Wu, B. Mayers, B. Gates, Y. Yin, F. Kim and H. Yan, Adv. Mater 15 (2003) 353.

[2] R. S. Wagner, W. C. Ellis, Appl. Phys. Lett 4 (1964) 89.

[3] C. Y. Gyu, W. Chunrui and I. P. Won, Semicond. Sci. Technol 20 (2005) 22.

[4] X. Jiang, T. Herricks, Y. N. Xia, Nano Letters,vol. 2, no. 12 (2002) 1333.

[5] A. Sambandam, X. Wen and S. Yang, Mater Chem and Phys 93 (2005) 35.

[6] H. Wu, D. Lin, and W. Pan, Applied Physics Letters, vol. 89, no. 13 (2006) 133125.

[7] K. Hauffe, Oxidation of Metals, Plenum Press, New York, NY, USA, 1965.

[8] F. Lanza, R. Feduzi, J. Fuger, J. Mater. Res. 5 (1990) 1739.

[9] D. Chen, G. Shen, K. Tang, Y. Qian, J. Crystal Growth 254 (2003)225.

[10] M. Cao, C.-T. Hsieh, J.-M. Chen, H.-H. Lin, H.-C. Shih, Appl. Phys.Lett. 82 (2003) 3316.

[11] P. A. Cox, Transition Metal Oxides: An Introduction to Their Electronic Structure and

Properties, Oxford University Press,New York, NY, USA, 20 (1992) 296.

[12] K.-H. Muller, High-Tc Superconductors and Related Materials, Kluwer Academic,

Dordrecht, The Netherlands, 86 (2001).

[13] A. Cruccolini, R. Narducci, R. Palombari, Sensors Actuators B 98 (2004) 227.

[14] V.R. Katti, A.K. Debnath, K.P. Muthe, M. Kaur, A.K. Dua, S.C. Gadkari, S.K. Gupta, V.C.

Sahni, Sensors Actuators B 96 (2003) 245.

[15] H. Fan, L. Yang, W. Hua, X. Wu, Z. Wu, S. Xie, B. Zou, Nanotechnology 15 (2004) 37.

[16] A. Santos, P. Yustos, A. Quintanilla, G. Ruiz, F. Garcia-Ochoa, Appl. Catal. B 61 (2005) 323.

[17] A.A. Ponce, K.J. Klabunde, J. Mol. Catal. A 225 (2005) 1.

[18] G. Larsen, S. Noriega, Appl. Catal. A 278 (2004) 73.

[19] C.T. Hsieh, J. M. Chen, H. H. Lin, H. C. Shih, Appl. Phys. Letter 83 (2003) 3383.

[20] L.S. Huang, S.G. Yang, T. Li, B.X. Gu, Y.W. Du, Y.N. Lu and S.Z. Shi, Journal of Crystal

Growth 260 (2004) 130.

[21] C.H.Xu, C.H.Woo, S.Q.Shi, Chemical Physics Letters 399 (2004) 62.

[22] J.C. Irwin, J. Chrzanowshi, T. Wei, Phys. C 166 (1990) 456.

[23] J.F. Xu, W. Ji, X.. Shen, S.H. Tang, J. Solid State Chem. 147 (1999) 516.

[24] J.D. Eshelby, Phys. Rev. 91 (1953) 755.

[25] A. Kumer, A.K. Srivastava, P. Tivari, R.V. Nandedkar, J. Phys. Condens. Matter 16 (2003) 8531.

Chapter – 3 Synthesis of highly-aligned cupric oxide nanowires

3.1 Introduction

Nanostructured materials have attracted much scientific attention due to their interesting size-dependent chemical and physical properties and potential technological applications. One-dimensional (1D) nanostructures such as nanowires, nanobelts, nanorods, and nanotubes have become one focus of intensive research as a result of their unique properties and potential usages [1]. Nanowires and nanorods of various semiconductor materials including Si, Ge, GaN, ZnO etc, have been the focus of intense studies in the past years. Different approaches, such as vapor-liquid-solid [2], vapor-solid [1] and template mediated [3] growth methods, have been used for the preparation of these 1D nanostructures.

Cupric oxide (CuO) with a known band gap of 1.2 eV has an interesting monoclinic crystal structure belonging to the Mott insulator material class whose electronic structure cannot be described by conventional band theory [4]. There has been increasing interest in developing 1D nanostructures of CuO for device applications such as gas sensor [5, 6], magnetic storage media [7], catalysts [8-10] and field emitters [11]. During the last couple of years 1D nanowires, nanorods, nanowhiskers and nanosheets of CuO have been synthesized by various growth techniques such as thermal decomposition of CuC_2O_4 precursors [12], hydrothermal decomposition route [13], self-catalytic growth processes [14] etc. One of the crucial factors in the synthesis of 1D nanostructure is the control of composition, size and crystallinity.

Moreover, from the point of view of studies of their fundamental properties as well as their applications, the method of preparation of the 1D nanostructures should be simple for producing bulk quantities and amenable to control of diameter and length. In comparison to complex chemical methods, thermal annealing of copper foils provides simple, convenient and fast methods for synthesizing CuO nanowires. Thermal oxidation is becoming an increasingly attractive method for synthesizing the nanostructures. Many studies of the growth of CuO nanowiers by thermal annealing of the copper foils in oxygen atmosphere have been reported [15-26]. Recent studies on CuO nanowires have focused on the influence of temperature, growth time and oxidative environment on the growth rate, size distribution and areal density of CuO nanowires [11, 22]. It has been shown that the growth time can be used to control nanowires length distribution [11], the growth temperature can be used to control the nanowires diameter distribution, and the O_2 and H_2O partial pressures strongly affect the nanowies areal density [22]. The surface condition of the copper substrate was also shown to significantly affect the nanowires growth [14, 16]. The growth of long, high density and aligned cupric oxide nanowires have rarely been reported in the literature. According to previous investigations, it seems very difficult to grow uniform and aligned vertical cupric oxide nanowires from pure metal thin films just by thermal oxidation and the very few approaches are reported in the literature for growing uniform and aligned vertical cupric oxide nanowires on the copper substrate. In this study, we report a simple process for growing high density, uniform and vertical aligned cupric oxide nanowires by thermal oxidation. We have investigated the effects of the grain size of copper substrate, orientation of grains and surface roughness of substrates on the growth of

cupric oxide nanowires. The nanowiers are characterized using scanning electron microscopy (SEM) transmission electron microscopy (TEM) and X-ray diffraction (XRD).

3.2 Experimental procedure

In order to investigate the effects of the grain size and orientation of copper substrates on the formation of cupric oxide nanowire during thermal oxidation, four copper foils (prepared by purchase) were used as substrates. Figure 2.1 shows the schematic diagram of the experimental setup for oxidation in cylinder air. The copper foils were cut into standard sizes of 1cm × 1cm. The substrates were cleaned in dilute hydrochloric acid to remove the native oxide layer and adsorbed impurities firstly, and then cleaned with acetone, methanol, and deionized water under an ultrasonic bath for 5min. Finally, they were dried by N_2 flow. The cleaned samples were placed onto a quartz boat. The quartz boat positioned in the center of a quartz tube was mounted in the middle of a horizontal tube furnace. The air gas was employed for the oxidation of copper foils. A flow of air gas firstly introduced into the quartz tube at a flow rate of 1 L/min for 20 min to remove air from the system, and then it was adjusted to 0.5 L/min. The tube furnace was heated to the set-point temperature (300, 400, 500 and 600°C in atmospheric pressure). After holding in the set-point temperature, the air gas flow was stopped and the N_2 gas flow was employed at a rate of 1L/min. The tube furnace was allowed to cool naturally to room temperature to prevent the thin film from cracking and further oxidation, caused by thermal stress and the atmospheric air if the film was directly taken out of the high temperature furnace. The substrate was pulled out of the furnace for further analysis. The crystal structure and phase composition were identified by X-ray diffraction (XRD, Rigaku

RINT-2100) using a 40 kV, 30 mA, Cu-Kα X-ray. A scanning step of degree of 0.02° was applied to

record the XRD patterns in the 2θ range of degree of 40 - 55°. The morphology of the CuO nanowires

were characterized by scanning electron microscope (SEM, Hitachi S-3000H) operated at 15 kV.

Transmission electron microscopy (TEM) observation and electron diffraction investigation were carried

out using a JEOL JEM-4000 EXII.

3.3 Results and discussion

3.3.1 Effect of crystallite size

In order to know the crystal structure and the corresponding grain size of copper foils, X-ray

diffraction was performed immediately after substrate cleaning. There are a set of Bragg peaks in the

XRD that could readily be indexed to the *fcc* structure of metal copper (Fm$\bar{3}$m, a = 3.615 Å, JCPDF no.

85-1326) (figure 3.1). The diffraction profiles of the copper foil A, C and B, D show very distinctive

features. In figure 3.1 there are two peaks on the copper foil A and C at *2θ* = 50.50° and *2θ* = 43.36°

corresponding to (200) plane and (111) plane of copper structures. Compared with the XRD pattern of the

copper foil A and C, only the peak at *2θ* = 50.50° corresponding to (200) reflection of the crystals in the

sample B and D appeared. Such a feature indicates that copper crystals in the sample B and D are

predominantly oriented with their a-axes perpendicular to the support surface. The average grain size can

be calculated using the Scherrer equation [22]:

$$D = \frac{0.9\,\lambda}{W\cos\theta} \qquad (3.1)$$
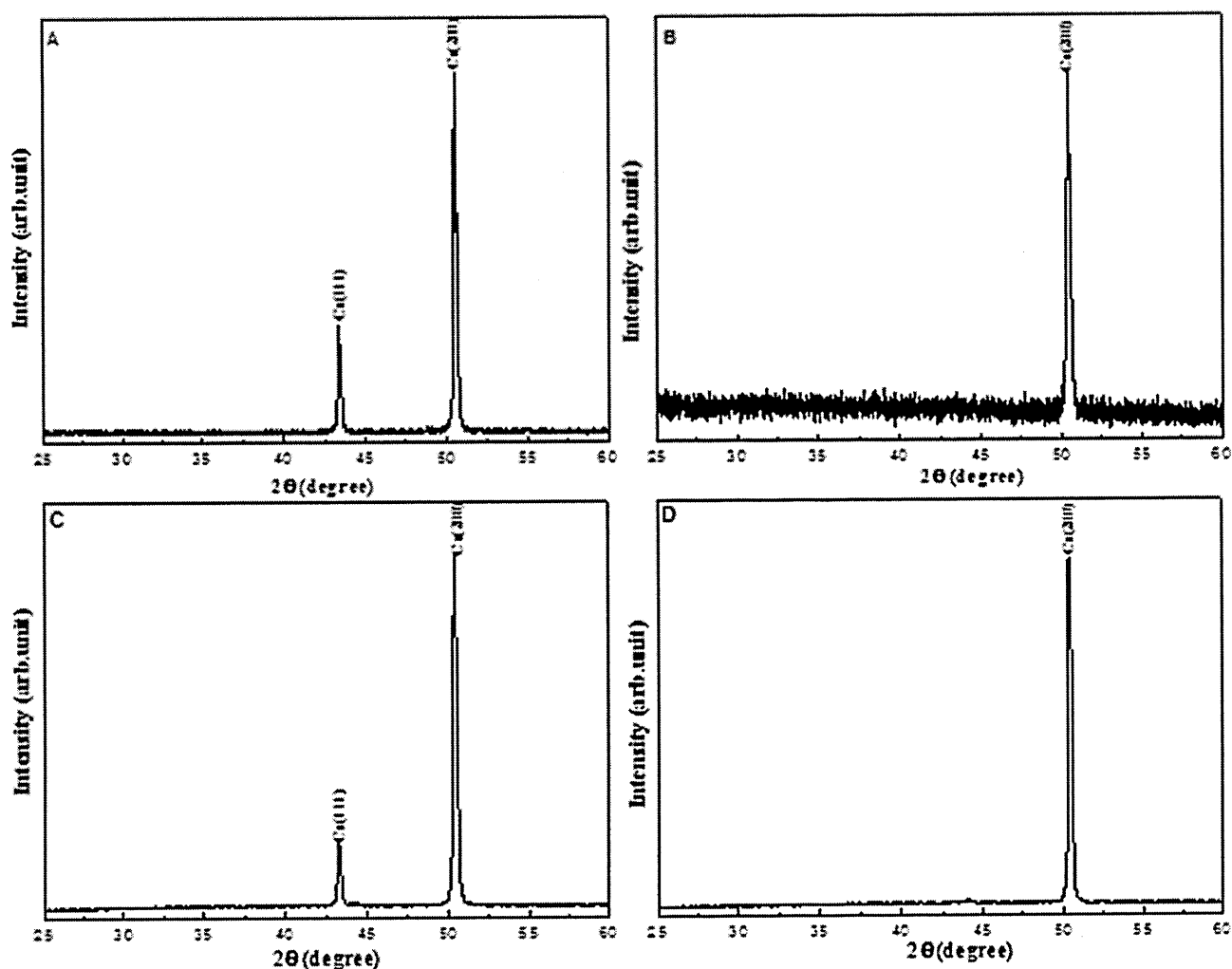
Figure 3.1 XRD patterns of (A) copper foil A, (B) copper foil B, (C) copper foil C and copper foil D

Table 3.1 Properties of four copper foils. The grain size and orientation of copper foils were characterized by XRD measurement.

Where λ is the X-ray wavelength, θ is the Bragg diffraction angle, and W is the full width at half maximum (FWHM) of the peak corresponding to θ. When calculated by using the peak corresponding to the (200) plane of copper, the resultant grain sizes in copper foil A are about 72.2 nm, in copper foil B are about 35.6 nm, in copper foil C are about 64.5 nm and in copper foil D are about 34.3 nm. The size of the grain in the copper foil A and C are about two times larger than that in the copper B and D. So number of grain in the copper foil B and D are the larger than it in the copper A and C. The properties of copper foil

A, B, C and D are summarized in table 3.1.

Table 3.1 Properties of four copper foils. The grain size and orientation of copper foils were characterized by XRD measurement.

	Grain size (nm)	Orientation of copper foils
Copper foil A	72.2	(111) and (200) orientation
Copper foil B	35.6	(200) orientation
Copper foil C	64.5	(111) and (200) orientation
Copper foil D	34.3	(200) orientation
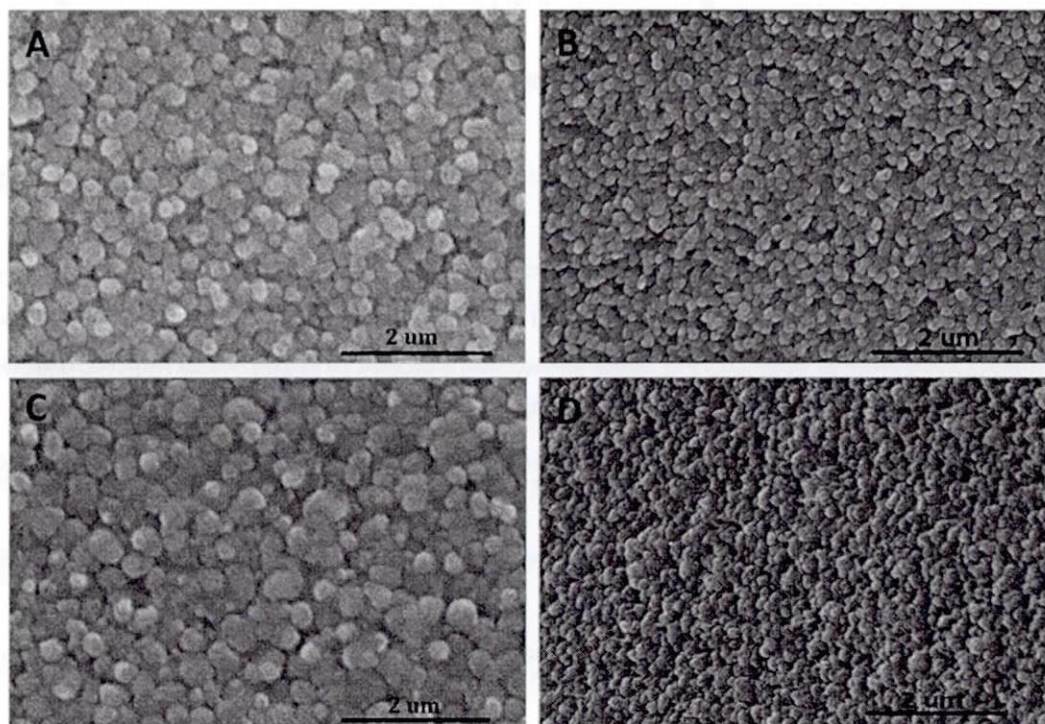
Figure 3.2 SEM images of copper foil (A) A, (B) B, (C) C, and (D) oxidized at 300 °C for 2 h in an air gas flow of 0.5 L/min.
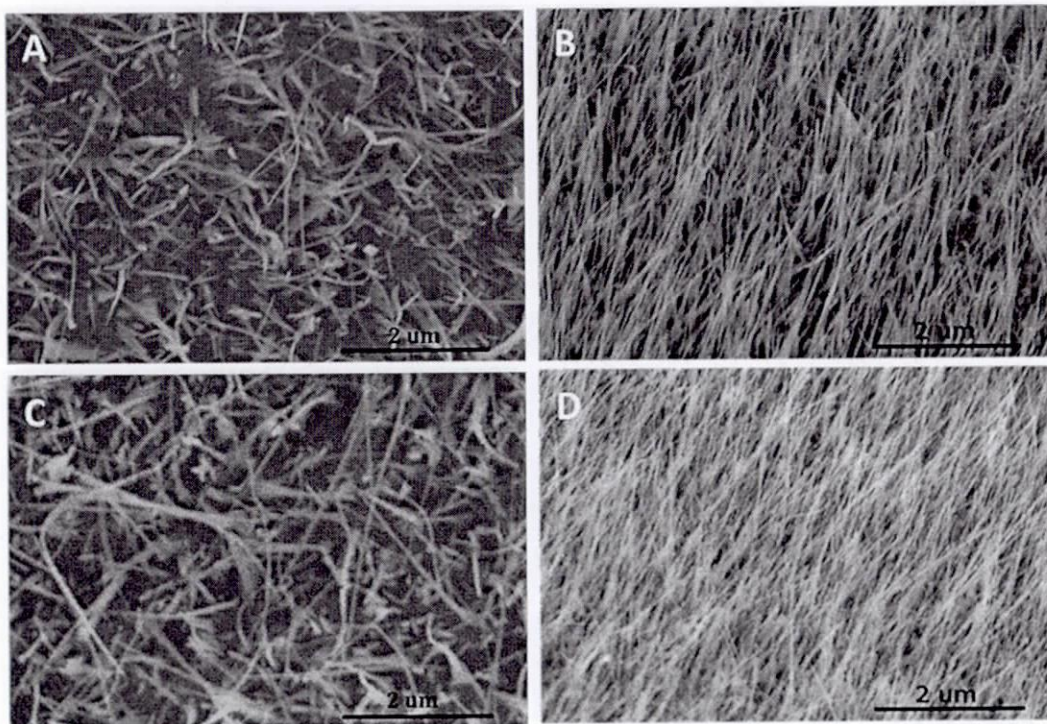
Figure 3.3 SEM images of copper foil (A) A, (B) B, (C) C, and (D) oxidized at 400 °C for 2 h in an air gas flow of 0.5 L/min.
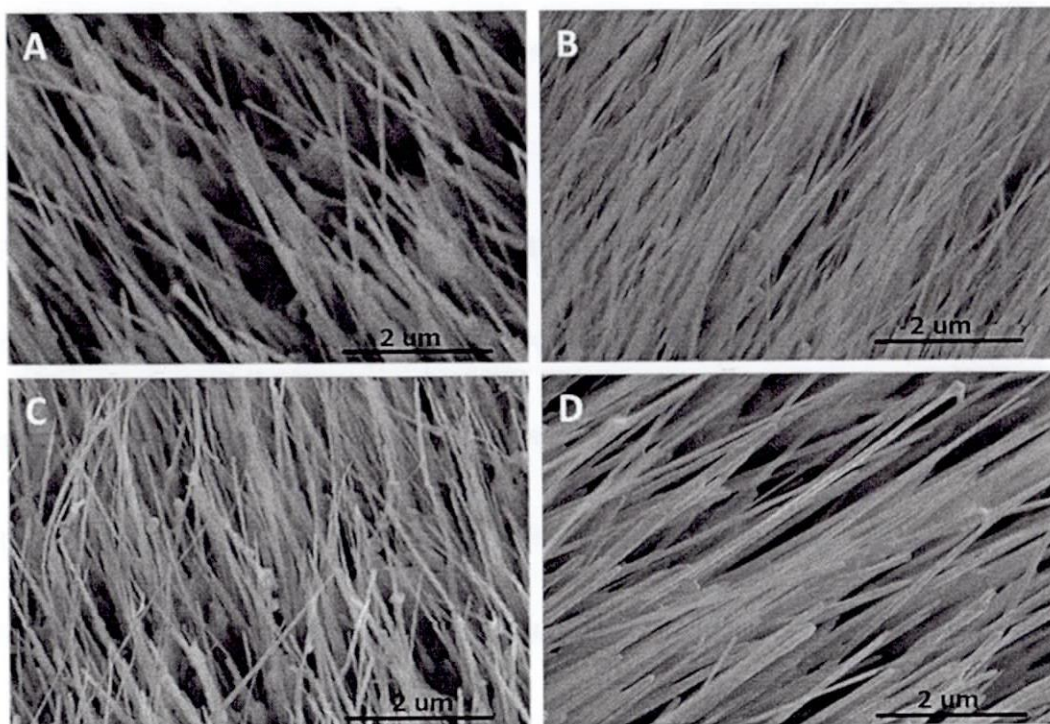
Figure 3.4 SEM images of copper foil (A) A, (B) B, (C) C, and (D) oxidized at 500 °C for 2 h in an air gas flow of 0.5 L/min.
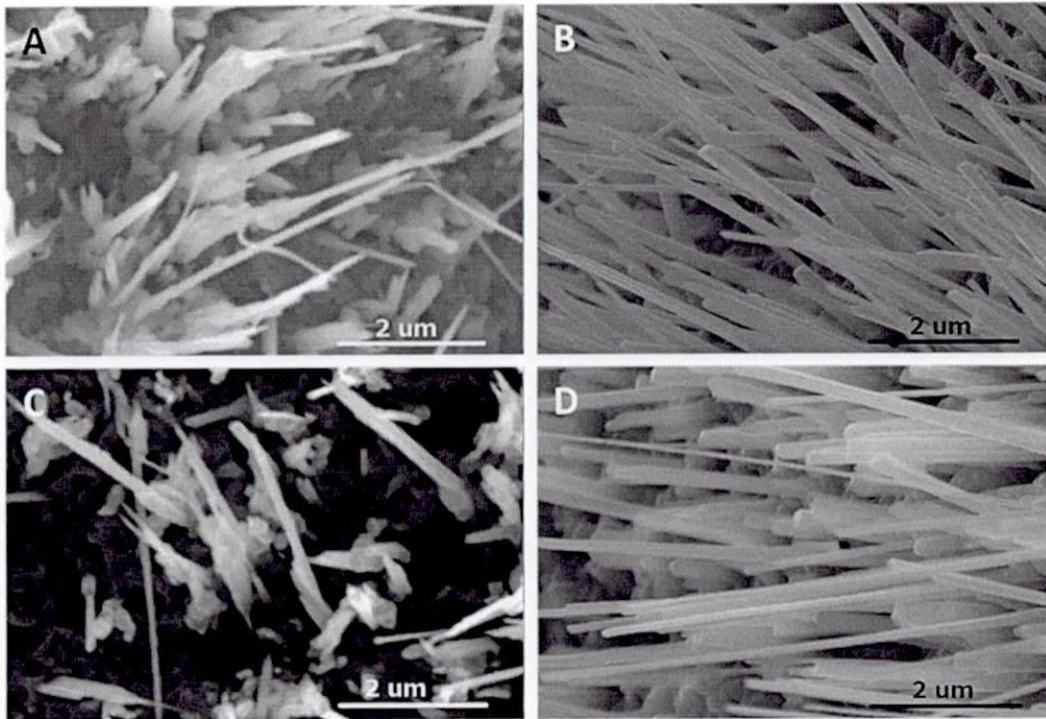
Figure 3.5 SEM images of copper foil (A) A, (B) B, (C) C, and (D) oxidized at 600 °C for 2 h in an air gas flow of 0.5 L/min.

3.3.2 Effect of oxidizing temperature

Figure 3.2 shows SEM images of surface morphologies after heating the copper foil A, B, C and D at 300 °C for 2 h in an air gas flow of 0.5L/min, respectively. As can be seen, oxide grains are observed on four substrates. The oxide grains on copper A and C are less compact than the others on the copper B and D. The measured oxide grain size on copper A and C are about 250 and 300 nm. The grains on the copper foil B and D are denser and the size are about 160 and 170 nm, without nanowires on the surface of the specimen. The oxide grains become larger as temperature increases. The oxide grains formed on copper foil B and D (smaller grain size) are much smaller than those formed on copper foil A and C (bigger grain size) at the early stage of oxidation. Due to a large number of nucleation sites on the smaller grain size of copper foils. From the morphology of the samples figure 3.3, it is observed that

nanowires formed at 400 °C. High density, more uniform and longer nanowires are formed on copper foil B and D compared with copper foil A and C. As the temperature is increased to 500 °C, there is also a very large amount of nanowires formed on the copper B and D as indicated in figure 3.4 (B) and (D). It can be seen that long and uniform nanowiers are formed on the entire surface and nanowires are mostly vertically along the substrate surface. The average diameters and length of the nanowires on copper foil B and D are about 80 nm and 7 μm and about 100 nm and 8 μm, respectively. Nevertheless, large-area and high density CuO nanowires can also grow from the copper A and C under an air gas flow as shown in figure 3.4 (A) and (C). The as-prepared nanowires on the copper foil A and C are not well vertically aligned along the substrate surface with the lengths of about 4 and 5 μm and the diameter of about 50 and 62 nm. They are desirable to grow large-area, uniform and vertically aligned CuO nanowires along the copper substrates surface such as applications in field emission emitters [23] and realization of nanosized-CuO/Al based energetic materials [24] for some applications. When the temperature is increased to 600 °C, there is a high density and a uniform size of nanowire still formed on the copper foil B and D as shown in figure 3.5 (B) and (D). In this process, the longer nanowires can be formed, which are longer than that on the copper foil A and C, with the length ranging from 5 to 15 μm and the diameter of the nanowires about 180 nm as shown in figure 3.5. A large amount of nanowires, with a low density, were observed on the copper foil A and C prepared at 600 °C with the length of 3 to 6 μm and the diameter of the nanowires from 100 to 400 nm. We can conclude that the grain size of copper foil has a great effect on the growth of nanowires. The smaller grain size of copper foil is favourable for the growth

of nanowires.

3.3.3 Cross-sectional characterization of CuO nanowires samples

Figure 3.6 shows the SEM images of the cross sections of oxidized the copper foil A and B at 500°C for 2 h. In order to measure the oxide layer thickness, an oxide flake was carefully removed from a copper substrate. When copper foil is oxidized at first the major product is Cu_2O and it is expected that CuO is formed through a second step of oxidation of Cu_2O [15, 27]. In this case, Cu_2O serves as a precursor to CuO. The outmost layer is always of CuO if the oxide consists of both Cu_2O and CuO. The fractional thickness of the CuO outmost layer in this bi-layer oxide layer mainly depends on the annealing temperature. In the figure 3.6 (A) the oxide layer is divided into the bottom layer of Cu_2O and the outermost layer of CuO [28]. Though measuring the substrate by the EDX, the CuO layer was about 0.9 μm thick, and the Cu_2O layer was about 4.2 μm in the copper foil A. However, for the copper foil B subjected to the same treatment as shown in figure 3.6 (B), the outermost CuO layer is thicker than that for the copper foil A, about 1.8 μm thick. The bottom Cu_2O layer is evidently thicker (about 5.8 μm). The total thickness of the layer on the copper substrate B is about 7.6 μm, which is thicker than that on the copper foil A (about 5.1 μm). The thicker oxide layer on the copper foil B is due to the higher oxidation rate. In principle, the copper ions and oxygen ions can diffuse across the scales much faster along the grain boundaries than through the bulk. The high oxidation rate of copper foil B would be due to the small grain size, resulting in faster overall rates of scale growth.

3.3.4 Effect of surface roughness

In order to study the influence of surface roughness on the growth of CuO nanowires, the copper foil B has been put into HCl acid for 1 and 3.5 h to make the surface roughness of copper substrate. The morphology of the treated copper foil B after treated with HCl for 1 and 3.5 h can be seen to be significantly different with as prepared one. The surface is very smooth and there are no defective areas on the surface when the HCl treatment was not performed (Figure 3.7(A)). However, as shown in Figure 3.8(B) and (C) there are many defective areas on the treated copper foil. Nanowires are synthesized on HCl treated copper substrates at 400 for 2 h in an air gas flow of 0.5L/min. From the morphology of the samples, it is observed that nanowires formed on the treated substrates are very high density and uniform size with the length ranging from 1.5 to 2 μm and the diameter from 20 to 30 nm as shown in Figure 3.8 (B) and (C). A very dense nanowire was produced on the treated substrates and no significant changes were observed when nanowire synthesized on the as prepared copper substrates (Figure 3.8(A)). We can conclude that the surface roughness of the copper substrate does not affect the growth of nanowires.
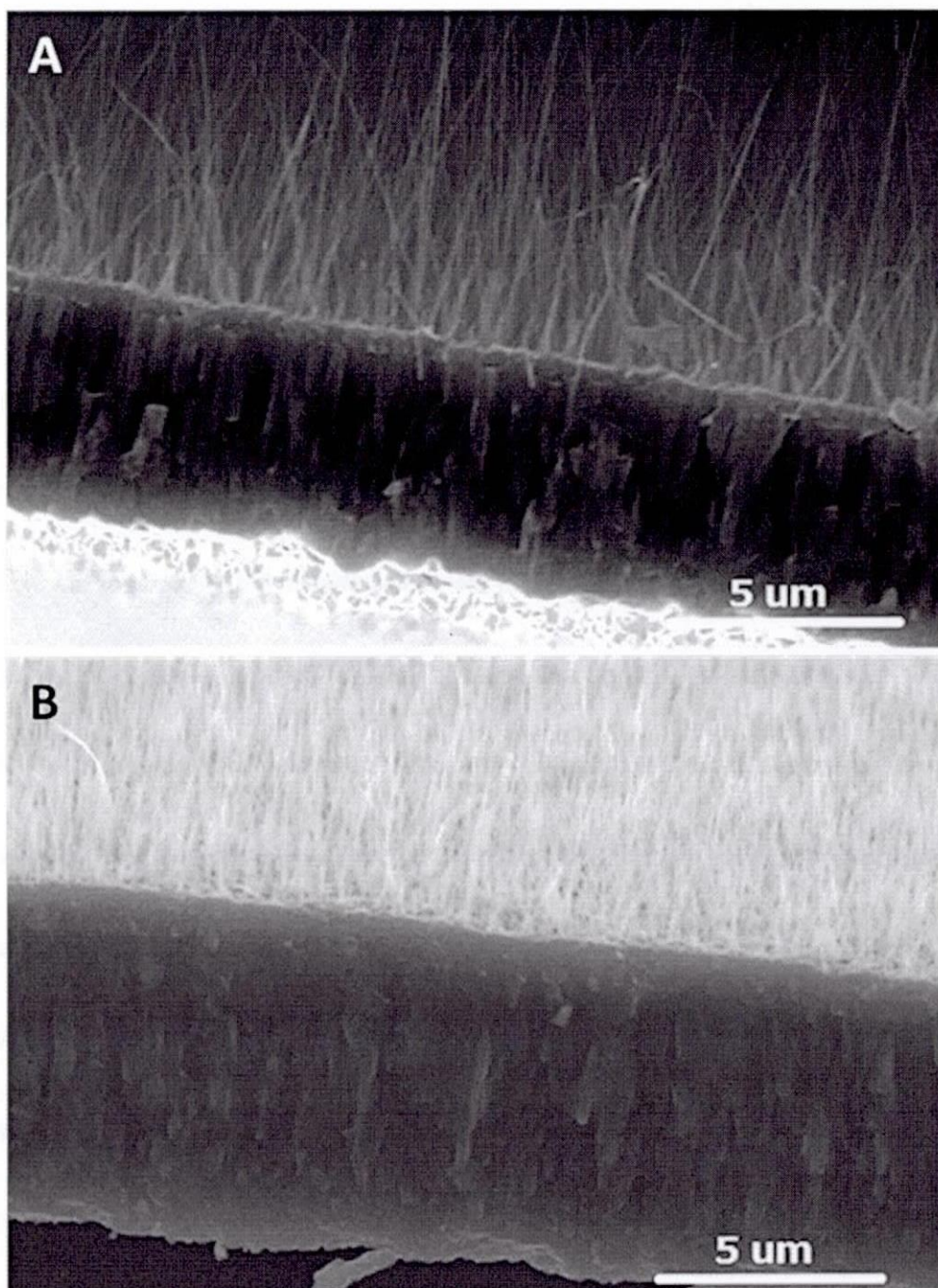
Figure 3.6 SEM images of cross-section of nanowires on (A) the copper foil A and (B) B. The nanowires were synthesized at 500 °C for 2 h.
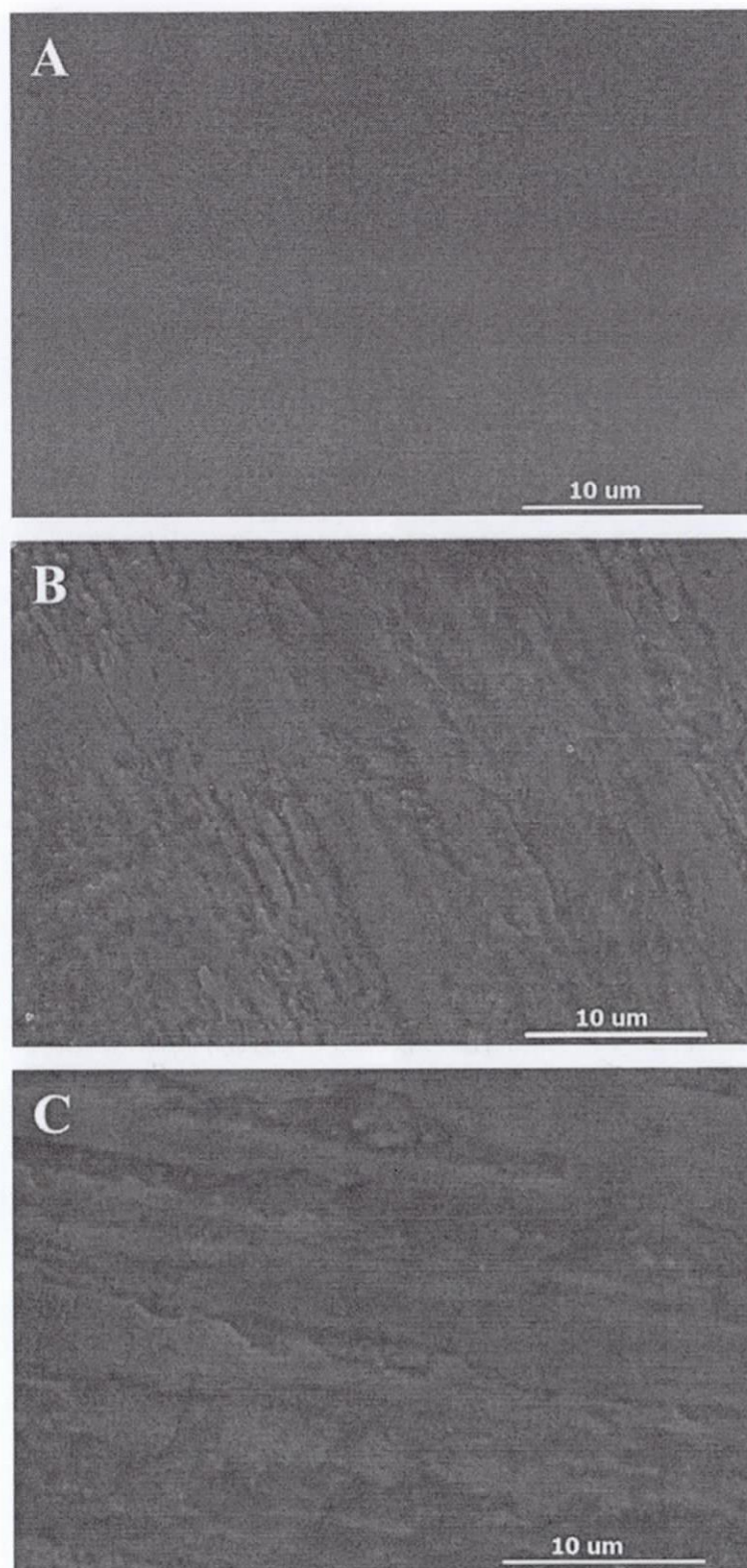
Figure 3.7 SEM images of the surface of copper foil B without (A) and with HCl treatment for (B) 1h and (C) 3.5 h.
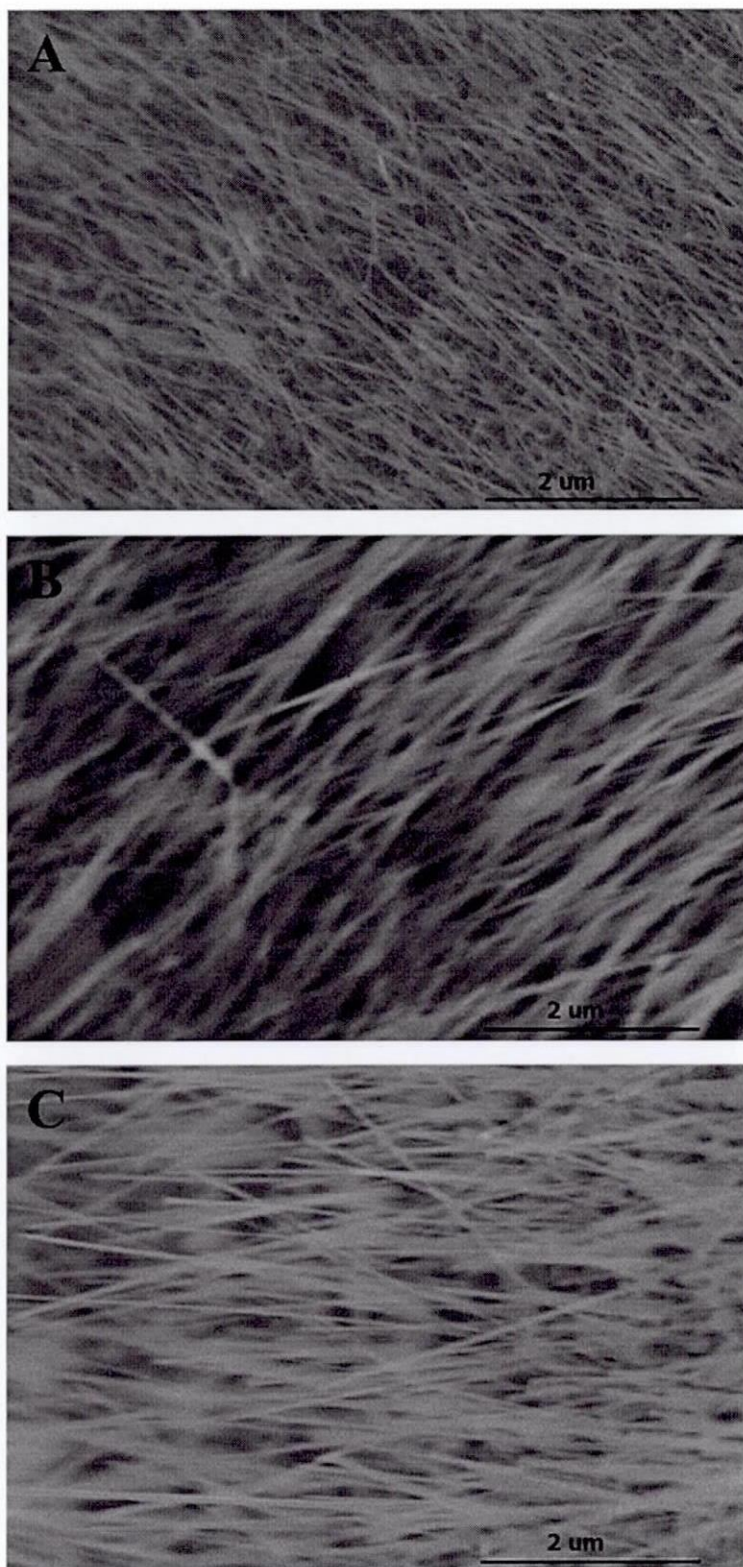
Figure 3.8 SEM images of CuO nanaowires synthesized at 400 °C for 2 h on copper foils without (A) and with HCl treatment for (B) 1 h and (C) 3.5 h.
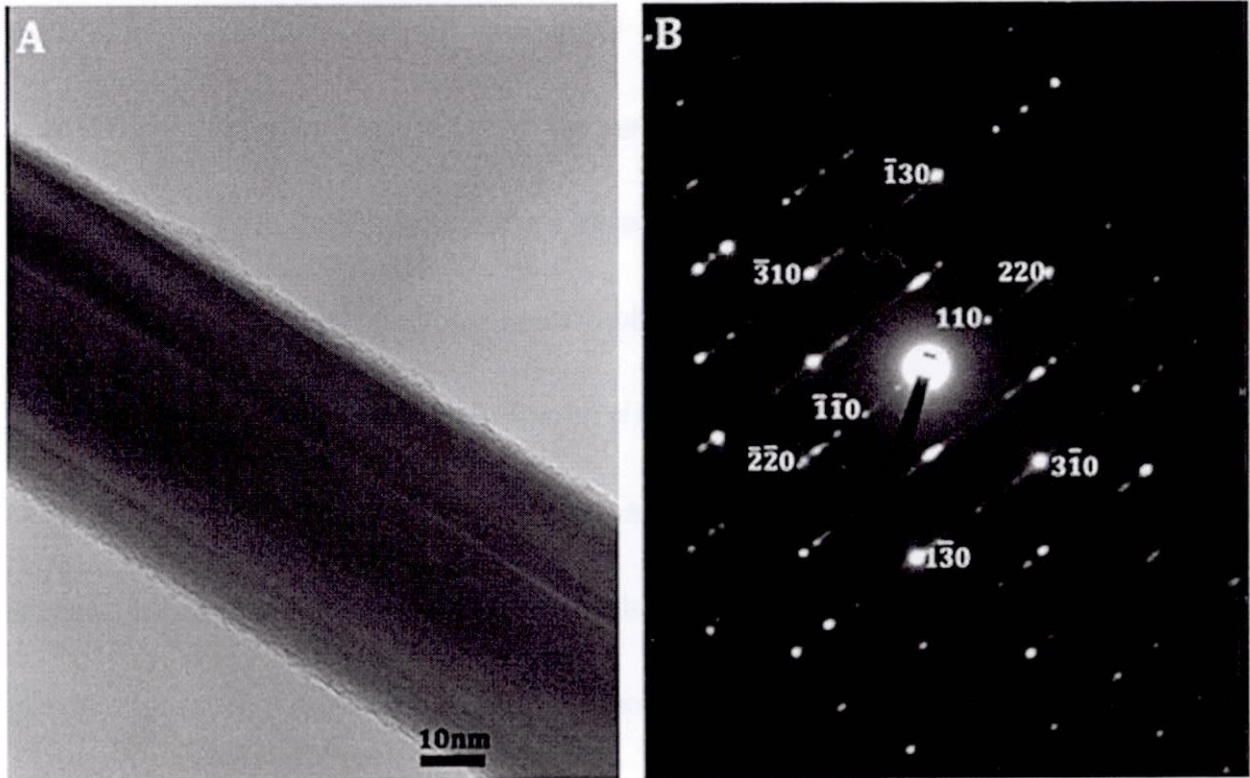
Figure 3.9 (A) TEM images and (B) SAD pattern of a single CuO nanowire of copper foil A prepared at 500°C for 2 h in air gas flow of 0.5L/min.
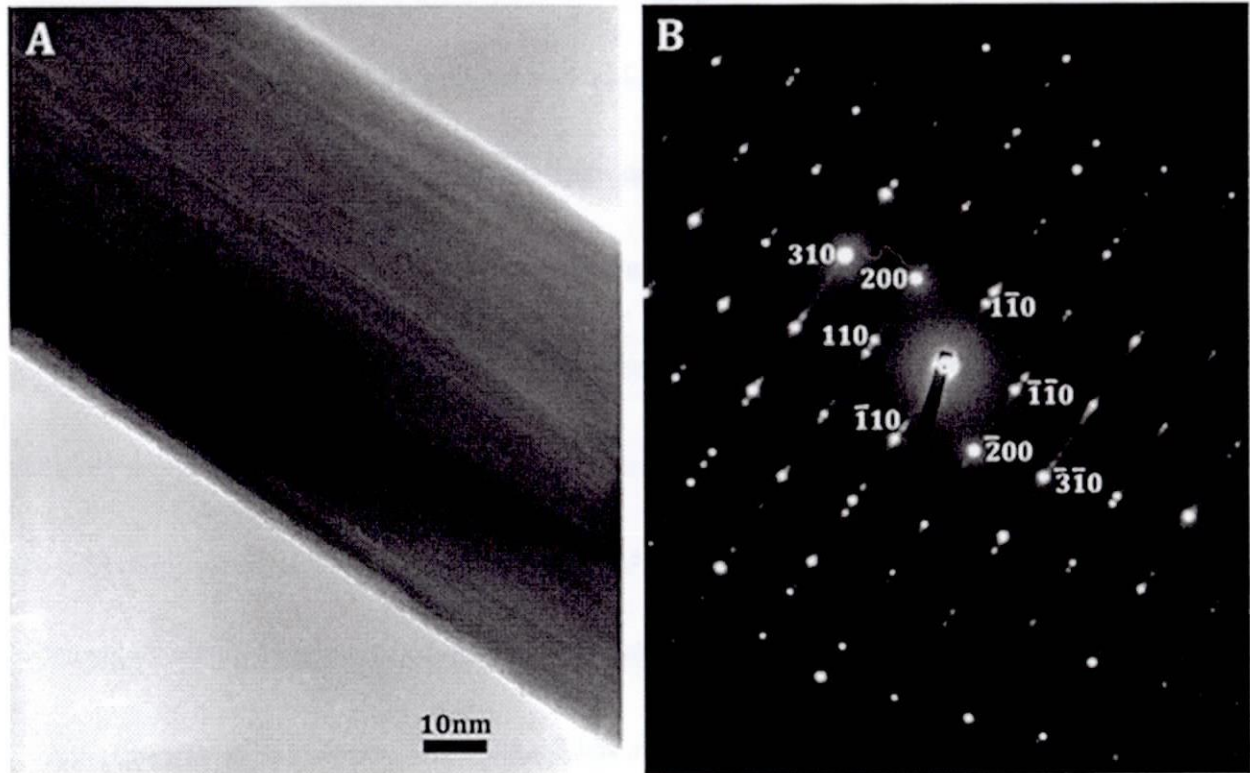
Figure 3.10 (A) TEM images and (B) SAD pattern of a single CuO nanowire of copper foil B prepared at 500°C for 2 h in air gas flow of 0.5L/min.

3.3.5 TEM characterization of CuO nanowires

We further characterized the size, structure and crystal of these nanowires using TEM and selected area diffraction (SAD) pattern. The used sample was prepared at 500 °C for 2 h. Figure3. 9 and 3.10 display TEM diffraction patterns of an individual nanowire of the copper foil A and B oxidized at 500°C for 2 h. In the image of the sample as shown in figure 3.10 (A), it is observed that the nanowire of the copper foil B has wire-like shape and the surface is very smooth with the diameter of about 70 nm. In comparison with the nanowire of the copper foil B, the nanowire's surface of copper foil A has roughness and smaller diameter of about 45 nm shown in figure 3.9 (A). A bigger diameter of nanowire is observed in figure 3.10 (A) compared to figure 3.9 (A), it may be attributed to have the larger number of grain boundaries on the copper foil B. Figure 3.9 (B) shows a TEM diffraction pattern of an individual nanowire from copper foil A prepared at 500°C for 2 h in air gas flow of 0.5L/min. It would be typically observed when the electron beam was focused on an individual nanowire along the [001] direction. The double diffraction is due to the twin plane within a nanowire. Figure 3.10 (B) also shows a TEM diffraction pattern of an individual nanowire from copper foil B prepared at 500°C for 2 h in air gas flow of 0.5L/min. The electron beam was focused on an individual nanowire along the [001] direction. Similarly, the double diffraction is caused by the twin plane within the nanowire, where each set diffraction spot is a single crystal which corresponds to the monoclinic structure of CuO with the lattice constants, $a = 0.469$ nm, $b = 0.343$ nm, $c = 0.513$ nm, and $\beta = 99.55°$.

The formation of nanowires occurs when two layers of copper oxides are gradually formed by

oxidation of copper [15, 26-28]. We examine our results based on mechanisms of nanowire growth reported in the literature. Goncalves et al. suggested that CuO nanowires growth occurs via grain boundary diffusion of copper ions through the Cu_2O layer of the oxygen ions through the outmost CuO layer [25]. Xu et al. also suggested that nanowire growth is via grain boundary diffusion [26]. This idea shares similarities with the model proposed recently for Fe_2O_3 nanowires formation [30]. However, Lu et al. and Yeon-Woong et al. reported that the mechanism of nanowires growing in this case is due to the relaxation of compressive stress [27, 28]. Here, we believe that the growth of nanowire occurs to reduce the stress generated during oxidation of copper by grain boundary diffusion process [20]. Now, we discuss how the proposed model can describe the obtained results. Long, high density and aligned cupric oxide nanowires are observed in figure 3.3, 3.4 and 3.5 (B) and (D); it can be attributed to grain boundary and the crystal direction with the effective relaxation of compressive stress. It is well known that the initial oxidation rate of a metal at intermediate temperatures (300 – 600 °C for copper) is too rapid to be attributed solely to lattice diffusion of the various ionic species in its oxide film [31]. The oxidation of copper at low temperatures is dominated by grain boundaries. The smaller grain size and the higher grain boundary energy can play an important role in increasing the effective diffusion coefficient of copper ions and oxygen in smaller crystallite size at intermediate temperatures as a result of grain boundary diffusion [32]. When copper foil oxidized to Cu_2O, and then Cu_2O oxidizing to CuO leads a compressive stress on the interface due to volume and structural change. The compressive stress drives outward diffusion of copper cations along grain boundaries, resulting in CuO nanowire growth on CuO grains [27]. Therefore,

the large numbers of grain boundaries increase the relaxation of the compressive stresses at the CuO and

Cu$_2$O layer interface. Consequently a high density of nanowires is observed in figure 3.3, 3.4 and 3.5 (B)

and (D) compared to figure 3.3, 3.4 and 3.5 (A) and (C). The oriented direction is favorable to the

diffusion of copper cations along grain boundaries in the copper film. It maybe affects the surface of

nanowire. The TEM images presented in figure 3.10 indicates a bigger diameter of nanowire and smooth

surface nanowire formed on the copper foil B. This also is attributed to the relaxation of compressive

stress by effective grain boundary diffusion. Depending on the oxidation temperature, the diffusion of the

atoms or ions may take place within the lattice, through grain boundaries in the oxide layer. As a result

nanowire density decreases as temperature increase, as seen in the sequence of SEM images of figure 3.5.

The oxide grains become larger as temperature increases on our experiment. Although we have tried to

raise the heating temperature to 800°C, large oxide grains are observed but no nanowires appeared on the

surface of substrate. When the temperature is higher than 800°C, copper oxidation is dominated by lattice

diffusion of copper ions; the influence of grain boundary diffusion would finally become small compared

to lattice diffusion. This explains the absence of nanowires for oxidations at 800°C. The relative

importance of grain boundary transport through a scale depends on the grain size of the oxide, on the

compressive stress of interface and on temperature and tends to become negligible at sufficiently high

temperatures [33]. By heating the copper foil with the smaller grain size with (200) oriented in an air gas

flow, the large numbers of grain boundaries are favorable to the relaxation of compress stress, resulting in

the growth of high density and smooth surface nanowires.

3.4 Conclusion

High density, smooth surface and aligned cupric oxide nanowires have been synthesized by heating copper foils with the smaller grain size and (200) oriented in an air gas flow. On the other hand, uniform, smooth surface and aligned nanowires cannot be obtained by heating copper foils with the bigger grain size and two crystal orientations. The difference is attributed to faster the relaxation of compress stress by outward diffusion of copper ions and inward diffusion of oxygen along the grain boundaries (both in the metal and in the layer for the smaller grain size of copper substrate). The small grain size of the copper foil B and C are favorable to the growth of nanowires due to the larger number of grain boundaries. Aligned cupric oxide and smooth surface nanowires could be produced by heating the (200) oriented copper foil. The surface roughness does not affect the growth of nanowires.

Reference

[1] Y. Xia, P. Yang, Y. Sun, Y. Wu, B. Mayers, B. Gates, Y. Yin, F. Kim, H. Yan, Adv Mater, 15 (2003) 353.

[2] R. S. Wagner and W. C. Ellis, Appl Phys Lett, 4 (1964) 89.

[3] K. S. Shankar and A. K. Raychaudhuri, Sci Eng C, 25 (2005) 738.

[4] P. A. Cox, Oxford University Press, NY, USA, 1992.

[5] A. Cruccolini, R. Narducci and R. Palombari, Sensors Actuators B, 98 (2004) 227.

[6] V. R. Katti, A. K. Debnath, K. P. Muthe, M. Kaur, A. K. Dua, S. C. Gadkari, S. K. Gupta and V. C. Sahni, Sensors Actuators B, 98 (2003) 245.

[7] H. Fan, L. Yang, W. Hua, X. Wu, Z. Wu, S. Xie, B. Zou, Nanotechnology, 15 (2004) 37.

[8] A. Santos, P. Yustos, A. Quintanilla, G. Ruiz and F. Garcia-Ochoa, Appl Catal B, 61 (2005) 323.

[9] A. A. Ponce and K. J. Klabunde, J Mol Catal A, 225 (2005) 1.

[10] G. Larsen and S. Noriega, Appl Catal A, 278 (2004)73.

[11] C. T. Hsieh, J.M. Chen, H. H. Lin and H. C. Shih, Appl Phys Letter, 83 (2003) 3383.

[12] F. Lanza, R. Feduzi and J. Fuger, J Mater Res,5 (1990)1739.

[13] D. Chen, G. Shen, K. Tang and Y. Qian, J Crystal Growth, 254 (2003) 225.

[14] C.T. Hsieh, J. M. Chen, H. H. Lin and H. C. Shih, Appl Phys Lett, 82 (2003) 3316.

[15] J. B. Liang, N. Kishi, T. Soga and T. Jimbo, Applied Surface Science, 257 (2010) 62.

[16] K. Zhang, C. Rossi, C. Tenailleau, P. Alphonse, J. Ching, Nanotechnology, 18 (2007) 8.

[17] R.C. Wang and C.H. Li, Crystal Growth & Design, 9 (2009) 2229.

[18] K. Zhang, Y. Yang, E. Pun and R. Shen, Nanotechnology, 21(2010) 7.

[19] J. Benjamin, Lu. Ganhua and C. Junhong, Journal of Nanomaterials, 2008 (2008) 7 .

[20] A. M. B. Goncalves, L. C. Campos, A. S. Ferlauto and R. G. Lacerda, Journal of Applied Physics, 106 (2009) 5.

[21] X. Jiang, T. Herricks and Y. Xia, Nano Lett, 2 (2002) 1333.

[22] C. H. Xu, C. H. Woo and S. Q. Shi, Superlattices and Microstructures, 36 (2004) 31.

[23] C. T. Hsieh, J. M. Chen, H. H. Lin and H. C. Shih, Appl Phys Lett, 83 (2003) 3383.

[24] C. Rossi, K. Zhang, D. Est`eve, P. Alphonse, J. Y. C. Ching, P. Tailhades and C. Vahlas, J Microelectromech Syst, 16 (2007) 919.

[25] A. M. B Goncalves, L. C. Campos, A. S. Ferlauto and R. G. Lacerda, J Appl Phys, 106 (2009) 34303.

[26] C. H. Xu, C. H. Woo and S. Q. Shi, Chemical Physics Letters, 399 (2004) 62.

[27] Y.W. Park, N.J. Seong, H.J. Jung, A. Chanda, S.G. Yoon, Journal of The Electrochemical Society, 157 (2010) 119.

[28] P. Shao, S. Deng, J. Chen, N. Xu, Nanoscale Research Letters, 6 (2011) 1.

[29] L. Yuan, Y. Wang, R. Memaa, G. Zhou, Acta Materialia, 59 (2011) 2491.

[30] A. G Nasibulin, S. Rackauskas, H. Jiang, Y. Tian, P. R. Mudimela, S. D. Shandakov, L. I. Nasibulina, J. Sainio and E. I. Kauppinen, Nano Res, 2 (2009) 373.

[31] J. M. Perrow, W. W. Smeltzer and J. D. Embury, Acta Metallurgica, 16 (1968)1209.

[32] Z. Han, L. Lu, H. W. Zhang, Z. Q. Yang, F. H. Wang and k. Lu, Oxidation of Metals, 63 (2005) 261.

[33] Y. Niu, F. Gesmundo, G. Farne, Y. S. Li, P. Matteazzi and G. Randi, Corrosion Science, 42 (2000)

1763.

Chapter – 4 Thin CuO films on quartz substrates prepared by thermal oxidation in air with water vapor

4.1 Introduction

In recent years, cupric oxide (CuO) thin films have attracted much interest due to their potential applications in optical and electronic devices. CuO has been known as a p-type semiconductor that exhibits a narrow band gap (1.2 eV) and a number of other interesting properties [1, 2]. CuO has also an interesting monoclinic crystal structure belonging to the Mott insulator material class whose electronic structure cannot be described by conventional band theory [3]. During the past years, in order to obtain high quality cupric oxide films, it has been prepared by various techniques such as thermal oxidation [4]; electro deposition [5]; chemical conversion [6]; chemical brightening [7]; spraying [8]; plasma evaporation [9]; reactive sputtering [10]; and molecular beam epitaxy [11]. Among various methods employed for the preparation of CuO films, CuO thin films by thermal oxidation at higher temperature are an inexpensive and convenient method. However, in most of these studies, a mixture of phases, like Cu, CuO and Cu_2O is generally obtained [12]. A copper foil is oxidized in air at 400 and 500 °C, the majority of copper foil converted into Cu_2O with only a small amount of CuO on the surface in the form of nanowires [13]. Huang et al reported CuO nanowires formed at 300 °C in oxygen by thermal oxidation of copper foils [14]. Hence it is the essential problem to find out the specific reaction parameters for producing pure CuO phase.

Here, we report the synthesis CuO films on quartz substrates by thermal oxidation in cylinder air with water vapor and conduct a detailed structural and optical investigation of CuO films.

4.2. Experimental details

Thin CuO films have been synthesized by thermal oxidation of copper films on quartz substrates in cylinder air with water vapor and in atmospheric air. Experimental detail of oxidation in atmospheric air as reported in [13]. 300 and 600 nm thick copper films were deposited on quartz substrates by using a thermal vacuum evaporator. The substrates were cleaned in acetone, methanol and deionized water under an ultrasonic bath for 5 min followed by drying with N_2 flow. The cleaned Cu on quartz substrate was placed onto a quartz boat. The quartz boat was positioned in the center of a quartz tube that was mounted in the middle of a horizontal tube furnace. One end of the quartz tube was attached to a nebulizer and other to the gas bubble. A flow of N_2 gas was first introduced into the quartz tube at a flow rate of 1 L/min for 30 min to remove ambient air from the system. Then flow rate was adjusted to 0.5 L/min. The tube furnace was heated to the set-point temperature and gas flow of N_2 was kept at a rate of 0.5 L/min. The system was allowed to cool naturally to room temperature to prevent the thin film from cracking, caused by thermal stress and further oxidized in air if the film was directly taken out of the high temperature furnace. The substrate is pulled out of the furnace for further analysis. The crystal structure and phase composition were identified by X-ray diffraction (XRD, Rigaku RINT-2100) using a 40 kV, 30 mA, Cu-Kα X-ray. A scanning step of degree of 0.02° was applied to record the XRD patterns in the 2θ range of degree of 25 - 60°. The morphology of the CuO was characterized by scanning electron

microscope (SEM, Hitachi S-3000H) operated at 25 kV. Optical studies were carried out with a

UV/VIS/NIR spectrophotometer (JASCO V-570).

4.3. Results and discussion

4.3.1. XRD characterization of CuO thin films

Figure 4.1 shows the XRD pattern of the 300 nm thick evaporated copper films oxidized at 450,

550 and 650 °C for 1 h in atmospheric air. Cu_2O and CuO phases are present when copper substrates were

oxidized in air [13].
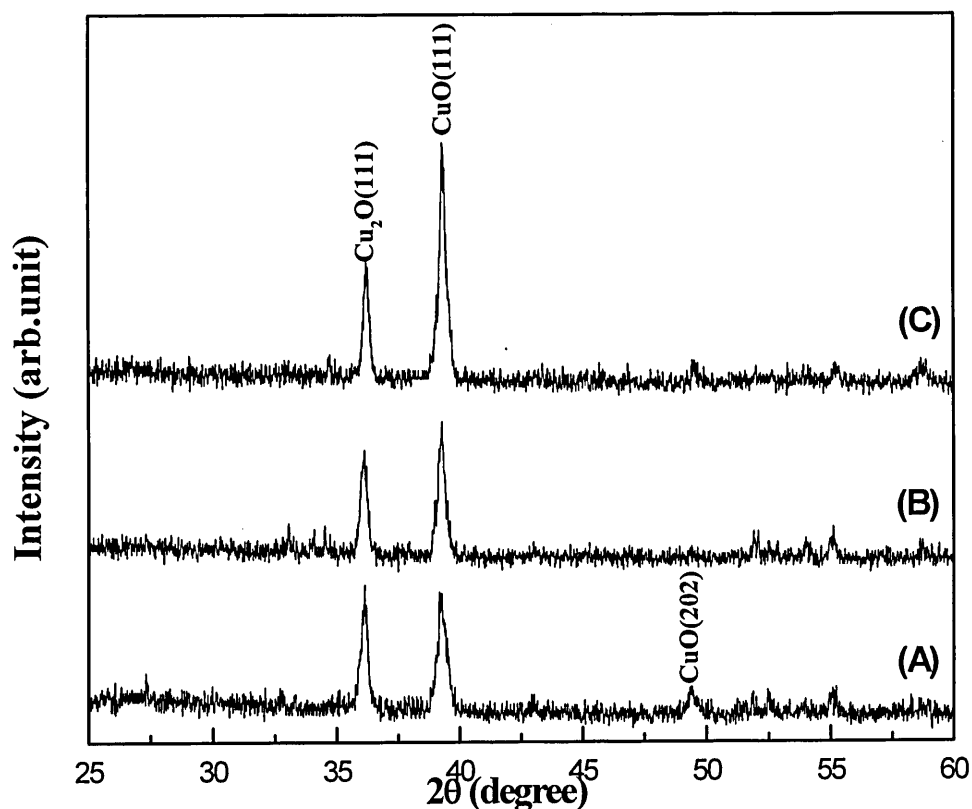
Figure 4.1 XRD patterns of the 300 nm thick evaporated copper films oxidized at (A) 450, (B) 550 and (C) 650 °C for 1 h in atmospheric air.
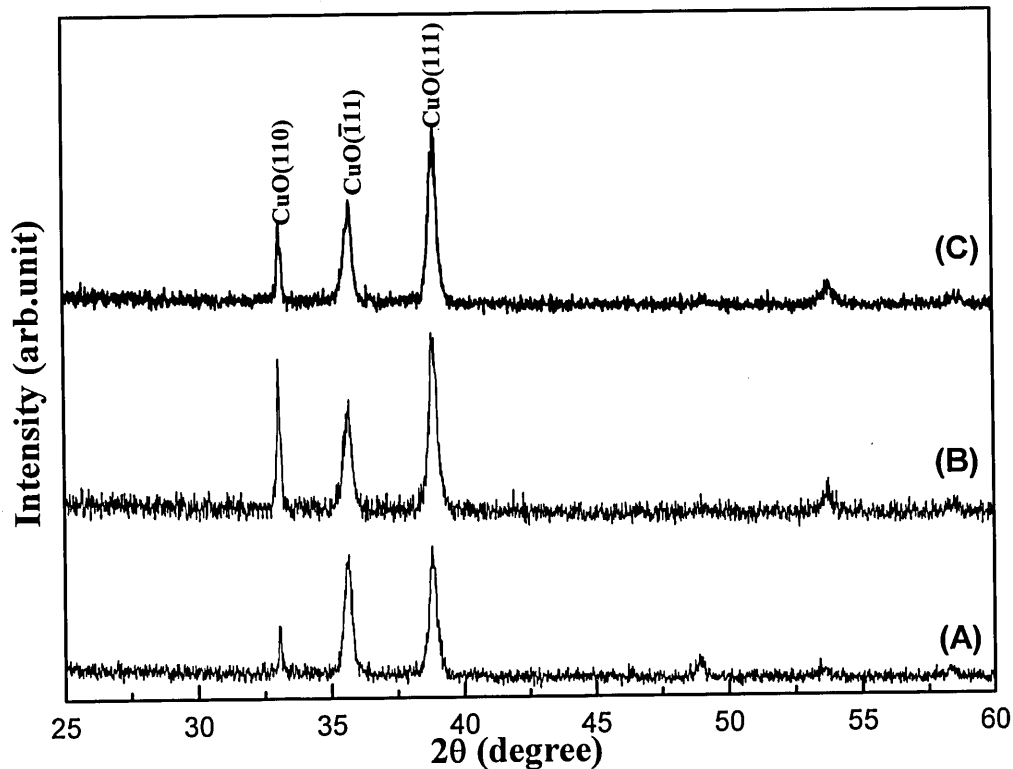
Figure 4.2 XRD patterns of the 300 nm thick evaporated copper films oxidized at (A) 450, (B) 550 and (C) 650 °C for 1 h in cylinder air with water vapor.

In this study, Cu_2O and CuO phases are also observed as shown in figure 4.1. XRD peak at $2\theta = 36.2°$ and

$2\theta = 38.7°$ can be readily indexed as (111) crystal plane of cubic Cu_2O and (111) monoclinic CuO, respectively. (111) plane of CuO become strong with increasing the heating temperature while CuO is

formed through a second step of oxidation of Cu_2O. A weak peak corresponding to CuO phases has also

been observed. However, as shown in figure 4.2 and 4.3, only CuO phase is observed after the 300 and

600 nm thick evaporated copper were oxidized at 450, 550 and 650 °C for 1 h in cylinder air with water

vapor. The XRD results show that CuO phase is the only oxidation product after the oxidation. XRD peak

at $2\theta = 33.1°$, $2\theta = 35.5°$ and $2\theta = 38.7°$ corresponding to (110), ($\bar{1}$11) and (111) plane of monoclinic

CuO structure, in addition (111) plane is the most prominent peaks in the 300 nm thick evaporated copper films. When evaporated copper film thickness increased to 600 nm, the XRD peak at $2\theta = 33.1°$ corresponding to (110) plane of monoclinic CuO structure become stronger with increasing the oxidation temperature. When the temperature rose to 650 °C, (110) and (111) plane of CuO monoclinic structure are the most prominent peak in the sample.
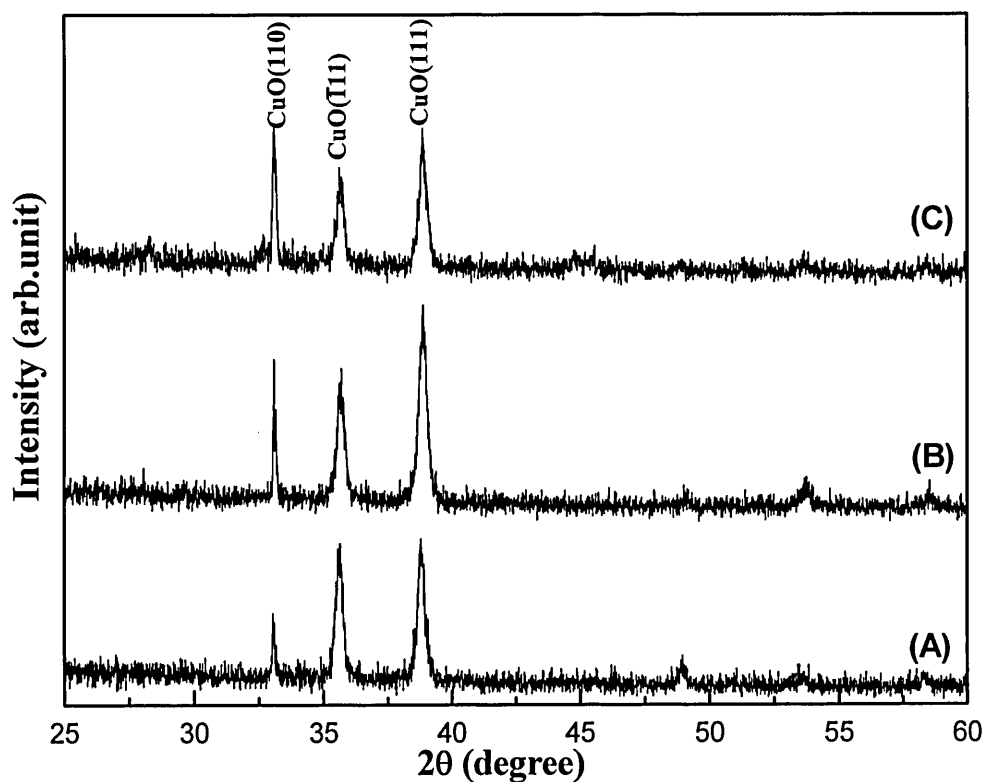
Figure 4.3 XRD patterns of the 600 nm thick evaporated copper films oxidized at (A) 450, (B) 550 and (C) 650 °C for 1 h in cylinder air with water vapor.

The evaporated copper thin film is all converted into CuO phase in the form of thin film. When oxidized in atmospheric air, the O_2 concentration decreases locally with the reaction near the thin film surface because the oxidation rate is larger than the diffusion rate. Employing a cylinder air with water vapor gas

flow is able to keep a relatively high O_2 concentration near the film that helps to convert the entire copper thin film into CuO. Our experiment shows that water vapor can significantly affect the formation of CuO thin film. Comparing figure 4.2 and 4.3 with figure 4.1 show that the single phase CuO thin film grown in cylinder air with water vapor is higher crystal quality than that of those formed in atmospheric air. This suggests that the water vapor mainly affects the nucleation rate of CuO. In this regard, the surface state of the oxide scale may affect the nucleation on the oxide scale. This is consistent with the observation that water vapors in cylinder air changes the morphology of oxide scale from multifaceted facets (figure 4.4 (A) to round facets (figure 4.4 (B)). The H_2O molecules may affect the absorption and break up of O_2 molecules on the scale surface during oxidation. This function of H_2O molecules may also be affected by the presence of O_2 in the oxidative environment. More research may be required to obtain a more complete understanding of the mechanism of the effect of water vapor.

4.3.2. Surface morphologies

Figure 4.4 show the SEM images of the 300 nm thick evaporated copper films oxidized at (A) 450, (C) 550 and ((E) 650 °C for 1 h in atmospheric air and at (B) 450, (D) 550 and (F) 650 °C for 1 h in cylinder air with water vapor. For the evaporated copper thin film oxidized at 450 °C in atmospheric air and in cylinder air with water vapor (figure 4.4 (A) and (B)), it can be seen, the copper thin film oxidized in atmospheric air is more compact compared to that oxidized in cylinder air with water vapor (figure 4.4 (B). its grain size is between 30 and 80 nm. The copper thin film oxidized in cylinder air with water vapor, its grain size is between 50 and 150 nm. After 1 h oxidized in atmospheric air at 550 °C, large oxide

grains are formed with big hole on the surface which is composed of several small crystal grains. When

the substrate temperature rose to 650 °C, the grain size don't increases obviously, but the hole became

bigger with increases the temperature. In comparison with heating in atmospheric air, heating in cylinder

air with water vapor produces large grain size.
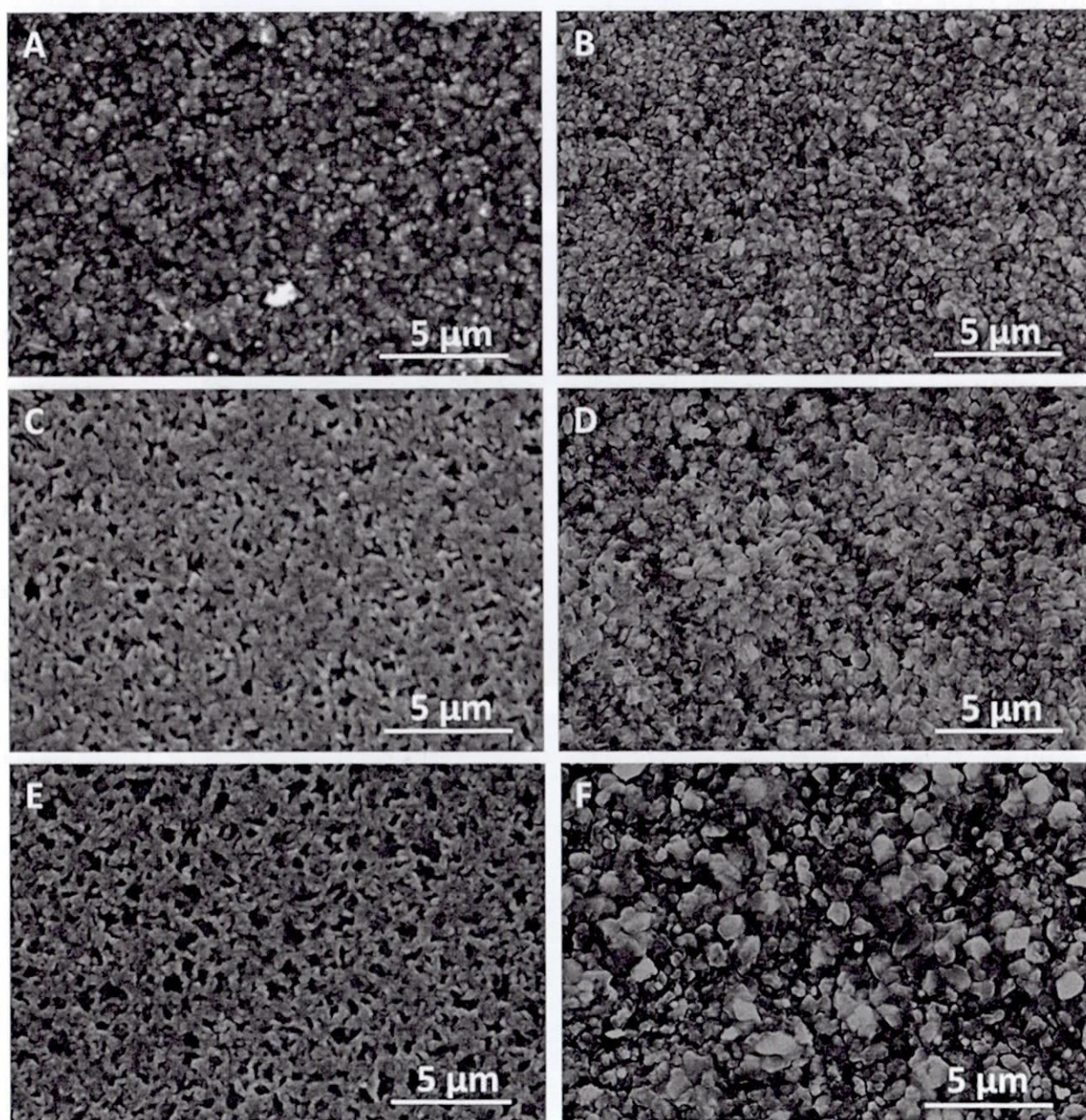
Figure 4.4 SEM images of the 300 nm thick evaporated copper films surface oxidized at (A) 450, (C) 550 and ((E) 650 °C for 1 h in static air and at (B) 450, (D) 550 and (F) 650 °C for 1 h in cylinder air with water vapor.
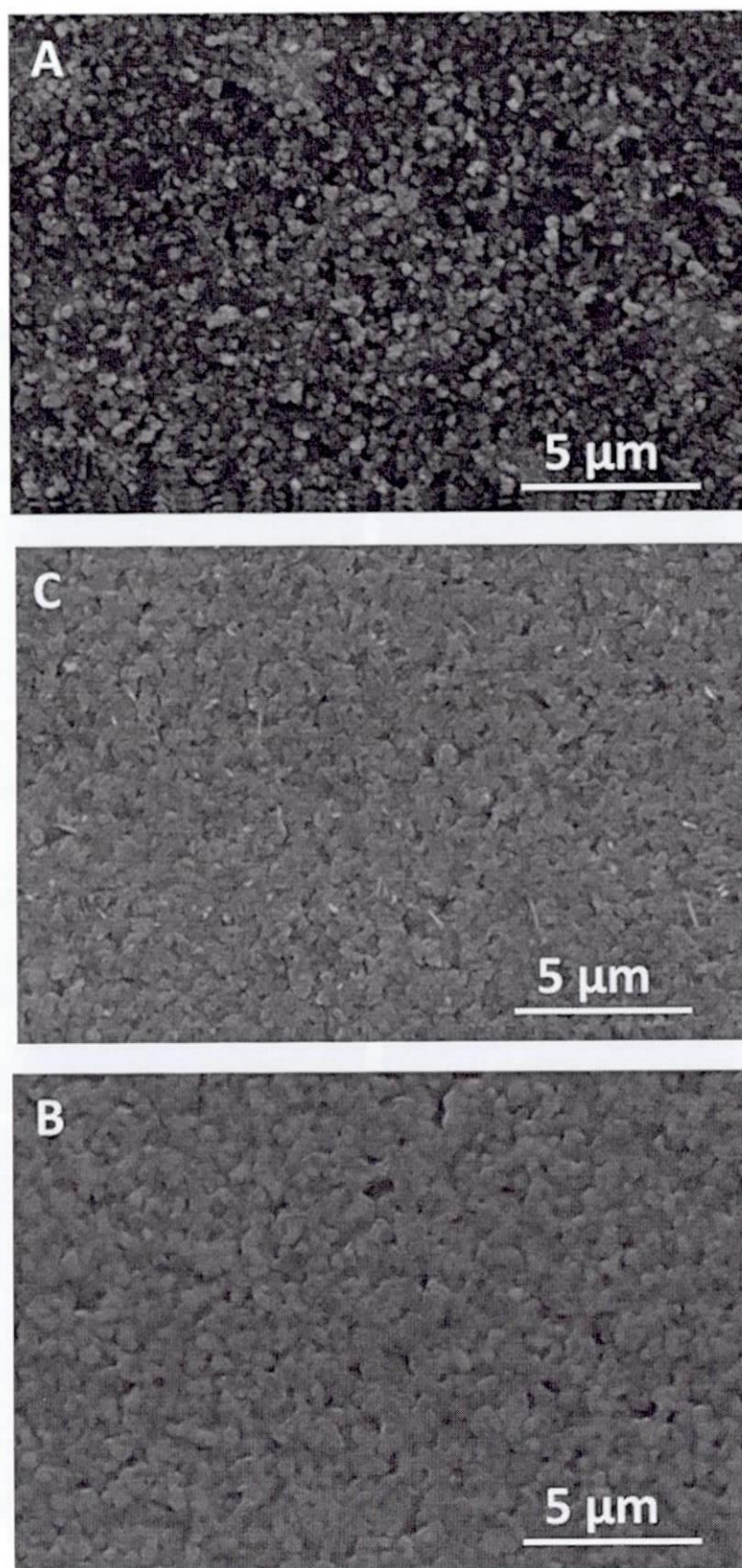
Figure 4.5 SEM images of the 600 nm thick evaporated copper films surface oxidized at (A) 450, (B) 550 and (C) 650 °C for 1 h in.

As shown in figure 4.4 (D) and (F) evaporated copper thin films after being oxidized in cylinder air with water vapor at 550 and 650 °C for 1 h, respectively, a large amount of oxide grains with size of about 500 nm were observed in the sample prepared at 550 °C. When the temperature rose to 650 °C, a large amount of oxide grains with non-uniform were also observed, its grain size ranging from 0.5 to 1.4 μm. The morphologies of grain size change, from small to big, as the oxidation temperature increases from 450 to 650 °C.

Figures 4.5 show the SEM images of the 600 nm thick evaporated copper thin films oxidized at (A) 450, (B) 550 and (C) 650 °C for 1 h in cylinder air with water vapor. A large amount of oxide grains with size of about 400 nm were also observed in the sample prepared at 450 °C. Comparing with the grains formed in the 300 nm thick sample (figure 4.4 (B), the grains formed in the 600 nm thick sample is more uniform and smaller. Figure 4.5 (B) shows that the sample prepared at 550 °C, have a large amount of oxide grains with uniform size. In this process the large oxide grains with size ranging from 400 to 600 nm are formed. When the temperature rose to 650 °C, the grain size don't increases obviously, but there is a very small amount of nanowire formed on the surface.

4.3.3. Optical properties

The optical parameters such as absorption coefficient and band gap are determined from optical absorption measurements. In the fundamental absorption region, the optical absorption coefficient (α) can be calculated using the following equation,

$$\alpha = \frac{1}{d} \ln \left[\frac{(1-R)^2}{T} \right] \qquad (4.1)$$

where d is the thickness of the films, R is reflectance and T is optical transmittance. Furthermore, the optical band gap E_g can be obtained,

$$\alpha h\nu = C(h\nu - Eg)^{1/2} \qquad (4.2)$$

where $h\nu$ is photon energy, C is proportionality constant which reflects the integrality of the crystal lattice.

The optical band gap of CuO thin films oxidized at various temperatures in cylinder air with water vapor were estimated using optical absorption data derived from optical measurements.
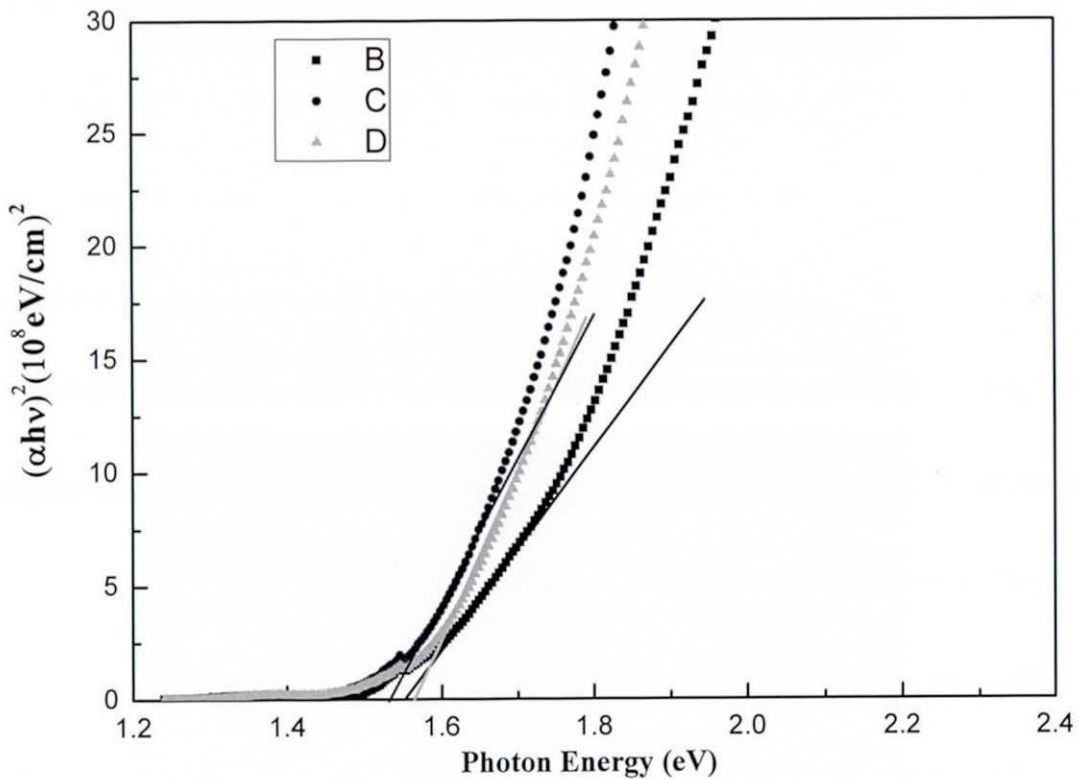
Figure 4.6 Plots of $(\alpha h\nu)^2$ versus $(h\nu)$ to determine the energy of the direct optical absorption edges for the 600 nm thick evaporated copper films oxidized at (A) 450, (B) 550 and (C) 650°C for 1 h in cylinder air with water vapor.

The copper oxide system is characterized by direct transition, so that the band values are obtained by extrapolating the linear portions of the plots (hv) versus $(\alpha hv)^{1/2}$ to the energy axis in Figure 4.6. The band gap values are estimated to be varying between 1.52 eV and 1.55 eV, which are in good agreement with literature values [15, 16] and corresponds to the band gaps of CuO phase [17]. However the Cu_2O phase was not detected by the X-ray diffraction and probably the presence of the amorphous component in the samples affect the band gaps of the films as shown in the amorphous component [18].

4.4. Conclusion

In the present work, we have successfully grown single CuO phase films in cylinder air with water vapor. The growth structural and optical properties of CuO films were investigated. It is observed that the diameter of oxide grain increases with increasing the oxidation temperature. X-ray diffraction studies indicate that the film is CuO phase and the only oxidation product. Furthermore, the optical gaps of cupric oxide films have been determined by the transmittance and reflectance spectra. It can serve as a starting material for studying Schottky or metal insulating semiconductor diodes with better characteristics based on contacts of CuO with various metals or compound semiconductors.

Reference

[1] Rakhshani, A. E. Solid-State Electron, 29 (1986) 7.

[2] Musa, A. O.; Akomolafe, T.; Carter, M. J. Sol. Energy Mater. Sol. Cells, 51 (1998) 305.

[3] Cox P A 1992 *Transition Metal Oxides: An Introduction to Their Electronic Structure and Properties*, Oxford University Press, NY, USA vol 20 P 296.

[4] Y.S. Gong, C.Lee, C.K. Yang, J.Appl.Phys. 77 (1995) 5422.

[5] Y.C. Zhou, J.A.Switzer, Mater.Res.Innovat.2 (1998) 22.

[6] A.B. Laurie, M.L. Norton, Mater. Res. Bull. 24 (1989) 213.

[7] A.B. Laurie, M.L. Norton, Mater. Res. Bull. 24 (1989) 1521.

[8] M. Ottosson, J.O. Carlsson, Surf.Coat.T echnol.78 (1996) 263.

[9] K.Santra, C.K.Sarkar, M.K.Mukherjee, B. Ghosh, Thin Solid Films 213 (1992) 226.

[10] V.F. Drobny, D.L. Pulfrey, Thin Solid Films 61 (1979) 89.

[11] R.Kita, K. Kawaguchi, T.Hase, T. Koga, R.Itti, T. Morishita, J.Mater . Res. 9 (1994) 1280.

[12] Y. Gong, C. Lee and C. Yang, J. Appl. Phys. 77 (1995) 5422.

[13] J. B. Liang, N. Kishi, T. Soga and T. Jimbo. Appl. Surf. Sci., 257 (2010) 62.

[14] L. S. Huang, S. G. Yang, T. Li, B. X. Gu, Y. W. Du, Y. N. Lu and S. Z. Shi. J. Cryst. Growth., 260 (2004) 130.

[15] T.J. Richardson, J.L. Slack, M.D. Rubin, Electrochromism of copper oxide thin films, presented at the 4th International meeting on Electrochromism, August 21–23, 2000, Uppsala, Sweden

[16] C. Guillen, J. Herrero, Sol. Energy Mater, 23 (1991) 31

[17] M.E. Abu-Zeid, A.E. Rakhshani, A.A. Al-Jassar, X.A.Youssef, Phys. Stat. Sol, A 93 (1986) 613

[18] J. Tauc, Amorphous and liquid semiconductors (New York,Plenum, 1974) Ch. 4

Chapter – 5 Thin cuprous oxide films prepared by thermal oxidation of copper foils with water vapor

5.1 Introduction

Cu_2O is spontaneously a p-type semiconductor since it contains negatively charged copper vacancies and probably interstitial oxygen [1]. Various attempts have been made to fabricate solar cells utilizing cuprous oxide as an active layer, because this semiconductor shows many interesting characteristics useful for solar cells production such as low cost, non-toxicity, good mobility, fairly high minority carrier diffusion length and direct band gap with a band gap of 2.1 eV. Although the theoretical limit of the energy conversion efficiency of a cuprous oxide based solar cell is about 20 % (just considering radiative recombination), the highest efficiency obtained up to now on this substrate is only 2 % [2]. Cuprous oxide thin films have been prepared by various techniques such as thermal oxidation [3-5], chemical vapor deposition [6], anodic oxidation [7], reactive sputtering [8], pulse laser deposition [9], electro-deposition [10] and plasma oxidation [11]. But thin films prepared by these methods are usually deposited on specific substrates, such as a quartz plates. In this paper we report a method to obtain self-supporting Cu_2O films with high quality. Cu_2O films can be obtained by using thermal oxidation of cupper foils with water vapor. Usually copper oxidized in air or oxygen produces two thermodynamically stable oxides, such as CuO and Cu_2O depending on the thermodynamic stability of the oxides [12]. But it is shown in this paper that only Cu_2O phase is formed when water vapor is used.

These will improve the study of electric junction in Cu_2O/Cu structure, and may hopefully lead to better rectifying junctions for use as photovoltaic cells with improved efficiency. The Cu_2O based Schottky diodes have been investigated by current-voltage (J-V) measurements.

5.2 Experimental details

Thin Cu_2O films have been synthesized by thermal oxidation of copper foils in air and water vapor. Experimental detail of oxidation in air as reported in [13]. Figure 2.1 shows the schematic diagram of the experimental setup for oxidation. The ultrasonic nebulizer is connected to quartz tube and N_2 gas cylinder. Copper foils (0.1 mm thick, 4N6) were used as substrates. The copper foils were cut into standard sizes of 1cm × 1cm. Foils were cleaned in dilute hydrochloric acid to remove the native oxide layer and adsorbed impurities and then washed with acetone, methanol, and deionized water under an ultrasonic bath for 5 min, respectively followed by drying with N_2 flow. The cleaned Cu substrate was placed onto a quartz boat. The quartz boat was positioned in the center of a quartz tube that is mounted in the middle of a horizontal tube furnace. One end of the quartz tube was attached to a nebulizer and other to the gas bubble. A flow of N_2 gas was introduced into the quartz tube at a flow rate of 1 L/min for 20 min to remove air from the system. Then flow rate was adjusted at 0.5 L/min. The tube furnace was heated to the set-point temperature–and gas flow of N_2 was kept at a rate of 0.5 L/min. The system was allowed to cool naturally to room temperature to prevent the thin film from cracking, caused by thermal stress and further oxidization in air if the film is directly taken out of the high temperature furnace. The substrate was pulled out of the furnace for further analysis. The crystal structure and phase composition

were identified by X-ray diffraction (XRD, Rigaku RINT-2100) using a 40 kV, 30 mA, Cu-Kα X-ray. A

scanning step of degree of 0.02° was applied to record the XRD patterns in the 2θ range of degree of 20 -

60°. The morphology of the Cu_2O was characterized by scanning electron microscope (SEM, Hitachi

S-3000H) operated at 15 kV. Cu_2O based Schottky diodes were fabricated to characterize electrical

properties of the thin films. As Cu_2O is a p-type semiconductor [14], Au and Cu were used as ohmic and

schottky contact materials, respectively. Au (100 nm) was deposit on the surface of Cu_2O thin films

prepared at 800 °C in water vapor. The oxide layer of the other side was removed by polishing to expose

the surface of the copper foil. The exposed copper was used as a schottky electrode. The current-voltage

(J-V) characteristics of the Au / Cu_2O / Cu diodes were measured using a semiconductor parameter

analyzer.

5.3 Results and discussion

5.3.1. Growth of Cu_2O thin films by thermal oxidation with water vapor

Figures 5.1(A) and (B) show the SEM images of the copper thin films after being heated in air

and water vapor at 700 °C for 2 h, respectively. Figure 5.1 (A) shows that CuO nanowires are formed on

the surface of the cupper foils annealed in air [13]. On the other hands, as shown in figure 5.1(B), Cu_2O

thin films having rugged rock like morphology are obtained by thermal oxidation in water vapor. In order

to study the influence of the oxidation temperature on the growth of Cu_2O thin film in water vapor, three

samples have been prepared at 700, 800 and 900 °C for 2 h, as shown in figures 5.2 (A) – (C). A large

amount of oxide grains with size of about 3 μm were observed in the sample prepared at 700 °C. Figure

5.2 (B) shows that the sample prepared at 800 °C, which has a large amount of oxide grains with non

uniform size. In this process the large oxide grains with size ranging from 2 to 12 μm are formed. As

shown in figure 5. 2(C), the oxide of about 15 μm grain sizes were observed in the sample prepared at

900 °C. From the morphology of these samples, it is observed that the size of oxide grain increases with

increasing the oxidation temperature. A SEM cross-section image of the sample heated at 700 °C reveals

that the sample consists of two layers as shown in Figure 5.2(D). The top layer is a Cu_2O thin layer with

thickness of about 5 μm that lies directly above the copper substrate. When the temperature rose to 800

and 900 °C, the thickness of Cu_2O layers were found about 5.8 and 6.7 μm, respectively. However, when

copper thin film is oxidized in air, the major product is Cu_2O, and then CuO is formed through a second

step of oxidation of Cu_2O [13].
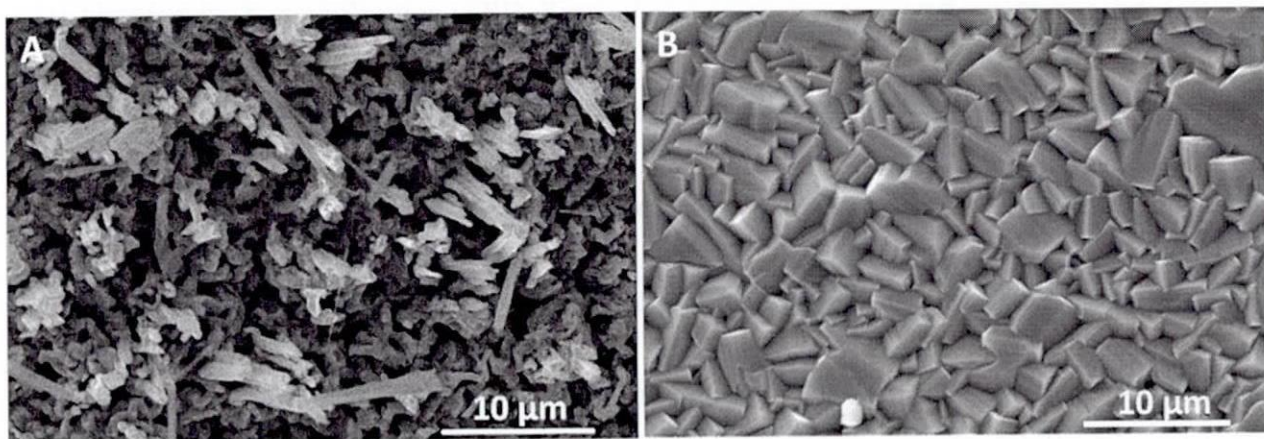
Figure 5.1 SEM images of the sample surface oxidized at 700 for 2 h: (A) in air and (B) in water vapor.
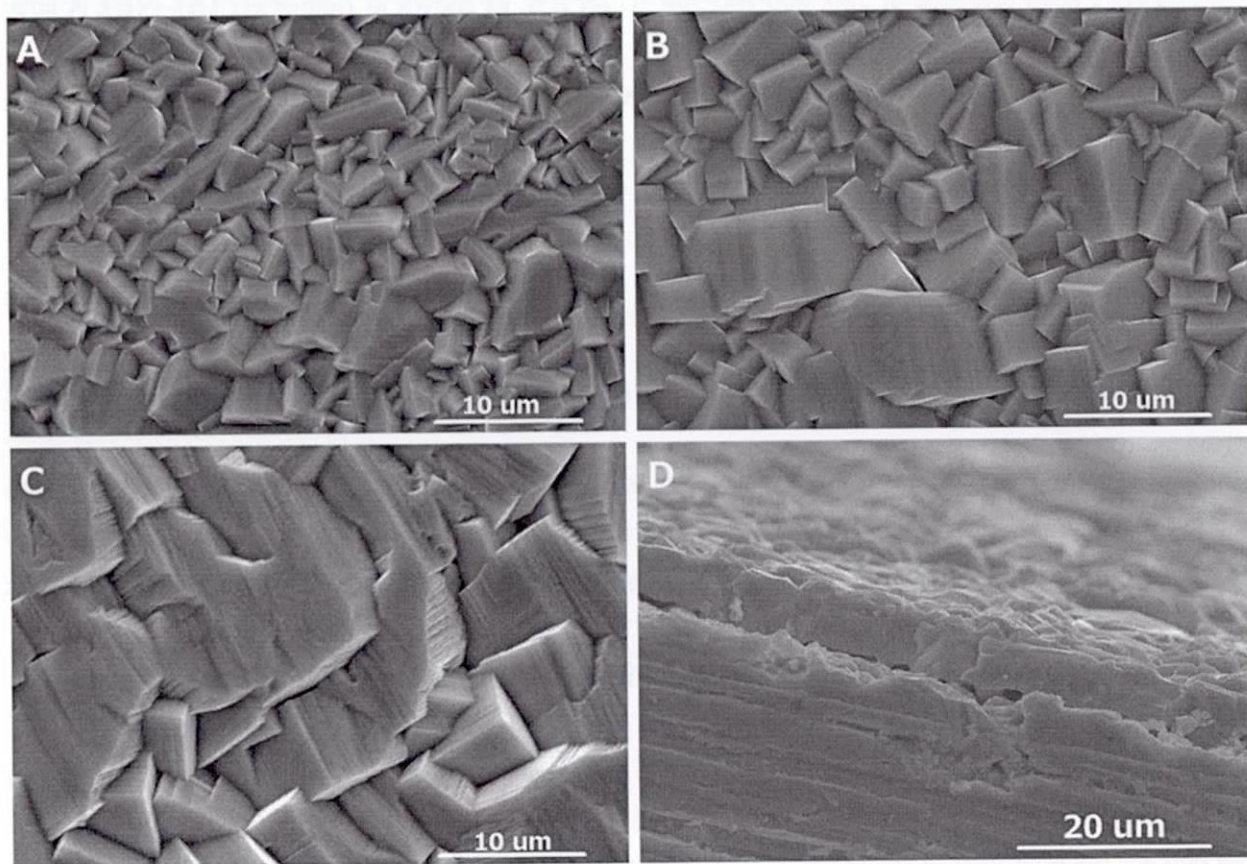
Figure 5.2 SEM images of the sample surface oxidized at (A) 700, (B) 800 and (C) 900 °C for 2 h in water vapor. (D) SEM image of cross-section of the sample oxidized at 700 °C for 2 h in water vapor
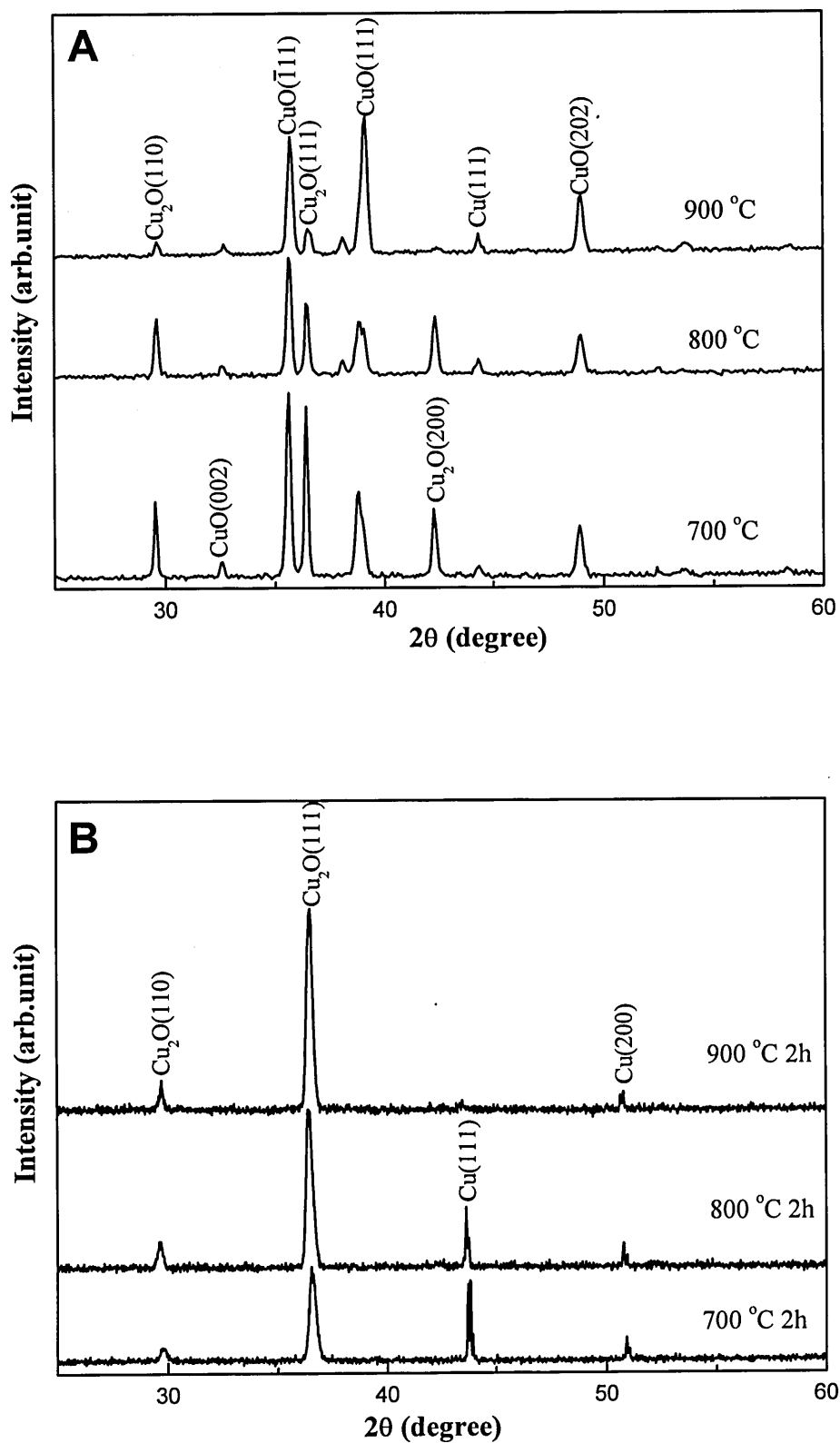
Figure 5.3 XRD patterns of the sample oxidized in air (A) and water vapor (B) at 700, 800 and 900 °C for 2 h.

5.3.2. XRD characterization of Cu_2O thin films

Figure 5.3 (A) shows the XRD pattern of the samples oxidized at 700, 800 and 900 °C for 2 h in air [13]. In this case, both Cu_2O and CuO phases are present when copper substrates are oxidized in air. XRD peak at $2\theta = 35.5°$ and $2\theta = 38.7°$ can be readily indexed as ($\bar{1}$ 11) and (111) crystal plane of monoclinic CuO. These two peaks become stronger with increasing the heating temperature. But (111) plane of Cu_2O becomes weak while CuO is formed through a second step of oxidation of Cu_2O. Other weak peaks corresponding to Cu_2O and CuO phases have also been observed. When the temperature rose to 900 °C, CuO became the main oxidation product with a small Cu_2O peak. This indicates a conversion from Cu_2O to CuO, and this is also confirmed by the fact that the colors of the samples changed from brick red (Cu_2O) to black (CuO). However, as shown in figure 5.3 (B), only Cu_2O phase is observed after the oxidation of samples at 700, 800 and 900 °C for 2 h with water vapor. The XRD results show that Cu_2O is the only oxidation products with a small amount of Cu after the oxidation at 700 and 800 °C. XRD peak at $2\theta = 36.3°$ and $2\theta = 29.7°$ corresponding to (111) and (110) plane of cubic Cu_2O structure, in addition (111) plane is the most prominent peak in the sample. The weak two peaks at $2\theta = 43.8°$ and $2\theta = 50.9°$ can be readily indexed as (111) and (200) crystal plane of cubic Cu. When the temperature rose to 900 °C, most of copper phases were oxidized. This indicates a conversion from copper to cuprous oxide which is evidenced by a color change from reddish brown color (Cu) to brick red (Cu_2O). Cu_2O can be obtained by oxidation in water vapor at higher temperature.

The oxygen partial pressure affects the oxide growth; when it's higher than the dissociation

pressure of Cu_2O and CuO. In this case mixture of Cu_2O and CuO may be formed. Water vapor's oxygen partial pressure is higher than the dissociation pressure of Cu_2O, but lower than the dissociation pressure of CuO. Therefore, only Cu_2O can be formed. Copper foil oxidized in air or oxygen forms two thermodynamically stable oxides CuO and Cu_2O [3-5]. Liang et al. reported a copper foil is oxidized in air at low temperature; the majority of copper foil is converted into Cu_2O with only a small amount of CuO on the surface in the form of nanowires [13]. Huang et al. reported CuO nanowires are formed at 300 °C in oxygen by thermal oxidation of copper foils [15]. In most of these studies, a mixture of CuO and Cu_2O phase is generally obtained. This is due to the environmental oxygen partial pressure is higher than the dissociation pressure of Cu_2O and CuO. The Cu-O phase diagram [16] shows that two types of oxide, Cu_2O and CuO may form during oxidation. Thermodynamically oxides form only if the ambient oxygen partial pressure is larger than the dissociation pressure of the oxide in equilibrium with Cu.

5.3.3. J-V characteristic of Cu_2O based diodes

Figure 5.4 shows the *J-V* characteristic of an $Au/Cu_2O/Cu$ Schottky diode. The dark J-V date shows a typical rectification behavior. The most common theory of Schottky barrier diode is based on the thermionic emission and according to this model, the current voltage relationship is given by;

$$I = I_S \left(exp \left(\frac{qV}{nkT} \right) - 1 \right) \qquad (5.1)$$

Where q is the electronic charge, V the voltage applied across the diode, k the Boltzmann constant, and T the absolute temperature, I_s the reserve saturation current and can be expressed by

$$I_S = SA^{**}T^2 exp \left(-\frac{q\emptyset_B}{kT} \right) \qquad (5.2)$$

Where S is the effective area of the diode, $A^{**}(= 100 \text{ A cm}^{-2} \text{ K}^{-2})$ is the Richardson constant [17], and $\emptyset_B$ is the Schottky barrier height of the diode. For the case of the diode with a high series resistance and

ideality factor, the relation between the applied forward bias V and the current I can be written as [18],

$$I = I_S \left[exp \left(\frac{q(V - IR_S)}{nkT} \right) \right]$$ (5.3)

When $V > 3kT/q$ [19]. A method to extract the series resistance Rs of ideal Schottky diode was first proposed by Norde [19].
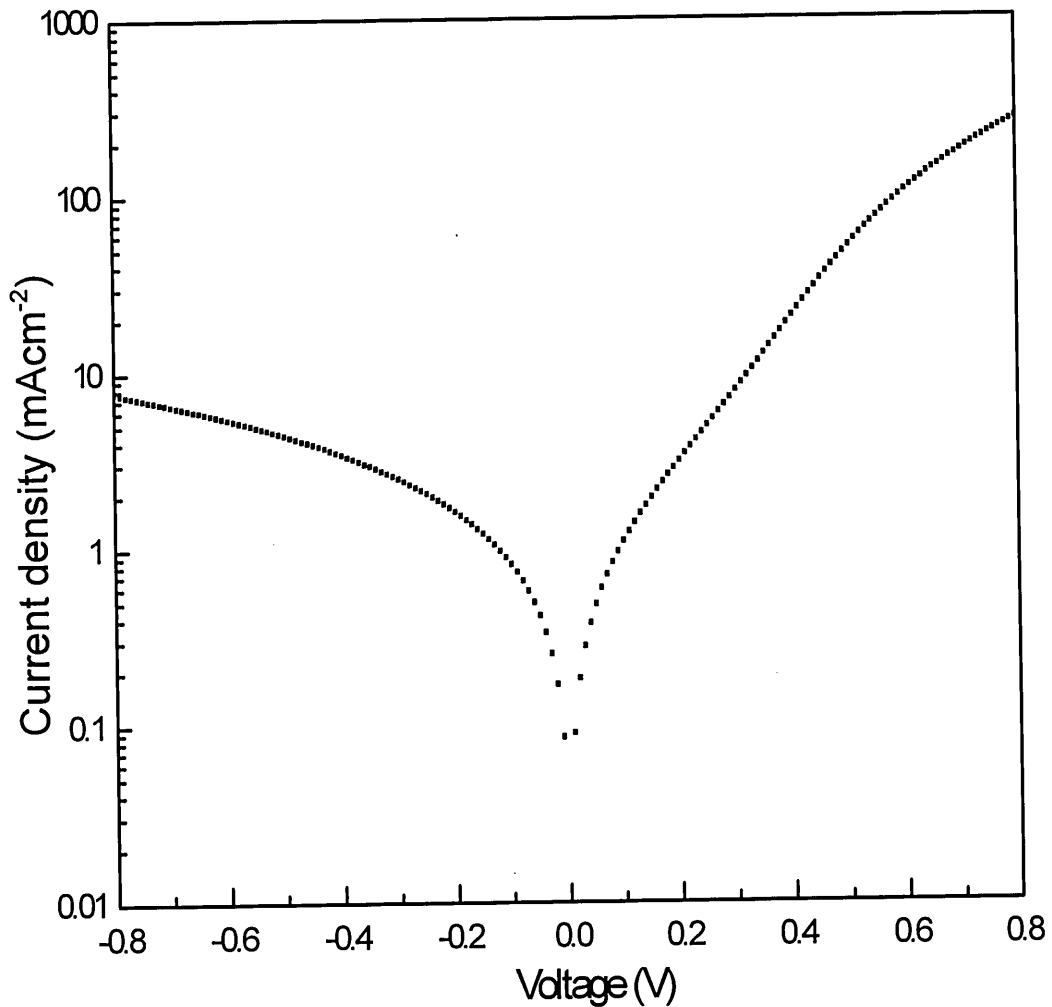
Figure 5.4 Current-voltage characteristics of an Au/Cu₂O/Cu diode.

Cheung [20] modified Norde's approach to extract the values of n and R_s from the forward bias I-V data of any Schottky diode. Equation (4) can be rewritten in terms of current density J (= I/S). Thus,

$$V = R_S SJ + n\emptyset_B + \frac{n}{\beta} \log \left(\frac{J}{A^{**}T^2} \right), \qquad (5.4)$$

Where

$$\beta = q/kT. \qquad (5.5)$$

Differentiating equation (5) with respect to J and rearranging terms, we obtain

$$\frac{dV}{d(logJ)} = R_S SJ + \frac{n}{\beta} \qquad (5.6)$$

Thus, a plot of dV / d (logJ) vs J will give R_sS as the slope and n/β as the y-axis intercept. The diode parameter obtained with an electrode area of $0.01 cm^2$ were $R_s = 20\ \Omega$ and a saturated reverse current density $J_s = 0.33\ mA/cm^2$ with a diode factor n = 3.8. The measured value of n is larger than two and therefore tunneling, recombination and generation currents in the depletion region and recombination through interface states at the Cu_2O/Cu junction are expected to play important roles [21].

5.4 Conclusion

In the present work, we developed a process to prepare Cu_2O films and studied the properties of the films. Cu_2O thin films were formed in water vapor in which the oxygen pressure was less than the dissociation pressure of CuO. It was observed that the diameter of oxide grain increased with increasing the oxidation temperature. X-ray diffraction studies indicated that the film was Cu_2O, the only oxidation products and cupric oxide (CuO) phase was absent. The current-voltage characteristics of the $Au/Cu_2O/Cu$ diodes exhibit rectification. The method is recommended as a fairly easy way for the fabrication of Cu_2O films. It can serve as a starting material for studying Schottky or metal insulating semiconductor diodes with better characteristics based on contacts of Cu_2O with various metals or compound semiconductors.

Reference

[1] O. Porat, I. Riess, Solid State Ionics 81 (1995) 29.

[2] A. Mittiga, E. Salza, F. Sarto, M. Tucci and R. Vasanthi, Appl. Phys. Lett. 88 (2006) 163502.

[3] Y. Gong, C. Lee and C. Yang, J. Appl. Phys. 77 (1995) 5422.

[4] A. O. Musa, T. Akomolafe and M. J. Carter, Sol. Energy Mater. Sol. Cells 51 (1998) 305.

[5] J. H. Part, K. Natesan, Oxid. Met 39 (1963) 411.

[6] T. Maruyama, Sol. Energy Mater. Sol. Cells 56 (1998) 85.

[7] M. Masui, T. Muranoi, R. Urao, Y. Momose, M.R. Islam, M. Takeuchi, Mater. Chem. Phys. 43

(1996) 283.

[8] M. Smith, V. Gotovac, Lj. Aljinovic, M. Lucic-Lavcevic, Surf. Sci. 335 (1995) 171.

[9] T. Mahalingam, J.S.P. Chitra, S. Rajendran, P.J. Sebastian, Semicond. Sci. Technol. 17 (2002) 565.

[10] T.J. Richardson, J.L. Slack, M.D. Rubin, Electrochim. Acta 46 (2001) 2281.

[11] C.A.N. Fernando, P.H.C. de Silva, S.K. Wethasinha, I.M. Dharmadas, T. Delsol, M.C. Simmonds,

Renewable Energy 26 (2002) 521.

[12] W.J. Tomlinson, J. Yates, J. Phys. Chem. Solids 38 (1977) 1205.

[13] J. B. Liang, N. Kishi, T. Soga, T. Jimbo, Appl. Surf. Sci. 257 (2010) 62.

[14] J. Herion, E.A Niekisch, G. Scharl, Sol. Energy Mater. 4 (1980) 101

[15] L S Huang, S G Yang, T Li, B X Gu, Y W Du, Y N Lu, S Z Shi, J. Cryst. Growth 260 (2004) 130.

[16] T.B. Massalski, Binary Alloy Phase Diagrams, second edn., vol. 2, ASM International, USA, 1990

[17] E.S. Ikata and S.K. Adjepong, J, Phys. D: App. Phys. 21 (1988) 1516

[18] Norde, H,Journal of Applied Physics 50 (7): (1979) 5052.

[19] Sze, S. M., "Physics of Semiconductor Devices 2nd ed.", John Wiley & Sons, New York, (1981) 362.

[20] S.K. Cheung and N.W. Cheung, Appl. Phys. Lett. 49 (1986) 85

[21] V.P. Singh, J.C. McClure, Sol. Energy. Mater. Sol. Cells 76 (2003) 369

Chapter – 6 Growth of high-quality (111) oriented cuprous oxide thin films oxidized in water vapor

6.1 Introduction

Cu_2O is a p-type semiconductor with a direct band gap of 2.1 eV; it contains negatively charged copper vacancies and probably interstitial oxygen [1]. There has been much interest in Cu_2O, since this semiconductor shows many interesting characteristics useful for solar cells production such as low cost, non-toxicity, good mobility, fairly high minority carrier diffusion length. Various attempts have been made to fabricate solar cells utilizing cuprous oxide as an active layer. Although the theoretical limit of the energy conversion efficiency of a cuprous oxide solar cell is about 20 %, the highest efficiency obtained up to now on this substrate is 3.83 % [2]. During the past years, in order to obtain high quality cuprous oxide films, it have been prepared by various techniques such as thermal oxidation [3-5], chemical vapor deposition [6], anodic oxidation [7], reactive sputtering [8], electro-deposition [9] have been used. Among various methods employed for the preparation of Cu_2O films, Cu_2O thin films by thermal oxidation at low temperature are an inexpensive and convenient method. However, copper foil oxidized in air or oxygen forms two thermodynamically stable oxides CuO and Cu_2O [3-5]. A copper foil is oxidized in air at 400 and 500 °C, the majority of copper foil converted into Cu_2O with only a small amount of CuO on the surface in the form of nanowires [10]. Huang et al reported CuO nanowires formed at 300 °C in oxygen by thermal oxidation of copper foils [11]. Therefore, the production of single phase

Cu_2O phase is difficult by thermal oxidation of copper foils in air and oxygen.

Here, we develop a new method to obtain (111) oriented single phase Cu_2O thin film with high quality. For the thermal oxidation of copper foils in water vapor, only Cu_2O phase is formed. We report the success of using copper foils and the evaporated copper substrates on the quartz glass to form Cu_2O films with water vapor and conduct a detailed structural and optical investigation of Cu_2O films.

6.2 Experimental details

Thin Cu_2O films have been synthesized by thermal oxidation of copper foils in air and water vapor. For the thermal oxidation of copper foils in air as reported in [8,10]. For the thermal oxidation of copper foils in water vapor, copper foils are adequately cleaned with acetone, methanol, and deionized water under an ultrasonic bath for 5 min and blow dried with N_2 flow. The cleaned sample is placed onto a quartz boat. The quartz boat is positioned in the center of a quartz tube that is mounted in the middle of a horizontal tube furnace. The one end of the quartz tube was attached to a nebulizer and other to the gas bubbler. Water vapor is obtained by passing N_2 gas through water vapor in a nebulizer. A flow of high purity N_2 gas is first introduced into the quartz tube at a flow rate of 1 L/min for 20 min to remove air from the system, and then this is adjusted to 0.5 L/min. The oxidation was carried out at 700, 800 and 900 °C for 2 h in water vapor. After being held at the set-point temperature, the N_2 gas flow is kept at a rate of 0.5 L/min. The system is allowed to cool naturally to room temperature to prevent the thin film from further oxidized in air if the film is directly taken out of the high temperature furnace. The samples are directly subjected to characterization by X-ray diffraction (XRD, Rigaku RINT-2100) using a 40 kV,

30 mA, Cu-Kα X-ray. The morphology of the Cu_2O was characterized by scanning electron microscope

(SEM, Hitachi S-3000H) operated at 15 kV. In order to determine the optical band gap of Cu_2O thin films,

500 nm thick copper films evaporated on the quartz substrate by the thermal vacuum evaporator were

used. Optical studies were carried out with a UV/VIS/NIR spectrophotometer (JASCO V-570). The

copper foils were oxidized in air with changing the temperature for comparison [8]. In this case, one end

of the furnace is opened to the atmosphere.

6.3 Results and discussion

6.3.1. Surface morphologies

Figure 6.1 show the SEM images of the samples after being heated in air and in water vapor at

700, 800 and 900 °C, respectively. Figure 6.1 (A) shows that the SEM image of the sample after being

oxidized in air at 700 °C for 2 h. It is observed that a few nanowires formed on the substrate with

diameter of the nanowires about 500 nm [8]. After 2 h oxidized at 800 °C, no nanowires are observed in

the sample in figure 6.1 (C), but large oxide grains are formed with big hole on the substrate which are

composed of several small crystal grains. When the substrate temperature reaches 900 °C, the grain size

increases obviously with more porous nature of the surface in figure 6.1 (E). In comparison with heating

in air, heating in water vapor produces homogeneous surface with high density grains. As shown in figure

6.1 (B), (D) and (F) copper thin films after being oxidized in water vapor at 700, 800 and 900 °C for 2 h,

respectively, a large amount of oxide grains with size of about 2 μm were observed in the sample

prepared at 700 °C which has homogeneous surface morphology. Figure 6.1 (D) shows that the sample

prepared at 800 °C, a large amount of oxide grains with non-uniform were also observed, it's grain size

ranging from 1.5 to 14 μm. When the temperature rose to 900 °C, the bigger oxide grain size of about 17

μm were observed in the sample as shown in figure 6.1 (F). The morphologies of grain size change, from

small to big, as the oxidation temperature increases from 700 to 900 °C.
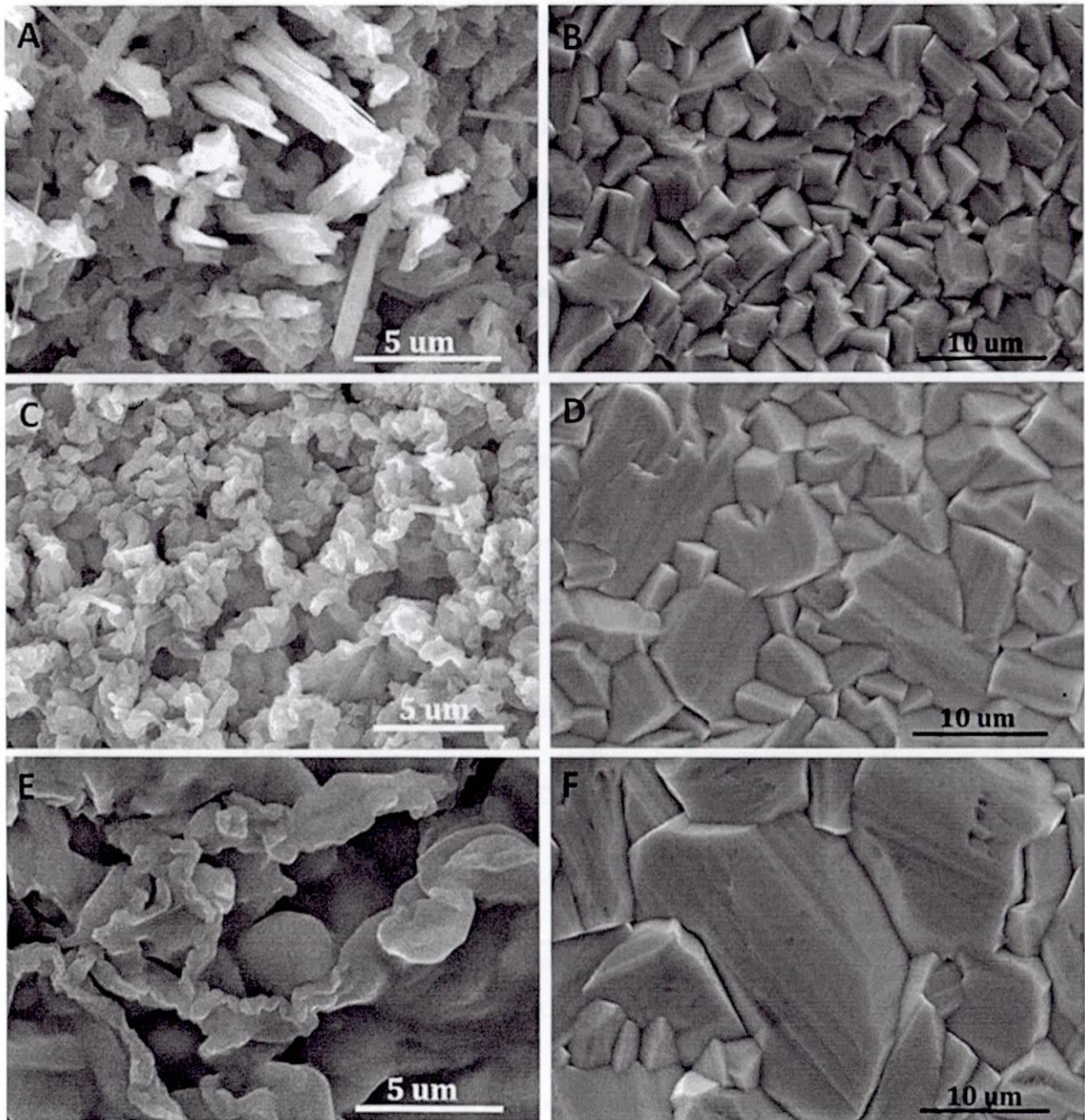
Figure 6.1 SEM images of the sample surface oxidized at (A) 700, (C) 800 and ((E) 900 °C for 2 h in air and at (B) 700, (D) 800 and (F) 900 °C for 2 h in water vapor.
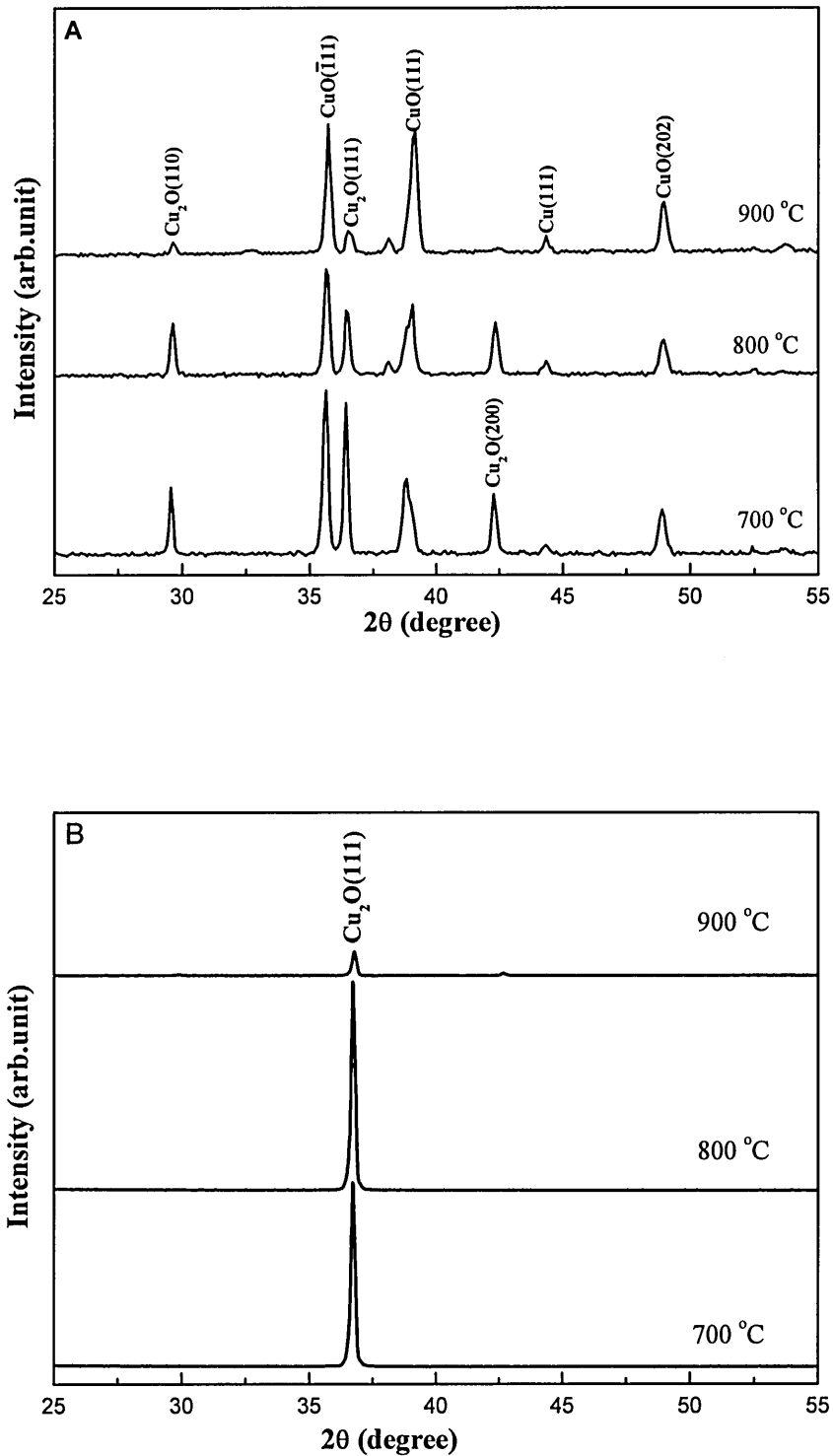
Figure 6.2 XRD patterns of the sample oxidized at 700, 800 and 900 °C for 2 h (A) in air and (B) in water vapor.

6.3.2. XRD characterization of Cu$_2$O thin films

Figure 6.2 (A) shows the XRD pattern of the samples oxidized at 700, 800 and 900 °C for 2 h in air. The XRD results show that CuO is the main oxidation products with a small amount of Cu$_2$O. XRD peak at $2\theta = 35.5°$ and $2\theta = 38.7°$ corresponding to ($\bar{1}11$) and (111) plane of monoclinic CuO structure. These two peaks become strong with increasing the heating temperature. The weak two peaks at $2\theta = 29.7°$ and $2\theta = 36.3°$ can be readily indexed as (110) and (111) plane of cubic Cu$_2$O structure. However, these two peaks become weak with increasing the oxidation temperature. This indicates a conversion from Cu$_2$O to CuO. In comparison with oxidation in air, oxidation in water vapor has higher crystal quality. Figure 6.2 (B) shows the XRD pattern of the samples oxidized at 700, 800 and 900 °C for 2 h in water vapor. Figure 6.2 (B) shows XRD data that exhibits sharp Bragg peaks indicating highly crystalline and single phase nature of the sample. The diffraction peak located at $2\theta = 36.3°$ correspond to (111) peak of Cu$_2$O. It means (111) peak is the only one peak in the samples and Cu$_2$O is the only oxidation products after oxidized in water vapor. As the oxidation temperature reaches 900 °C, the (111) peak became weaker in water vapor. In figure 6.2 (A), both Cu$_2$O and CuO phases are present when the samples are oxidized at high temperature in air. However, in figure 6.2 (B), only Cu$_2$O is observed after copper film is oxidized at high temperature in water vapor. The results show that the single phase Cu$_2$O thin film grown in water vapor is high crystal quality as compared with oxidation in air. According to the bulk phase diagram [12], Cu$_2$O and CuO can form if the ambient oxygen partial pressure is larger than the dissociation pressure of two types of the oxide in equilibrium with copper. When copper film oxidized in

air the environmental oxygen partial pressure is higher than the dissociation pressure of Cu_2O and CuO.

Therefore, two types of oxide can be formed in air [8-10]. However, copper film oxidized by a N_2 gas

flow with water vapor is able to keep relatively low oxygen partial pressure near film that the higher and

pure Cu_2O films can be obtained. This is consistent with our results that only Cu_2O and not CuO are

formed on samples oxidation in water vapor. These processes are also consistent with the bulk phase

diagram.
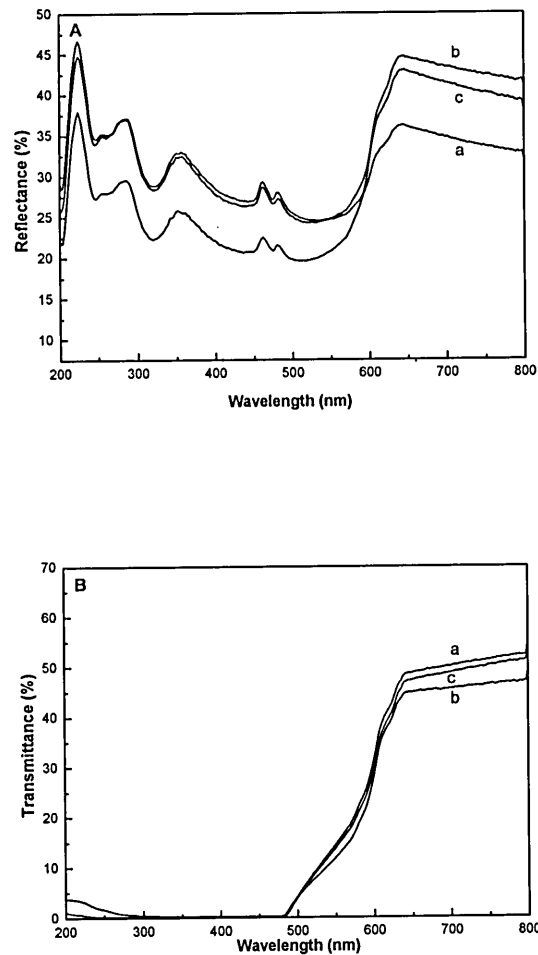
Figure 6.3 Optical reflectance (A) and transmission spectrums (B) of the deposited copper thin films oxidized at (a) 700, (b) 800 and (c) 900 °C for 6 h in water vapor.
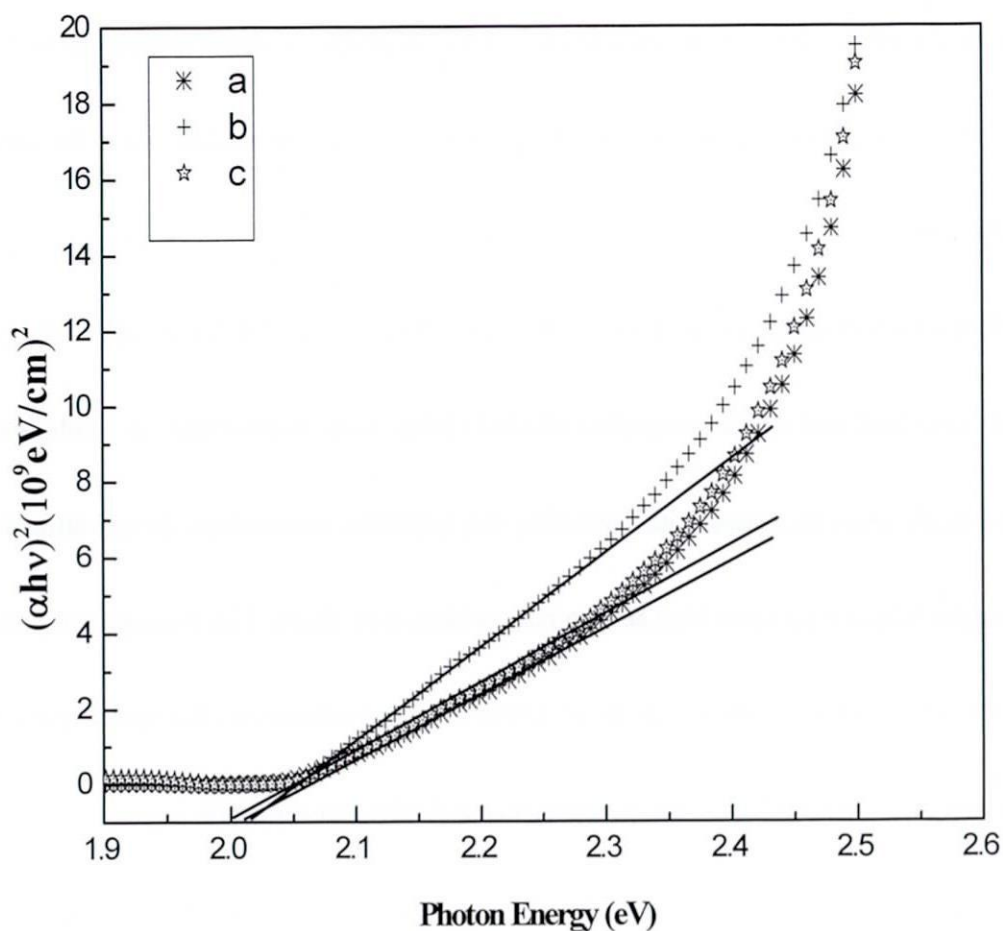
Figure 6.4 Plots of $(\alpha h\nu)^2$ versus $(h\nu)$ to determine the energy of the direct optical absorption edges for Cu_2O films oxidized at (a) 700, (b) 800 and (c) 900°C.

6.3.3. Optical properties

The transmission and reflection spectra were measured for Cu_2O thin films after being heated in water vapor at (a) 700, (b) 800 and (c) 900 °C for 6 h. The optical transmittance (T) and reflectance (R) spectra are shown in Figure 6.3 (a) and (b), respectively. In the fundamental absorption region, the optical absorption coefficient (α) can be calculated from the T and R data using the equation (4.1). Furthermore, the optical band gap Eg can be obtained by using the equation (4.2). The relationship of $(\alpha h\nu)^2$ and photon

energy (hv) is shown in Figure 6.4. Using the linear extrapolation method, the values of E_g are determined

to be 2.01 eV, 2.0 eV and 2.02 eV for samples a, b and c, respectively, which are similar to other reports

on cuprous oxide films [13]. The observed band gap does not depend on particle size in the current study.

6.4 Conclusions

In the present work, we have successfully grown (111) oriented Cu_2O films with water vapor.

The growth structural and optical properties of Cu_2O films were investigated. It is observed that the

diameter of oxide grain increases with increasing the oxidation temperature. X-ray diffraction studies

indicate that the film is Cu_2O and Cu_2O is the only oxidation products. The films grown in water vapor

shows a (111) preferred orientation with much better crystal. Furthermore, the optical gaps of cuprous

oxide films have been determined by the transmittance and reflectance spectra.

References

[1] O. Porat and I. Riess. Solid State Ionics, 81 (1995) 29.

[2] T. Minami, Y. Nishi, T. Miyata and J. Nomoto. Applied Physics Express, 4 (2011) 062301.

[3] Y. Gong, C. Lee and C. Yang. J. Appl. Phys., 77 (1995) 5422.

[4] A. O. Musa, T. Akomolafe and M. J. Carter. Sol. Energy. Mater. Sol. Cells., 51 (1998) 305.

[5] J. H. Part and K. Natesan. Oxidation of Metals, 39 (1993) 411.

[6] T. Maruyama. Sol. Energy Mater. Sol. Cells., 56 (1998) 85.

[7] M. Masui, T. Muranoi, R. Urao, Y. Momose, M. R. Islam and M. Takeuchi. Mater. Chem. Phys., 43 (1996) 283.

[8] M. Smith, V. Gotovac, L. Aljinovic and M. Lucic-Lavcevic. Surf. Sci., 335 (1995) 171.

[9] T. Mahalingam, J. S. P. Chitra, S. Rajendran and P. J. Sebastian. Semicond. Sci. Technol., 17 (2002) 565.

[10] J. B. Liang, N. Kishi, T. Soga and T. Jimbo. Appl. Surf. Sci., 257 (2010) 62.

[11] L. S. Huang, S. G. Yang, T. Li, B. X. Gu, Y. W. Du, Y. N. Lu, S. Z. Shi. J. Cryst. Growth., 260 (2004) 130.

[12] T. B. Massalski, Binary Alloy Phase Diagrams, second edn., vol. 2, ASM International, USA, 1990.

[13] J. F. Pierson, A. Thobor-Keck and A. Billard. Appl. Surf. Sci., 210 (2003) 359.

Chapter – 7 Conclusion

7.1 Conclusion of this work

There is a long standing need for cheap and clean energy sources as the world population continues to increase with increasing energy consumption per person. Use of fossil fuels and unclear plants in an increasing rate to meet the energy demand poses a serious threat to environment as well as to their availability. A frequently mentioned solution to the problem of increasing requirements for energy and dwindling energy sources is to tap the energy in sunlight. The solar energy falling on the earth's surface each year is over 2,000 times the amount presently required by the human race, making for a seemingly inexhaustible supply. Until now, solar cells are regarded as the prime candidate for solar energy conversion for effective utilization by human civilization. However, the various solar cells fabricated to date are far too expensive to use on a commercial basis. With respect to present high efficient solar cell materials, cupric oxide nanowire is a material of highly stable, cheap, non-toxic which can be obtained from precursors those are sufficiently available in nature. It is a potential candidate for cheap solar cell material.

CuO nanowires have been synthesized by heating a Cu foil in an ambient condition. The copper foil samples were oxidized in air between 300 and 800 °C. The diameters of nanowires can be controlled by changing the annealing temperature. The morphology, composition, and structure were analyzed by using X-Ray Diffraction (XRD) and Scanning Electron Microscope (SEM). Increasing the oxidation

temperature may produce a reduction in the density, but increase in the diameter and strength of the nanowires, causing them to adopt a straight morphology. It is observed that the aspect ratio and number density of these nanowires are critical functions of various growth parameters, namely, the annealing time and the annealing temperature. While the annealing temperature affect both the aspect ratio and number density, the main effect of the annealing time is on the aspect ratio of these nanowires. The EDX measurements indicate that the growth process began with the formation of thin layer of Cu_2O, then thick layer of CuO and finally, nanowires are grown on the CuO. Moreover, from TEM analysis, the CuO nanowires exhibited bi-crystalline property with monoclinic structure.

The effects of copper foils with the smaller grain size, (200) oriented and surface roughness was systematically investigated on the growth of cupric oxide nanowires. Long, high density and aligned cupric oxide nanowires have been synthesized by heating copper foils with the smaller grain size and (200) oriented in static air. Annealing copper thin foil in static air produce large area, uniform and vertically aligned nanowires along the thin film surface. Long and aligned nanowires can only be formed within a narrow temperature range from 500 to 600 °C, with diameters between 80 and 160 nm. On the other hand, uniform and aligned nanowires cannot be obtained by annealing copper foils with the bigger grain size and two crystal orientations. The difference is attributed to faster the relaxation of compress stress by outward diffusion of copper ions and inward diffusion of oxygen along the grain boundaries (both in the metal and in the layer for the smaller grain size of copper substrate). We have studied how different the surface roughness of substrates affects the growth of cupric oxide nanowires. It is observed

that the growth of nanowires do not depend on the surface roughness of substrates, only the grain size of copper affects the growth of nanowires. The small grain size of the copper foil is favorable to the growth of nanowires due to the larger number of grain boundaries.

Single CuO phase films were prepared by thermal oxidation of copper thin films evaporated onto quartz substrate in cylinder air with water vapor. It was found that in cylinder air with water vapor single CuO phase are formed, whereas mixture of random oriented CuO and Cu_2O are formed when oxidized in atmospheric air. The growth structural and optical properties of CuO films were investigated. It is observed that the diameter of oxide grain increases with increasing the oxidation temperature. X-ray diffraction studies indicate that the film is CuO phase and the only oxidation product. Furthermore, the optical gaps of cupric oxide films have been determined by the transmittance and reflectance spectra. It can serve as a starting material for studying Schottky or metal insulating semiconductor diodes with better characteristics based on contacts of CuO with various metals or compound semiconductors.

High quality crystals of cuprous oxide thin films were synthesized on copper substrates by thermal oxidation of copper foils with water vapor. This method proved to be good for preparing cuprous oxide films with high purity and large grain size. X-ray diffraction studies revealed the formation of Cu_2O films with (111) and (110) peaks. From the SEM images it is observed that the size of oxide grain increases with increasing the oxidation temperature. The top layer of the sample is a Cu_2O thin layer with thickness of about 5 μm that lies directly above the copper substrate heated at 700 °C. The films grown in water vapor shows a (111) preferred orientation with much better crystal. Furthermore, the optical gaps of

cuprous oxide films have been determined by the transmittance and reflectance spectra. The current-voltage characteristics of the Au/Cu$_2$O/Cu diodes exhibit rectification. The method is recommended as a fairly easy way for the fabrication of Cu$_2$O films. It can serve as a starting material for studying Schottky or metal insulating semiconductor diodes with better characteristics based on contacts of Cu$_2$O with various metals or compound semiconductors.

7.2 Suggestion of the future work

CuO nanowires still belong to the experimental world of laboratories. However, they may complement or replace carbon nanotubes in some applications. Some early experiments have shown how they can be used to build the next generation of computing devices. To create active electronic elements, the first key step was to chemically dope a semiconductor nanowire. This has already been done to individual nanowires to create p-type and n-type semiconductors. The next step was to find a way to create a p-n junction, one of the simplest electronic devices. The main objective of this dissertation is aimed at fabrication of solar cell from cupric oxide nanowires which can be carry out as its bulk and thin film properties showed to be suitable for solar cell and because of very low cost, non-toxie nature, stability and availability of this material, probability of homojunction from n-type zinc oxide with p-type cupric oxide nanowires device will be the ultimate future scope of this work.

Acknowledgement

necessary facilities for carrying out this research.

List of publication

[1] Cross-sectional characterization of Cupric Oxide Nanowires grown by Thermal Oxidation of Copper

Foils

JianBo Liang, Naoki Kishi, Tetsuo Soga, Takashi Jimbo:

Applied Surface Science 257 (2010) 62 ~ 66.

[2] Synthesis of highly-aligned cupric oxide nanowiers by thermal oxidation of copper foils

JianBo Liang, Naoki Kishi, Tetsuo Soga, Takashi Jimbo:

Journal of Nanomaterials Volume 2011, Article ID 268508,

[3] Thin cuprous oxide films prepared by thermal oxidation of copper foils with water vapor

JianBo Liang, Naoki Kishi, Tetsuo Soga, Takashi Jimbo, Mohsin Ahmed:

Thin solid films (in press)

[4] Growth of high-quality (111) oriented cuprous oxide thin films oxidized in water vapor

JianBo Liang, XuYang Li, Naoki Kishi, Tetsuo Soga:

Materials science and engineering B (submitted)

Conference

[1] Growth of cupric oxide nanostructure by thermal oxidation of copper

梁剣波,曽我哲夫,神保孝志:

電子情報通信学会技術研究報 ED2008－1~21 [電子デバイス] (2008 年 5 月 15 ~ 16 日,名古屋)

pp.47~50.

[2] Cupric oxide nanowires synthesis by thermal oxidation of copper

JianBo Liang, Naoki Kishi, Tetsuo Soga, Takashi Jimbo:

In NANO-SciTech 2008 international Conference on Nanoscience and Nanotechnology (Malaysia, November 2008), pp.97~

[3] CuO-ZnO core shell nanowires and ZnO nanoparticle CuO nanowire integrated structures

JianBo Liang, Naoki Kishi, Tetsuo Soga, Takashi Jimbo:

In Nanomaterials Seminar for Reducing Environmental Risk in Asia (Nagoya, December 2009), pp.74~

[4] 熱酸化により CuO ナノワイヤーの合成

梁剣波, 岸直希, 曽我哲夫, 神保孝志:

,第 57 回応用物理学会関係連合講演会(2010 年 3 月 17～20 日,神奈川)

[5] Synthesis of copper oxide nanowires by thermal oxidation of thin copper foils

JianBo Liang, Naoki Kishi, Tetsuo Soga, Takashi Jimbo:

In EM-NANO 2010 the Third International Symposium on Organic and Inorganic Electronic Materials and Related Nanotechnologies (Toyama, June 2010), pp.50 ~

[6] Synthesis and characterization of highly-aligned cupric oxide nanowiers by thermal oxidation of copper foils

JianBo Liang, Naoki Kishi, Tetsuo Soga, Takashi Jimbo:

In the 4th International Workshop on Advanced Ceramics (Nagoya, December 2010), pp.64~